

5-2002

Distribution of Patterned Ground and Surficial Deposits on a Debris-covered Glacier Surface in Mullins Valley and Upper Beacon Valley, Antarctica

Andrew M. Lorrey

Follow this and additional works at: <http://digitalcommons.library.umaine.edu/etd>

 Part of the [Geology Commons](#), [Glaciology Commons](#), and the [Sedimentology Commons](#)

Recommended Citation

Lorrey, Andrew M., "Distribution of Patterned Ground and Surficial Deposits on a Debris-covered Glacier Surface in Mullins Valley and Upper Beacon Valley, Antarctica" (2002). *Electronic Theses and Dissertations*. 597.
<http://digitalcommons.library.umaine.edu/etd/597>

This Open-Access Thesis is brought to you for free and open access by DigitalCommons@UMaine. It has been accepted for inclusion in Electronic Theses and Dissertations by an authorized administrator of DigitalCommons@UMaine.

**DISTRIBUTION OF PATTERNED GROUND AND SURFICIAL DEPOSITS ON
A DEBRIS-COVERED GLACIER SURFACE IN MULLINS VALLEY AND
UPPER BEACON VALLEY, ANTARCTICA**

By

Andrew M. Lorrey

B.A. Boston University, 1998

A THESIS

Submitted in Partial Fulfillment of the

Requirements for the Degree of

Master of Science

(in Geological Sciences)

The Graduate School

The University of Maine

May, 2002

Advisory Committee:

George H. Denton, Libra Professor of Geological Sciences and Quaternary and
Climate Studies

Daniel F. Belknap, Professor of Geological Sciences, Marine Sciences, and
Quaternary and Climate Studies

Kirk Maasch, Associate Professor of Geological Sciences and Quaternary and
Climate Studies

**DISTRIBUTION OF PATTERNED GROUND AND SURFICIAL DEPOSITS ON
A DEBRIS-COVERED GLACIER SURFACE IN MULLINS VALLEY AND
UPPER BEACON VALLEY, ANTARCTICA**

By Andrew M. Lorrey

Thesis Advisor: Dr. George H. Denton

An Abstract of the Thesis Presented
in Partial Fulfillment of the Requirements for the
Degree of Master of Science
(in Geological Sciences)
May, 2002

Beacon Valley is located in the western Dry Valleys, Antarctica, adjacent to the East Antarctic Ice Sheet (EAIS). The surficial material on the floor of Beacon Valley is segmented into large polygonal landforms separated by trenches. Buried beneath the polygons and surficial material is massive ground ice. One hypothesis is that the buried ice in upper Beacon Valley is glacier ice originating from local debris-covered glaciers. The networks of polygons and trenches form as the buried ice undergoes thermal contraction and sublimation. Contraction cracks that penetrate the surficial material and buried ice in Beacon Valley contain Late Miocene age volcanic ashes. The ashes post-date the buried ice. The preservation of such old ice implies a continuous extreme polar condition in Beacon Valley since late Miocene time.

An alternative explanation is that the buried ice in Beacon Valley is modern ground ice that formed from percolation of melted, wind-blown snow that subsequently froze within the sediment mantle. Polygonal landforms would result from the seasonal freeze-thaw of the modern ground ice and surficial material. Continual freeze-thaw

action, or cryoturbation, would create a mass of coalesced, modern ice lenses covered with older sediment. The buried ice in this case could be young, and hence could not be used to imply stable climatic conditions in Beacon Valley since the late Miocene.

Polygons cover the surface of a debris-covered glacier that fills part of upper Beacon Valley and Mullins Valley. A survey of the debris-covered glacier surface indicates that polygons mature with distance from the equilibrium line. The polygon morphology highlights the transport path of the buried ice in upper Beacon Valley, which can be sourced to the cirque (accumulation zone) at the head of Mullins Valley. The buried ice in upper Beacon Valley is part of a coherent, massive ice body of glacial origin.

A gray diamicton is draped over the buried ice. It has textural and weathering characteristics akin to englacial, buried ice sediment. This diamicton is classified as a till that formed from sublimation of buried ice. The sublimation till (28% sand, 69% gravel, and 3% mud) is sorted by narrow contraction cracks in the buried ice that results in sand wedge deposits (83% sand, 11% gravel, and 6% mud). The grain-sizes that comprise sublimation till and sand wedges indicate that sediment is initially derived from sublimation of the buried ice.

Deep polygon trenches develop over thermal contraction cracks in the buried ice, and create traps for wind-blown sediment (reworked sublimation till, sand wedge sediment and volcanic ash.) The tops of some contraction cracks were void of sediment, indicative of a sediment starvation. In this case, any primary volcanic ashfall could descend directly into active sand wedges. As sublimation occurs, sand wedges containing volcanic ash can slump over the sublimation till and buried ice.

The stratigraphy of massive weathered sand, with stringers of volcanic ash, resting on sublimation till and buried ice is widespread in upper Beacon Valley. Because the contraction cracks and sand wedges are secondary to the buried ice, the ashes contained in them can afford a minimum age for the buried ice. This study supports the concept of the ash chronology previously used (Sugden *et al.*, 1995) to date the buried ice at late Miocene age, and argues for persistent polar conditions in Beacon Valley since that time.

ACKNOWLEDGMENTS

My sincerest appreciation and thanks are extended to George Denton, who provided me with the opportunity and physical means to complete fieldwork for this degree. Dr. Denton's continual guidance about all matters scientific and social has contributed to making me a better scientist and human being.

I thank Dave Marchant, for introducing me to Antarctic glacial geology, for helping in the development of thesis and mapping plans, and for general guidance in the field. Eric Moore was an indispensable companion in the field, as he provided instruction on both excavation and sampling techniques at various locations and helped with development and completion of a large-scale mapping project in Beacon Valley.

Many hours were spent in preparation for the 1998-99 field season with Adam Lewis, whose hard work and intellectual discussion I greatly appreciate. I extend my thanks to Daniel Belknap for instruction and use of equipment in the sedimentology laboratory.

I thank D.W. Caldwell, Duncan FitzGerald and Ilya Buynevich of Boston University for giving me an education in geology.

My gratitude is extended to family and friends for their continual support.

This research was supported by the Division of Polar Programs of the National Science Foundation, through grants awarded to George Denton.

TABLE OF CONTENTS

ACKNOWLEDGMENTS.....	ii
LIST OF TABLES.....	vii
LIST OF FIGURES.....	viii
I. INTRODUCTION.....	1
Antarctica and Climate Change.....	1
Background and Previous Work.....	3
The Onset of Polar Conditions in Antarctica.....	5
Pliocene Deglaciation Hypothesis.....	6
Onset of Polar Conditions in Middle Miocene Time: Evidence From the Dry Valleys.....	7
II. THE PROBLEM.....	11
Patterned Ground in Beacon Valley.....	11
Models of Polygon Formation.....	13
Goal.....	22
Objectives.....	22
III. PHYSICAL AND GEOLOGIC SETTING.....	24
Physical Geography.....	24
The Dry Valleys.....	24
Beacon Valley.....	26
Bedrock Geology of Beacon Valley.....	29
Beacon Supergroup Sedimentary Rocks.....	29
Basement Rocks.....	29

	Ferrar Dolerite Intrusive Rocks.....	31
	Sirius Group.....	31
IV.	METHODS.....	32
	Field Methods.....	32
	Laboratory Methods.....	34
V.	RESULTS.....	35
	Morphology of Polygons.....	36
	Stratigraphy in Excavations.....	45
	Excavation DLE 98-004.....	45
	Sediments and Stratigraphy.....	45
	Buried Ice.....	48
	Debris Bands.....	48
	Stratigraphic Interpretation.....	48
	Excavation DLE 98-005.....	50
	Sediments and Stratigraphy.....	50
	Buried Ice.....	50
	Debris Bands.....	53
	Stratigraphic Interpretation.....	56
	Excavation DLE 98-007.....	58
	Sediments and Stratigraphy.....	58
	Buried Ice with Included Clasts.....	59
	Stratigraphic Interpretation.....	59

Excavation DLE 98-010.....	62
Sediments and Stratigraphy.....	62
Buried Ice.....	63
Stratigraphic Interpretation.....	63
Excavation DLE 98-013.....	66
Sediments and Stratigraphy.....	66
Buried Ice and Debris Bands.....	66
Contraction Cracks.....	67
Stratigraphic Interpretation.....	67
Excavation DLE 98-014.....	70
Sediments and Stratigraphy.....	70
Buried Weathered Dolerite Clasts.....	70
Stratigraphic Interpretation.....	71
Excavation DLE 98-017.....	75
Sediments and Stratigraphy.....	75
Volcanic Ash Stringers.....	75
Ice-cemented Volcanic Ash.....	76
Buried Ice.....	76
Stratigraphic Interpretation.....	79
Sedimentology.....	80
Sorting.....	80
Grain Maturity.....	83
Oxidation and Lithology.....	85

VI.	DISCUSSION.....	87
	Morphology.....	87
	Development of Trenches.....	89
	Sediment Distribution.....	93
	Linkage Between Polygon Characteristics.....	96
	Stratigraphy.....	102
	Development of Stratification.....	102
VII.	CONCLUSIONS.....	112
	REFERENCES.....	114
APPENDIX A-	SEDIMENTOLOGY DATA.....	119
APPENDIX B-	POLYGON MAPPING DATA.....	123
APPENDIX C-	MAP C.1 EXCAVATION SITE MAP.....	124
	MAP C.2 POLYGON MAPPING SITES.....	125
	BIOGRAPHY OF THE AUTHOR.....	126

LIST OF TABLES

TABLE 1- Descriptions and interpretations of stratigraphic units seen in the field.....	81
TABLE A.1- Sedimentology data; weathered quartz and dolerite sand unit (actual sample weights).....	119
TABLE A.2- Sedimentology data; weathered quartz and dolerite sand unit (percent grain-size by weight).....	120
TABLE A.3- Sedimentology data; unweathered gray diamicton unit (actual sample weights).....	121
TABLE A.4- Sedimentology data; unweathered gray diamicton unit (percent grain-size by weight).....	122
TABLE B.1- Polygon mapping data.....	123

LIST OF FIGURES

Figure 1-	Antarctica and the surrounding Southern Ocean.....	2
Figure 2-	Cenozoic benthic foraminifera oxygen isotope record.....	4
Figure 3-	Polygon networks on the floor of Beacon Valley.....	12
Figure 4-	Contraction crack/ cryoturbation polygon.....	15
Figure 5-	Contraction crack/ sublimation polygon.....	18
Figure 6-	The Dry Valleys of Antarctica.....	25
Figure 7-	Satellite map of Beacon Valley.....	28
Figure 8-	Bedrock geologic map of the Beacon Heights area.....	30
Figure 9-	Map-view and cross-section of polygon measurements.....	37
Figure 10-	Aerial photographs of Beacon and Mullins Valley.....	40-44
Figure 11-	Excavation DLE 98-004.....	46,47
Figure 12-	Relict polygon nets.....	52
Figure 13-	Excavation DLE 98-005.....	54,55
Figure 14-	Cross-section through an ice-cemented sand wedge.....	56,57
Figure 15-	Excavation DLE 98-007.....	60,61
Figure 16-	Excavation DLE 98-010.....	64,65
Figure 17-	Excavation DLE 98-013.....	68,69
Figure 18-	Excavation DLE 98-014.....	73,74
Figure 19-	Excavation DLE 98-017.....	77,78
Figure 20-	Ternary plot of all sediment samples.....	82
Figure 21-	Contrast in grain-maturity from samples DLS 98-010C and D.....	84
Figure 22-	Contrast in oxidation and lithology.....	86
Figure 23-	Observed changes in polygon morphology.....	88

Figure 24-	Diagram of change in polygon relief.....	90
Figure 25-	Diagram of change in trench angle and relationship between trench angle and polgyon relief.....	91
Figure 26-	Diagram of change in trench width and relationship between trench angle an trench width.....	92
Figure 27-	Diagram of sediment thickness with increasing distance from the equilibrium line.....	94
Figure 28-	Profile of a debris-covered glacier.....	95
Figure 29-	Schematic diagram of a polygon environment.....	99
Figure 30-	Polygon cannibalization process.....	100
Figure 31-	Contraction crack/ sublimation polygon model.....	105
Figure 32-	Stretching of volcanic ash wedge into a stringer.....	106
Figure 33-	Development of sand wedges and overlying polygon trenches.....	107
Figure 34-	Photograph of healed contraction cracks.....	109
Figure 35-	Burial of former desert pavements.....	111

I. INTRODUCTION

Antarctica and Climate Change

The Antarctic Ice Sheet and the surrounding Southern Ocean together (**Figure 1**), are important components in Earth's climate. Multiple parts of Earth's climate are influenced by the presence of a continental-scale ice sheet on Antarctica, including global sea level, ocean chemistry and planetary albedo. The cold, polar environment of Antarctica has created an enormous heat sink, effectively steepening the latitudinal thermal gradient of the Southern Hemisphere and increasing the vigor of atmospheric circulation (Zachos *et al.*, 1996).

The East Antarctic Ice Sheet composes a major part of the Antarctic Cryosphere System and plays a large role in global climate. The response of the East Antarctic Ice Sheet to long and short-term perturbations in Earth's climate is one of the keys to understanding global climate change. The past conditions that prevailed over the East Antarctic Ice Sheet can be correlated with changes at the ice sheet margin through the interpretation of the glacial geology of deglaciated landscapes. Past and present dynamics of the East Antarctic Ice Sheet can then be used to develop models for future glaciations and climate change (Hughes, 1998). Some current models have illustrated the effects of general climatic amelioration during the Tertiary. Long-term climatic changes during the late Tertiary have included the initiation and growth of Northern Hemisphere ice sheets and have influenced the course of global biotic evolution and geographic distributions of humankind (Flower and Kennett, 1994).

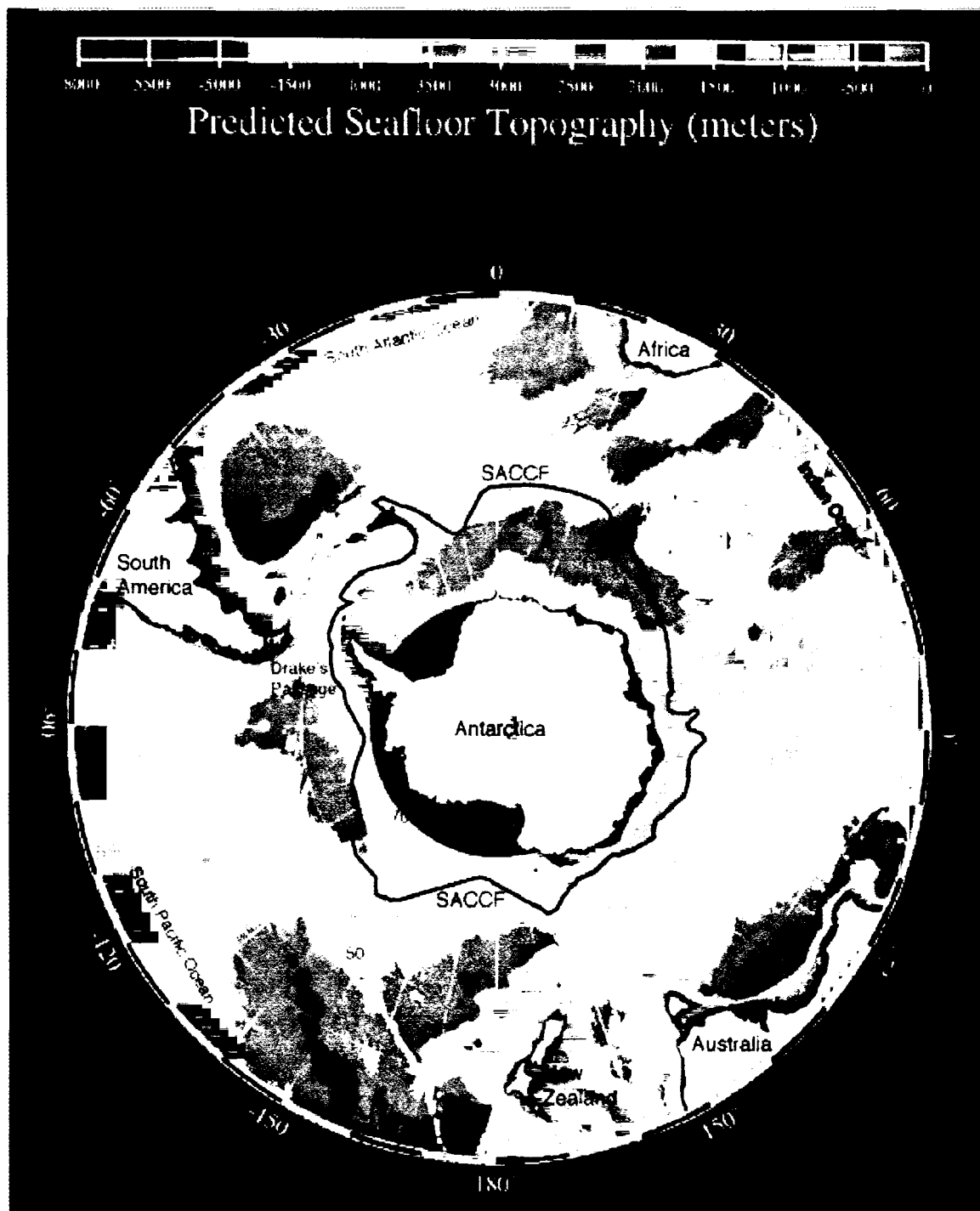


Figure 1- Antarctica and surrounding Southern Ocean. Shown on the map is the approximate location of the Southern Antarctic Circumpolar Current Front (SACCF) and seafloor bathymetry. Bathymetric depths are in meters. (Modified from NOAA web site graphic image file <http://www.ngdc.noaa.gov/mgg/image/predict.gif>)

Global climate has become progressively warmer since the end of the 19th Century (Gutzler, 2000). The Antarctic Ice Sheet may be susceptible to the current trend in rising global temperatures. A mass-balance instability in the East Antarctic Ice Sheet would cause a 60 m rise in global sea level if the entire ice sheet melted (Hughes, 1998; Drewry, 1982). A sea-level rise of this proportion would have a devastating affect on the socio-economic centers of today's world, which are located near present-day coastlines.

Background and Previous Work

Long-term Cenozoic climate change in Antarctica occurred as a series of punctuated of step-like decreases in deepwater temperature taking place over the last 55 million years (Miller *et al.*, 1987; Flower and Kennett, 1994; Barrett, 1997) (Figure 2). The relative amounts and types of biota within sediments from deep-sea cores taken in the South Pacific Ocean have been interpreted as evidence of a major cooling of the continent and formation of the first glaciers in Antarctica during the Eocene (Margolis and Kennett, 1970.) The migration of Australia and South America from sub-polar to mid-latitudes, coupled with the opening of the Drake Passage in the late Oligocene-early Miocene changed the ocean circulation around Antarctica from a meridional to a near-circumpolar current system. The establishment of the Antarctic Circumpolar Current (ACC) was completed when the Drake Passage opened, which produced changes in ocean basin bathymetry and enhanced the development of Antarctic bottom water

(Flower and Kennett, 1994; Kennett, 1977). The establishment of a vigorous circumpolar oceanic current around Antarctica at a high polar latitude is responsible for the thermal isolation and growth of ice sheets on the continent (Barrett, 1996).

A large step in the deepwater benthic foraminifera $\delta^{18}\text{O}$ records indicate that a major climatic change may have taken place in high latitude oceans during the middle Miocene (Miller *et al.*, 1987). The middle Miocene step in the benthic foraminifera $\delta^{18}\text{O}$ is thought to be associated with an increase in Antarctic deepwater production and growth of the East Antarctic Ice Sheet (Flower and Kennett, 1994). Evidence of an expanded East Antarctic ice sheet during this time is found in the Dry Valleys in the form of preserved glacial deposits and erosional features. Some of these glacial deposits have been dated as middle Miocene in age (Marchant *et al.*, 1993a). The glacial deposits and erosional features found in the Dry Valleys suggest basal melting conditions existed for an expanded East Antarctic Ice Sheet that overrode the Transantarctic Mountains during middle Miocene time.

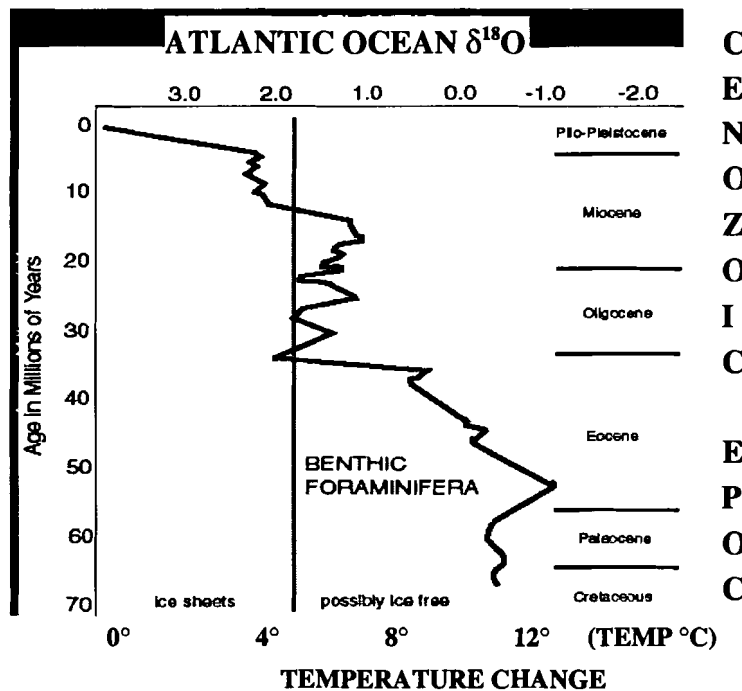


Figure 2- A Summary of Cenozoic benthic foraminiferal oxygen isotopic records from the Atlantic Ocean (modified from Miller *et al.*, 1987). The black line is an average from core data that were used as a proxy for ice volume and/or deep-water temperature change in the Atlantic Ocean over the last 70 million years.

Subglacial erosional features are found in the Quartermain Mountains contemporaneous with ice overriding the Dry Valleys during middle Miocene time. These erosional features include striated bedrock surfaces, molded clasts, and stoss-and-lee bedrock features that contain potholes and plunge pools formed from subglacial meltwater on the lee side of bedrock obstructions (Denton *et al.*, 1993). Conspicuously absent in terrain overridden by Miocene-age ice are ice-marginal features and deposits created by meltwater, such as outwash plains or kame terraces. The absence of such deposits is taken as evidence for ice dissipation during middle Miocene time under cold, polar conditions identical to the present climate in the Dry Valleys (Marchant *et al.*, 1993a).

The Onset of Polar Conditions in Antarctica

At least two views pertain to the stability of the East Antarctic Ice Sheet during late Cenozoic time. One view is that the East Antarctic Ice Sheet has been robust and stable ever since the initiation of a full-bodied Antarctic Circumpolar Current, shortly after the opening of the Drake Passage at the Oligocene/early Miocene boundary. A different view is that the East Antarctic Ice Sheet existed in a temperate climate until the late Pliocene, and hence was susceptible to changes in ocean and atmospheric circulation on a global scale, waxing and waning during periods of global cooling and warming. This hypothesis has been used to infer the collapse of the East Antarctic Ice Sheet and deglaciation of East Antarctica during periods of global warmth, such as experienced during the Pliocene. Demise of an ice sheet the size of the one now covering East Antarctica would cause a sea level rise of approximately 60 m (Drewry, 1982).

Pliocene Deglaciation Hypothesis

The hypothesis of East Antarctic deglaciation during the Pliocene hinges on the inferred age of the Sirius Group, a tillite found as remnants in numerous localities in the Transantarctic Mountains (Denton *et al.*, 1993). The age and paleoenvironmental interpretation of the Sirius Group has been subject to controversy (Webb *et al.*, 1984; Webb and Harwood, 1991; Barrett *et al.*, 1992; Marchant *et al.*, 1993a, b; Burckle and Potter, 1996). A Pliocene age was assigned to the deposit on the basis of enclosed recycled marine diatoms (Webb *et al.*, 1984). These diatoms are found within a matrix of reworked glaciolacustrine/glaciomarine sediments. Paleoglacial flow directions inferred from a striated bedrock surface underlying the Sirius Group indicate that an ice sheet overrode the Dry Valleys from the southeast. The paleoglacial flow direction implies emplacement of the Sirius Group from an overriding ice sheet that flowed across the Wilkes and Pensacola Basins. Both basins are located behind the Transantarctic Mountains, deep in the interior of East Antarctica. Therefore, the presence of Pliocene diatoms derived from this area would mean that East Antarctica must have been ice free during the late Pliocene before an ice sheet formed in this region.

The paleoclimatic significance of the Sirius Group is enhanced by the discovery of *in situ* woody twigs and stems of *Nothofagus* within outcrops of the tillite found in the Beardmore Glacier region (Webb and Harwood, 1987). The existence of *Nothofagus beardmorensis* as far as 85° South latitude implies that yearly temperatures must have exceeded 5°C for at least three months out of the year (Hill and Truswell, 1993). The likelihood of a polar ice sheet being present during such a warm period is improbable if

beech trees were growing at such high latitudes during the Pliocene. However, a temperate ice sheet could have existed in East Antarctica at the same time as trees growing in the Beardmore Glacier region.

Onset of Polar Conditions in Middle Miocene Time: Evidence from the Dry Valleys

The opposing hypothesis to a temperate ice sheet in the interior of East Antarctica during the Pliocene is that the East Antarctic Ice Sheet has been a permanent feature existing in a polar condition since middle Miocene time (Marchant and Denton, 1996; Hall *et al.*, 1993; Denton *et al.*, 1993). The stability hypothesis refutes the biostratigraphic age assigned to the Sirius Group from the included diatoms. Ice cores from the interior of the East Antarctic Ice Sheet have yielded marine diatoms, demonstrating diatom transport by aeolian processes over large distances (Kellogg and Kellogg, 1996, 1997). Miocene-Holocene diatoms occur in some Paleozoic, Mesozoic and Cenozoic sedimentary, igneous and metamorphic rocks in the Dry Valleys (Burckle and Potter, 1996). The presence of young diatoms at widespread geographical localities and in older rocks highlights the plausibility of diatom inclusion in the Sirius Group from random aeolian fallout (Burckle and Potter, 1996). The biostratigraphic association of diatoms to the Sirius Group would then be unfounded if the marine diatoms included in the deposits are merely aeolian contaminants. A more appropriate age for the Sirius Group, based on early to mid Tertiary geographic distributions of *Nothofagus*, would likely be Oligocene (Burckle and Pokras, 1991).

If the diatom evidence that contradicts a Pliocene age interpretation of the Sirius Group were completely disregarded, then a question can still be asked about the plausibility of an East Antarctic Ice Sheet collapse: if the East Antarctic craton was

subject to deglaciation during the Pliocene, then where are the temperate glacial deposits associated with such an ice-sheet collapse?

The glacial deposits preserved in the Quartermain Mountains and the western Asgard Range in the Dry Valleys are not indicative of massive temperate deglaciation during a warm Pliocene epoch. Between 15 Ma and 13.6 Ma, an expanded East Antarctic Ice Sheet overran both of these regions. The preserved succession of glacial deposits in Arena Valley consisting of the Sessrumnir, Inland Forts, and Altar tills exhibit characteristics of deposition from temperate ice prior to 15 Ma. The Monastery Colluvium that is superposed on these tills is interpreted as evidence for an ice-free and semi-arid environment shortly after deglaciation (Marchant *et al.*, 1993a). The Sessrumnir and Inland Forts till overlain by the Koenig Colluvium form a similar stratigraphic succession in the western Asgard Range (Marchant *et al.*, 1993b). Minor colluvium deposition in these areas resumed sometime between 13.6 Ma and 11.3 Ma. Sedimentation since 11.3 Ma has been nearly nonexistent. The absence of temperate glacial deposits and the colluvium deposited a semi-arid environment in both Arena Valley and the western Asgard Range demonstrate persistent cold, polar conditions during the East Antarctic Ice Sheet recession from the western Dry Valleys (Marchant *et al.*, 1993a).

Volcanic ash deposits have been found interbedded with some of the glacial deposits and colluvium in Arena Valley and the western Asgard Range (Marchant *et al.*, 1993a; b). The ash deposits contain grains with fibrous glass shards, delicate spires, and euhedral grains containing intact bubble vesicles. The Arena Valley volcanic ash deposits exhibit little if any signs of weathering and retransport after primary airfall

deposition, and are indicative of being *in situ* or near *in situ* volcanic ashfall. The Arena Valley volcanic ash deposits located in the Quartermain Mountains, range in age from 11.3-4.34 Ma and overlie the Monastery Colluvium. Chemical stability of these ashes is implied because they are weathered to less than 5% clay in total composition (Marchant *et al.*, 1993b).

The chemical stability of the volcanic ashes in Arena Valley and the western Asgard Range suggests that the warm climate conditions necessary for weathering of ash to clay were not present after time of airfall deposition in western Dry Valleys. The delicate sedimentologic features of ash grains and lack of clay content in ash deposits argue against the existence of a temperate ice sheet during the Pliocene. Hence, the ashes used to date the colluvium are interpreted as *in situ*, being preserved in an unaltered state since 11.3 Ma. The preservation and lack of alteration of the Monastery Colluvium and the volcanic ashes that date the deposit argue for the antiquity of the present glacial landscape contained in the western Dry Valleys in a persistent cold, polar climate since 11.3 Ma (Marchant *et al.*, 1993b).

The antiquity of the Dry Valleys landscape is further supported by the degree to which surface clasts have been exposed and weathered at the land surface. Cosmogenic exposure age dates on dolerite boulders and bedrock from Insel Mountain, located in the Olympus Range, have yielded ages that place the formation of the present Dry Valleys landscape at more than 6.5 Ma (Schäfer *et al.*, 1999). Such great exposure ages demonstrate extremely low, persistent erosion rates since the initiation of cold, polar desert conditions in Antarctica.

Beacon Valley is located in the western Dry Valleys alongside the East Antarctic Ice Sheet. Changes in East Antarctic Ice Sheet geometry, ice-sheet dynamics and paleoenvironment of the Dry Valleys would be recognized in Beacon Valley because of its geographic position relative to the East Antarctic Ice Sheet. Potter and Wilson (1984) reported that much of the broad floor of Beacon Valley contained a surficial mantle superposed on buried ice. It was hypothesized that the buried ice was relict, stagnant glacial ice from local debris-covered glaciers that had flowed into upper Beacon Valley and relict Taylor Glacier ice that advanced into central Beacon Valley (Potter and Wilson, 1984). Ash deposits found in contraction cracks in the sediments overlying the buried ice have since been dated at 8.1 Ma (Sugden et al., 1995), and thereby provide a minimum age for the buried ice. The preservation of ancient buried ice in Beacon Valley is an important piece of evidence supporting the stable ice sheet hypothesis. The East Antarctic Ice Sheet would have not melted away since the late-Miocene if small debris-covered glaciers and relict late-Miocene-age Taylor Glacier ice have persisted in Beacon Valley prior to and through the Pliocene warm period.

II. THE PROBLEM

Patterned Ground in Beacon Valley

The fact that patterned ground covers the floor of Beacon Valley raises questions pertaining to landscape antiquity and stability in the western Dry Valleys. Quantitative geomorphologic studies of patterned ground were undertaken in the Dry Valleys region in an attempt to determine the age of polygonal features using modern growth rates of polygonal cracks in various geomorphic settings (Berg and Black, 1966; Black, 1973; 1982). During the winter season in permafrost regions, cold ground temperatures create thermal contraction cracks in perennially frozen surficial material. The result of expansion and contraction of the ground over an extensive permafrost landscape is a polygonal array of cracks perpendicular to the ground surface (Black, 1982).

Geomorphic surfaces that are disrupted by arrays of polygons highlight a potential problem with using an apparently “ancient” surface as a means of assessing the entire landscape stability of a particular region. The polygons on the floor of Beacon Valley are small-scale features ($<0.25 \text{ m}^2$ - $.02 \text{ km}^2$) superimposed on the large-scale landscape ($\approx 525 \text{ km}^2$). Examples from the Canadian Arctic, Alaska and Spitzbergen demonstrate that landscapes exhibiting active, wide, closely spaced sand wedges undergoing geologically modern cryoturbative processes (Hallet, 1990a, b; Hallet and Prestrud, 1986).

The landscape in Beacon Valley contains surficial sediments riddled with polygonal cracks (**Figure 3**). A contemporary polygon study conducted at the mouth of Beacon Valley used modern contraction crack growth rates to extrapolate polygon ages. The polygons ($10\text{-}25\text{m}^2$) near the margin of Taylor Glacier were estimated to have taken



Figure 3-Polygon networks on the floor of Beacon Valley

The polygonal network and surface debris on buried ice mantling the floor of upper Beacon Valley. Note snow in the trenches that separate individual polygons. The linear snowbank in the center of the photo demarcates the end of a debris-covered glacier.

between 5000 and 6000 years to form (Black, 1973; 1982). However, discoveries of apparently *in situ* ash fall deposits contained in polygon cracks in middle Beacon Valley have been dated at 8.1 Ma (Sugden *et al.*, 1995b), which would imply that the polygons form on a time scale orders of magnitude greater than a few thousand years.

Do the presence of polygons mean that the landscape is truly young, and that the ashes cannot be used to date the overall landscape? How can ash wedges be preserved in an apparently active mesoscale landscape? Are the mechanisms that form polygons in the Arctic or lower Beacon Valley characteristically representative of polygon formation for middle and upper Beacon Valley? These are puzzling questions. The ancient ice buried beneath polygons in middle Beacon Valley and the ash stratigraphy that dates this ice are lines of evidence that support the persistence of cold, polar conditions in the Dry Valleys region since Miocene time. But what if the ice beneath the surface of Beacon Valley was in fact, modern ground ice, currently cryoturbating and forming polygons? Determining the nature of the buried ice, the processes that form the polygons, and the stratigraphy contained in Beacon Valley are important to forming an accurate interpretation of paleoclimate of the western Dry Valleys.

Models of Polygon Formation

One particular type of formation of patterned ground has been established for Arctic polygons. This Arctic model of polygon formation relies on cryoturbation as a means of developing sorted polygon networks. The freeze-thaw action of sand wedges and expanding-contracting ground ice or permafrost results in self-organization of surficial material on the basis of grain size (Hallet and Pestrud, 1986; Hallet, 1990a; b) in environments that contain extensive water. The long-term, convection-like cycling of

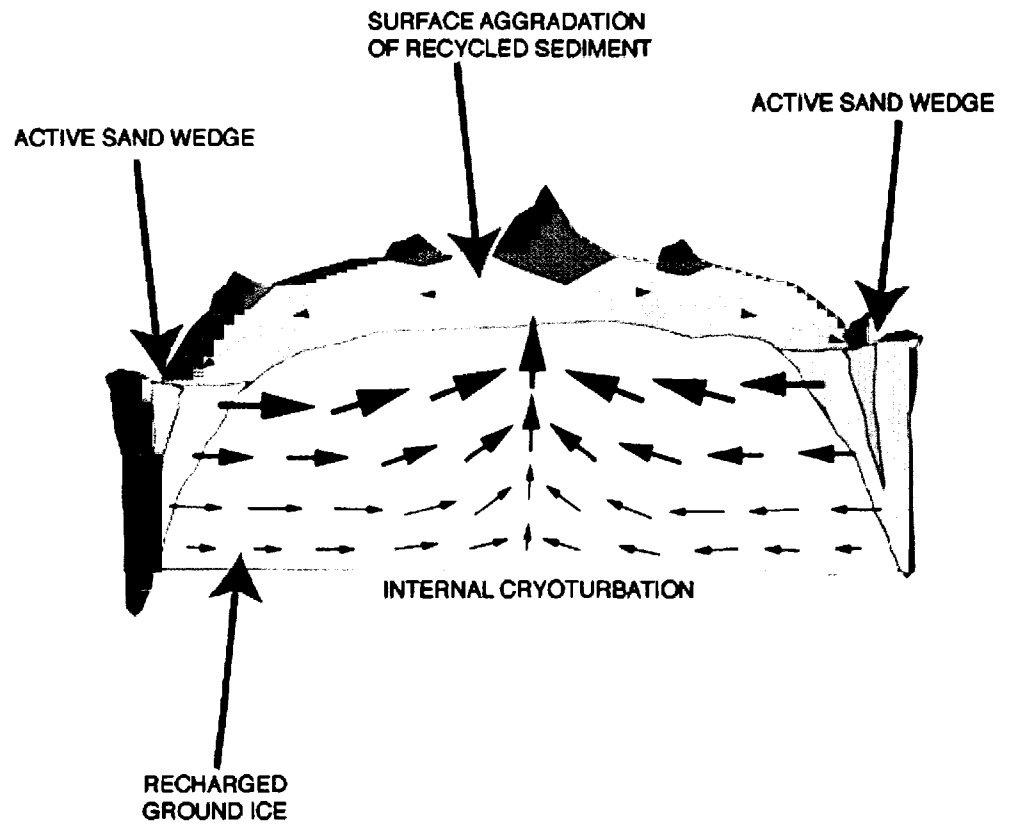
material through polygons from season to season causes material to migrate and move from the bottom of bordering, active sand wedges up through the center of a polygon. After material reaches the surface and center of a sorted polygon, it is eventually cycled to the edge by creep processes into the tops of surrounding active sand wedges (**Figure 4**).

The cryoturbative processes responsible for this particular type of polygon formation disrupts geomorphic surfaces by creating an inversely sorted vertical stratigraphic column (Rosato *et al.*, 1987). With this mechanism of polygon formation, the persistence of extreme surface stability would be unlikely. The obliteration of stratigraphy from long-term and seasonal ice loss, as well as the vertical motion of soils resulting from cryoturbative processes, is the result of the lateral and vertical sorting of clasts within a polygon. The disruption of the uppermost geomorphic surface of a polygon-riddled landscape is a foregone conclusion in this particular scenario. In addition, data from some polygons in the Dry Valleys indicate that the ratio of polygon size to sand-wedge growth rate is indicative of the ground surface being reworked on the order of thousands of years (Black 1973, 1982).

The significance of polygons forming under the Arctic model has two implications for paleoenvironment. The first is that buried ice underlying the polygons may be secondary to the sediment cover, and may contain material that has been pervasively reworked. Volcanic ashes included in such polygons could not be used to date the buried ice. The second paleoenvironmental implication is that there may be geologically modern, active cryoturbative processes occurring on a small-scale, superimposed on an ancient macroscale landscape.



Figure 4- Contraction Crack/Cryoturbation Polygon

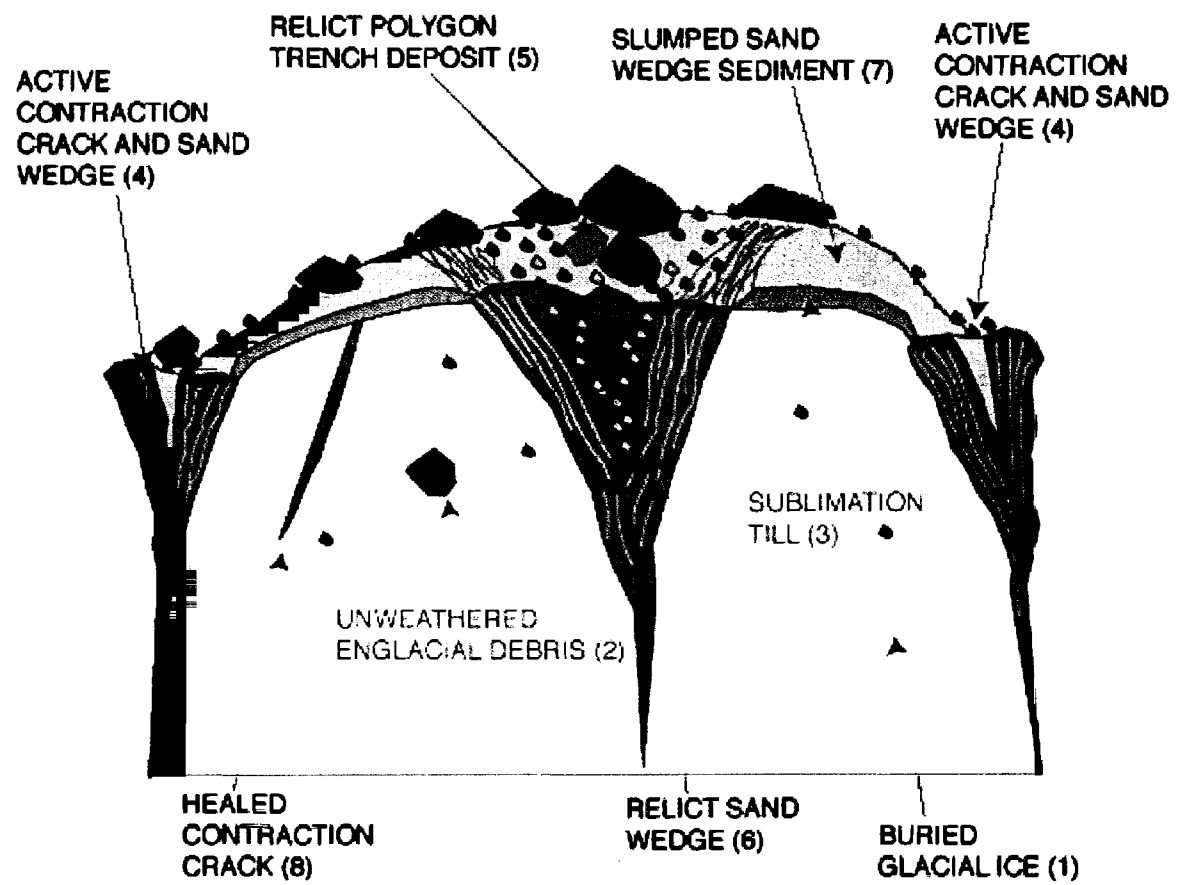


An alternative model for polygon formation in Beacon Valley relies on simple thermal contraction of underlying, ancient glacial ice (**Figure 5**). The ancient glacial ice in this case is part of a remnant debris-covered glacier. A debris-covered glacier is composed of a small, steep accumulation area in a cirque marked by snow accumulation and rock fall from the headwall. As glacier ice moves from the accumulation zone into the ablation zone, rockfall debris accumulates on the ice surface, forming a protective layer from wastage (Clark *et al.*, 1998). Due to the protective nature of the debris mantle on the surface of the buried ice, the ablation zone in a debris-covered glacier system can be much larger area than the accumulation zone.

Thermal contraction cracks form the geometrical basis of the polygonal network on the surface of the debris-covered glacier. The debris-covered glacier moves slowly enough for the cracks to occur and remain open for long intervals. The sides of contraction cracks provide additional surface area for sublimation. As sublimation progresses, englacial sediment is deposited at the surface of the buried ice as a sublimation till. Some contraction cracks continue to grow wider, causing some sublimation till to fall into the open cracks. The sediments that fall into a crack are separated through the process of preferential sieving, dominated primarily by the crack width. Some contraction cracks never open or expand beyond a few centimeters in width. The immature contraction cracks heal from re-expansion of surrounding ice by thermal expansion or because sediment that has fallen into the crack has become ice cemented. Ice cementation of sediment in contraction cracks, as well as on the ablation sediment-ice surface interface, may greatly reduce or stop sublimation and vapor transport of preserved ancient ice all together (Marchant, personal communication, 1998).



Figure 5 - Contraction Crack/ Sublimation Polygon



The buried ice and the sediment cover comprise the ablation zone of a debris-covered glacier. The sediment within the buried ice originated as both rock fall and wind-blown material in the accumulation zone (Ackert, 1998; Potter and Wilson, 1984). Sediments sublimate out of the buried ice in the ablation zone. Rock fall supplies additional material to the debris-covered glacier sediment mantle in the ablation zone. Englacial sediment and the sublimation till that directly mantles the buried ice are compositionally identical. Linear cracks open as the buried ice undergoes seasonal thermal contraction. Because the opening of a contraction crack is small, only sand can penetrate to depth in an open crack. Repetitious opening and healing of one contraction crack would form a sand wedge, a V-shaped deposit of vertically bedded sand. Slumped sand-wedge deposits would be draped over the sublimation till as sublimation of the buried ice progressed. The sediment in a slumped sand-wedge is sorted, oxidized and weathered, and the sublimation till is not. The sand-wedge sediments and slump sediments retain a distinction from the englacial sediment and the sublimation till because transportation occurs only from the buried ice to the surface and into the contraction cracks, but not back into the buried ice.

This particular model of polygon formation involves a sedimentary process in the sand wedges where, by the origin of the buried ice and deposition, stratigraphy is not disrupted in the center of polygons. This sedimentation process is also unconventional according to the Law of Superposition, which states that in a series of flatlying, undisturbed sedimentary layers or rocks, the oldest layer will be found at the bottom of the sequence. Here, material is added to the underside of the stratigraphic column overlying the buried ice while ablation occurs. This process occurs uniquely on a debris-

covered glacier surface because the majority of surficial material is emerging at the ice-sediment interface instead of being deposited subaerially on the surface of the debris-covered glacier.

Because the sediment at the top of the stratigraphic column overlying the buried ice was deposited first, the uppermost geomorphic surface has the longest exposure history. Former contraction-crack deposits, as well as ash-filled contraction cracks may be preserved in centers of polygons. Any surficial sediment or volcanic ash deposit would have been deposited after the formation of the buried ice. Intact, *in situ* ash wedges can be used to provide minimum absolute dates for the deposition of surficial sediments and the buried ice. This model of polygon formation would allow the buried ice to be relatively dated from the ashes contained in the sand wedges and surficial material. Because the valley is proximal to the ice sheet, buried ice relatively dated at Miocene age could then be used to imply long-term stability of East Antarctic Ice Sheet.

Goal

The goal of this study is to determine the origin of the buried ice and stratigraphy in upper Beacon and Mullins Valley. A secondary and equal goal is to determine what processes are controlling the formation and distribution of the polygonal landforms superposed on the buried ice. It is evident that the polygonal landforms are related to the seasonal kinematics of the buried ice, but why are their distributions and sizes uneven throughout Beacon Valley? Are the polygons a result of the presence of young, subsurface ground ice, directly resulting from current and possibly past fluctuations or breakdowns in polar conditions? Is the buried ice in Beacon Valley ancient, stagnating and sublimating away slowly, over millions of years in a stable cold, polar environment? The interpretation of the polygon distribution, the stratigraphy resulting from their formation, and the processes that form them in upper Beacon Valley are important to understanding the paleoenvironmental history of the western Dry Valleys.

Objectives

The following objectives must be completed in order to determine the overall paleoenvironment in Beacon Valley. Accomplishing these tasks will result in understanding a unique geomorphic process responsible for landscape formation in upper Beacon Valley, and will assess the relative stability of the current climate exhibited in the western Dry Valleys region.

- 1.) Describe the morphology, stratigraphy, sedimentology, lithology, and weathering characteristics of surficial deposits in upper Beacon and in Mullins Valley.

- 2.) Identify distinct stratigraphic units overlying buried ice. Determine the genesis of stratigraphic units by grain-size and texture analyses, conducted in the field and laboratory.
- 3.) Describe buried ice in upper Beacon and in Mullins Valley. Determine local origin of ice from the characteristics of encapsulated sediments.
- 4.) Describe the polygon geomorphology in upper Beacon and in Mullins Valley from field measurements and aerial photographs.
- 5.) Construct detailed maps of polygon characteristics and their distributions in upper Beacon and in Mullins Valley.
- 6.) Develop a process model for polygon formation in this area of the western Dry Valleys.
- 7.) Assess the validity of volcanic ash stratigraphy used to date buried ice in Beacon Valley.
- 8.) Determine the overall paleoenvironment in upper Beacon Valley.

III. PHYSICAL AND GEOLOGIC SETTING

Physical Geography

The Dry Valleys

The Dry Valleys region (77°-78° S, 160°-163° E) is a large, ice-free sector of the Transantarctic Mountains located along the western edge of the Ross Embayment near McMurdo Sound (Figure 6). The blocking action of the Transantarctic Mountains in the western portion of the Dry Valleys is responsible for diversion of ice around this area. Ice flow is routed around the Dry Valleys block of the Transantarctic Mountains to the north through the Mackay Glacier and south through the Mullock Glacier. The deflection of ice flow, coupled with katabatic winds that sweep into the Dry Valleys from the polar plateau are responsible for the physical geography of long, ice-free, east-west trending valleys that connect the periphery of the East Antarctic Ice Sheet to the Ross Embayment.

Taylor Dome, a marginal dome of the East Antarctic Ice Sheet, drains into upper Wright and Taylor Valley, two of the largest ice-free valleys in the Dry Valleys. The environment of the Dry Valleys today is marked by cold, polar desert that exhibits a hyper-arid precipitation regime. The amount of sublimation occurring in the Dry Valleys exceeds precipitation at all localities, except where windblown snow exceeds sublimation. Sublimation is largely responsible for glacier ablation in the Dry Valleys today (Chinn, 1980; Denton *et al.*, 1993).



Figure 6- The Dry Valleys of Antarctica
 Dry Valleys sector of the Transantarctic Mountains alongside McMurdo Sound. (From USGS Ross Island and Vicinity Topographic Map). The box in the lower left corner encompasses Beacon Valley.

Beacon Valley

Beacon Valley (77 °S, 161° E) is the largest ice-free valley in the Quartermain Mountains, a block of isolated mountains on the western edge of the Dry Valleys (**Figure 6**). The long axis of Beacon Valley trends northeast-southwest. The surface elevation of the main valley floor in upper Beacon is approximately 1400 m. The northern end or mouth of Beacon Valley is dammed by a lateral lobe of Taylor Glacier, an outlet of Taylor Dome on the edge of the East Antarctic Ice Sheet. The south end, or head of Beacon Valley is flanked by high mountains. Mount Feather at 2985m is the highest mountain on the southern flank of Beacon Valley. The east and west walls of Beacon Valley are both lined with numerous cirques. The East Antarctic Ice Sheet is banked against the southern side of the Quartermain Mountains on the southern end and the backside of the cirques on the western edge of Beacon Valley (**Figure 7**). The mouth of Beacon Valley contains recessional moraines that mark the former position of Taylor Glacier in Beacon Valley. Mean annual temperature has not been calculated for Beacon Valley; however in nearby Wright Valley mean annual temperature is -19.8°C at 123m above sea level. If one assumes an adiabatic lapse rate of 1°C/100m increase in elevation, then the mean annual temperature in Beacon Valley is approximately -29°C to -34°C (Schwerdtfeger, 1984). The annual precipitation of less than 10 mm water equivalent as calculated in Wright Valley is probably slightly less than that of Beacon Valley. A slightly higher value may be more acceptable because of snow transported into the valley by katabatic winds blowing off the bordering polar plateau.

The south end of Beacon Valley splays into smaller cirques and associated valleys. Three of these valleys are occupied by debris-covered glaciers, supported by

accumulation of local snowfall and of wind-blown snow derived from the East Antarctic Ice Sheet (Sugden *et al.*, 1995; Potter and Wilson, 1984). A prominent supraglacial lake demarcates the equilibrium line of each glacier. The ablation surfaces of these debris-covered glaciers are covered with numerous arcuate, cross-valley ridges. An extensive network of polygonal cracks segments the surficial materials mantling the debris-covered glaciers. The cracks and polygonal landforms range in size from a few meters to hundreds of meters in length.

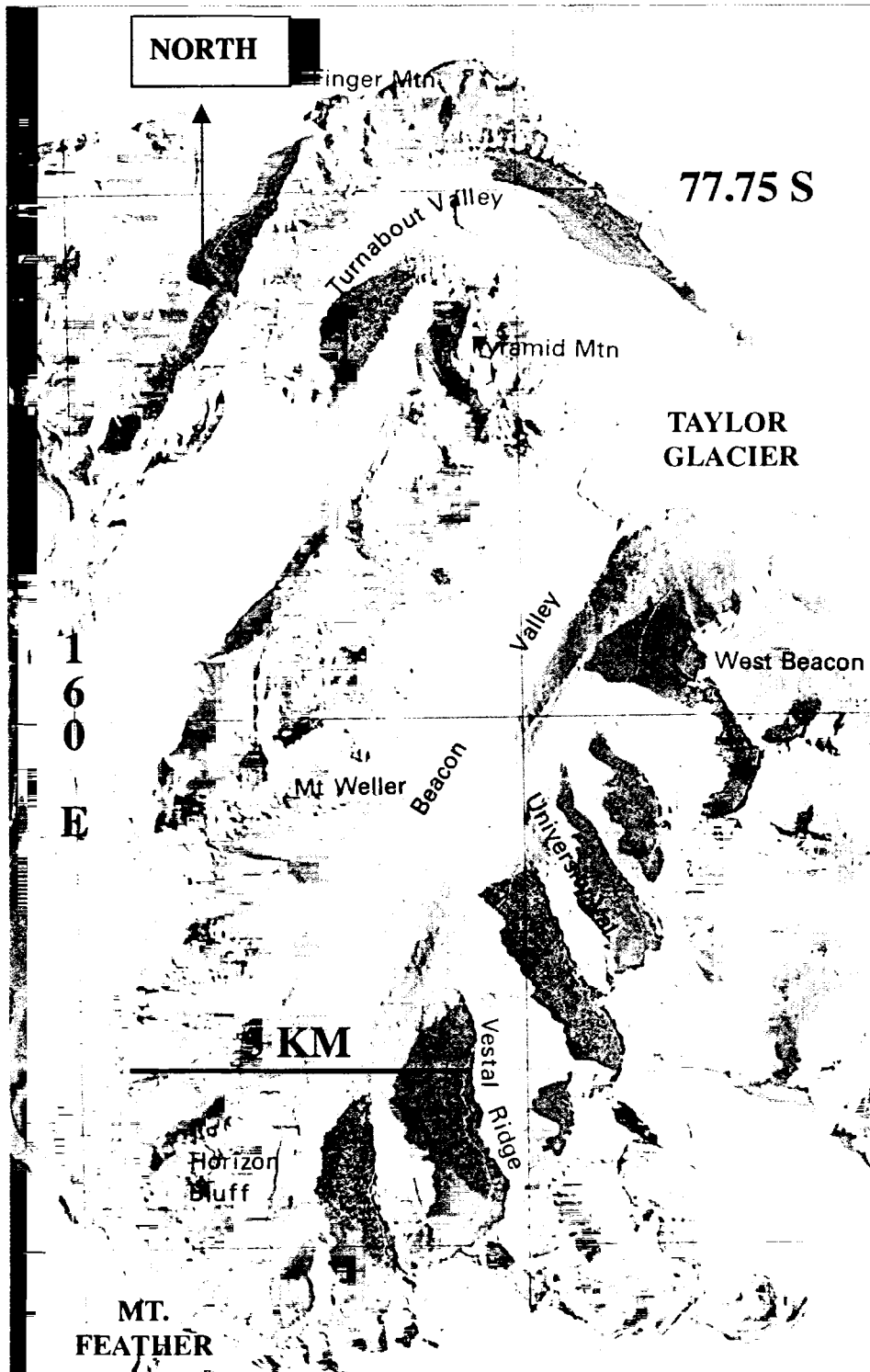


Figure 7- Satellite topographic map of Beacon Valley, Antarctica
 (From USGS Antarctic Satellite Image Map, McMurdo Dry Valleys
 Quadrangle)

Bedrock Geology of Beacon Valley

Beacon Supergroup Sedimentary Rocks

Inferred from the regional geology, the unexposed basement complex of the Quartermain Mountains is presumably truncated by the Kukri Erosional Surface (McKelvey *et al.* 1977). Oriented in a near flat-lying position over the erosional surface are Devonian to Triassic Beacon Supergroup, which can be divided into a lower Taylor Group and an upper Victoria Group. The Taylor Group is composed of quartzose sandstone interbedded with green, red, and purple siltstones sandstones. The Maya Erosional Surface is an unconformity that separates the upper Victoria Group and the lower Taylor Group. The Victoria Group is composed of a succession of Permian and Triassic glacial sediments that are separated by sandstones containing coal measures (McElroy and Rose, 1987). The Triassic sedimentary rocks in this unit, specifically the Feather Conglomerate and Lashly Formation, crop out in exposures on Mount Feather, located in the southernmost end of Beacon Valley.

Basement Rocks

Precambrian to early Paleozoic igneous/metamorphic rocks of granite, granitic gneiss, and migmatite, compose the unexposed basement complex underlying Beacon Valley and the Quartermain Mountains. Outcrops of basement rocks are isolated to a singular locality outside Beacon Valley, in a strip two kilometers long against the south side of the Taylor Valley, due east of Arena Valley (McElroy and Rose, 1987).

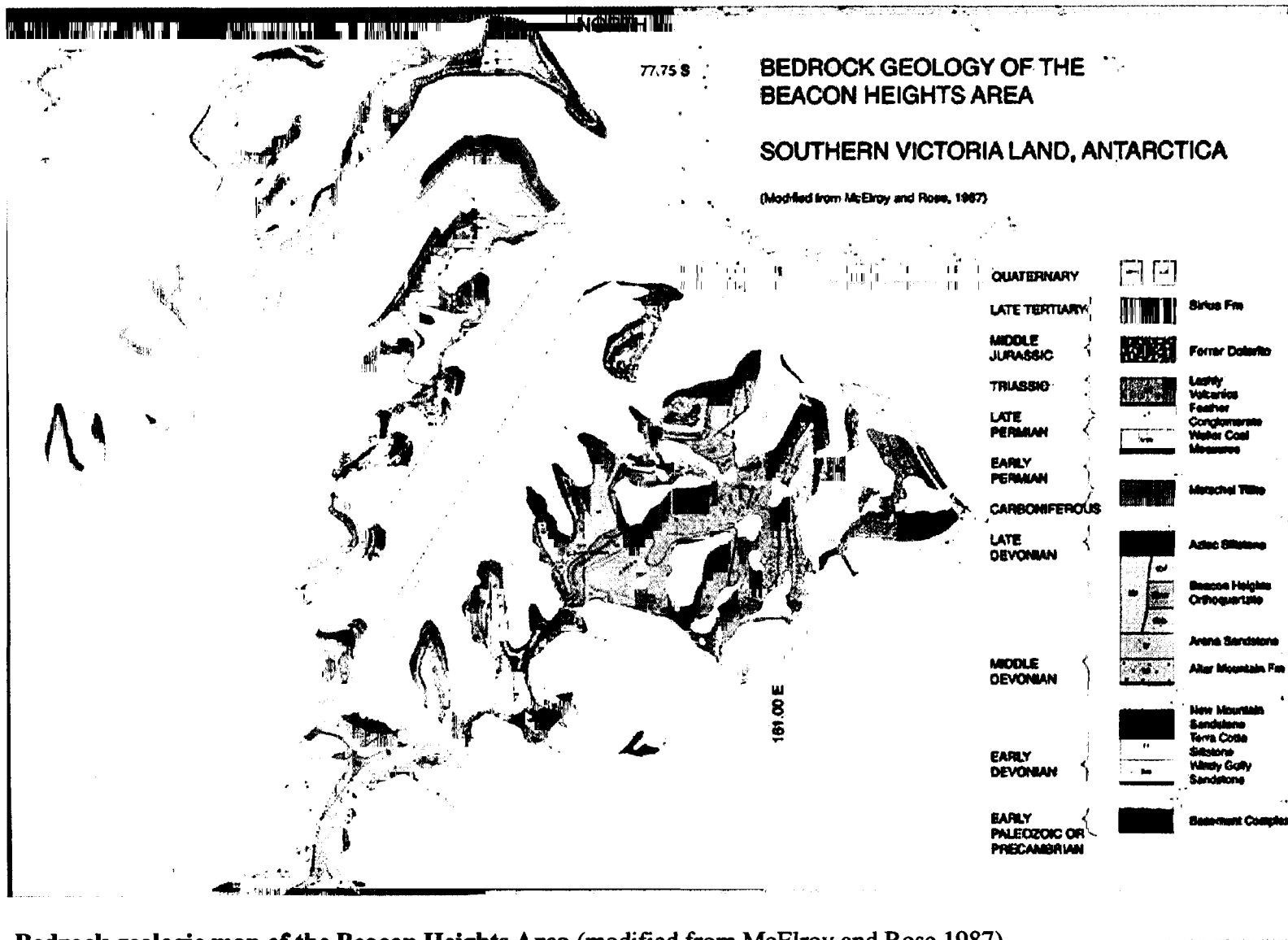


Figure 8- Bedrock geologic map of the Beacon Heights Area (modified from McElroy and Rose, 1987)

Ferrar Dolerite Intrusive Rocks

The Beacon Supergroup is intruded by the Ferrar Dolerite, massive sills of mafic igneous rock of Jurassic age that cut bedrock throughout the Transantarctic Mountains (Elliot *et al.* 1985.) These sills range in size from just over 20 m to over 250 m thick in Beacon Valley, and here are seen at four distinct levels below, above and within the Beacon Supergroup.

Sirius Group

The uppermost stratigraphic bedrock unit in Beacon Valley is the Sirius Group, a small outcrop of tillite (0.6 km²) located at 2800 m on the north flank of Mount Feather. This deposit contains clasts of Beacon Supergroup sedimentary rocks, Ferrar Dolerite, and basement granitic rocks that are supported by a greyish-green matrix of fine-grained sediment. Paleoglacial flow indicators in this deposit include long axis orientations of clasts in the tillite and striations found on a pavement underlying the deposit. The striations imply ice flow over this area trending 145°-335° (Brady and McKelvey, 1979.)

IV. METHODS

Field Methods

Fieldwork was conducted during the 1998-99 austral summer. A preliminary map of the field area was made using aerial photographs prior to and during the field season. Detailed fieldwork focused on upper Beacon Valley and on Mullins Valley, a tributary to Beacon Valley. Specific excavation sites were targeted in an attempt to characterize the surficial deposits on a debris-covered glacier. Excavations of surficial deposits were dug by hand, using a pick and shovel. Twenty major excavations were conducted to describe the surficial deposits in the field area. A minimum volume of one cubic meter of sediment was excavated at all but one site. The 20 large excavations were used for the purpose of studying stratigraphic and sedimentologic characteristics of surficial deposits, as well as for sampling sediment and buried ice. Forty-two smaller pits were dug in a systematic fashion in the field area during a survey of polygons. The polygon survey afforded additional data about sediment thickness and stratigraphy overlying the buried ice in the field area.

Detailed notes about sediment characteristics and stratigraphy were taken during excavation. Pits were photographed and sampled. All sediment samples were sieved at -4 phi in the field to separate material smaller than granules from clasts that were greater than 8 mm in diameter. An attempt was made to collect at least 50 clasts from each sediment sample for weathering analysis in the laboratory. Volcanic ashes found on the surface or in an excavation pit were carefully sampled using a trowel. Morphology of ash stringers and wedges were noted, and preliminary textural analysis of ash grains were

conducted in the field using a 10x power hand lens to determine the viability of collecting an ash sample for isotopic dating.

Multiple bulk samples of buried ice were collected at 10 excavations for $\delta^{18}\text{O}$ and sediment-content analyses. In addition, at nine sites ice was collected as intact blocks for fabric analysis. Ice fabric blocks were oriented with a large arrow etched into the top of the block, corresponding to true north. Ice-cemented sand wedges were sampled at many excavation sites for $\delta^{18}\text{O}$ and sediment analyses. All samples containing ice were collected using an ice ax. At two sites, cores of buried ice were taken using a Snow, Ice, and Permafrost Research Equipment (SIPRE) auger. Modern snow from perennial snowbanks was collected for $\delta^{18}\text{O}$ analyses to be used as a comparison to buried ice.

At 42 additional sites in the field area, physical characteristics of patterned ground were measured. The resulting data were used to create maps of the distribution of patterned ground. Polygon length, width, and relief (the distance from the top of a polygon to the bottom of the contraction crack bordering it) were measured using a 50 m tape. Trenches bordering the polygons were also surveyed at each locality. Trench angles were measured with a Brunton pocket transit. Trench width was also measured using a 50 m tape. The size of the largest boulder at each site was recorded, as was the relative degree to which surface sediment was sorted. All sites were photographed with an 85 cm ice ax for scale, so sites could be compared in side-by-side photographs at a later date.

Numerous transects through the field area were conducted to collect surface samples of Ferrar Dolerite, to be used at a later time for cosmogenic exposure age dating. Surface samples were photographed, and latitude and longitude was recorded at each

collection site using a Garmin Global Positioning System. For the purpose of determining time of exposure to direct sunlight at each site, angles to the horizon were shot at the eight major azimuths of the compass using a Brunton pocket transit. The top and bottom of each sample, along with the sample number, were labeled with a permanent marker on the surface of the sample collected. The position of each sample site was recorded on an aerial photograph of the field area.

Laboratory Methods

Laboratory methods include sediment grain-size analyses of fine-gravel, sand and mud, lithology and surface texture description of gravel ($<4\phi$). Sediment sampled from excavations was segregated into gravel, sand, and mud fractions by wet sieving, using deionized water and a dispersant (0.5% Calgon). Gravel was separated at 0.5 ϕ intervals using sieves and a mechanized shaker. Sand and mud fractions were desalted using deionized water. The sand fraction of samples was analyzed at 0.25 ϕ intervals using the University of Maine Rapid Sediment Analyzer Operating System. The mud fraction of samples was analyzed through the use of a Micromeritics 5000ET Sedigraph.

At least 50 clasts from each hand-dug excavation that contained gravel were analyzed for lithology, grain shape, and various surface textures used to assess the degree to which a deposit was weathered. Using a binocular microscope at the Boston University geomorphology laboratory, volcanic ashes were sampled for crystals to be used in $^{40}\text{Ar}/^{39}\text{Ar}$ total fusion dating by Adam Lewis, Eric Moore and Jane Willenbring.

V. RESULTS

The first part of this section contains details and results of the mapping project that was conducted on the debris-covered glacier contained in upper Beacon and Mullins Valley. The morphology of the polygons and the surrounding trenches are described here. The data for all measurements taken can be found in Appendix B.

The second part of this section affords descriptions of type localities in the field area that highlight important stratigraphy in this study. The description of the stratigraphy for each excavation focuses on the surficial sediments mantling the buried ice. Also contained here are description of other unique features contained in excavations that are related to the stratigraphy, such as debris bands in buried ice, ice cemented sediments, ice-cemented sand and volcanic ash wedges. Brief descriptions and classification of all stratigraphic units seen in the field can be found in Appendix D. Locations of all excavations can be found in Appendix C, Map 1.

The third part of this section focuses on the sedimentology of the stratigraphic units recognized in the field. Described in this section are sedimentological characteristics such as sorting, weathering, texture, and lithologic composition. Grain-size and other statistical data pertaining to the sampled stratigraphy in these excavations can be found in Appendix A.

Morphology of Polygons

The physical characteristics of the polygon centers and the trenches separating them vary widely across the debris-covered glacier surface. The measurable physical dimensions of these landforms (**Figure 9**) include polygon area (mean length and mean width of the landform) and polygon relief. Measurable characteristics of the surficial sediments contained in a polygon include the sediment thickness overlying the buried ice, the sorting of the sedimentary cover on a polygon surface and the maximum boulder size (largest surface clast) on a polygon surface.

Physical characteristics of the trenches bordering a polygon include the distance between upper surfaces of adjacent polygons (trench width), the slope angle into the trench and sorting of boulders contained in trenches. All of the aforementioned characteristics were measured at 42 sites across the surface of the debris-covered glacier and at selected excavation localities contained in Mullins/Beacon Valley (Map 2, Appendix C.)

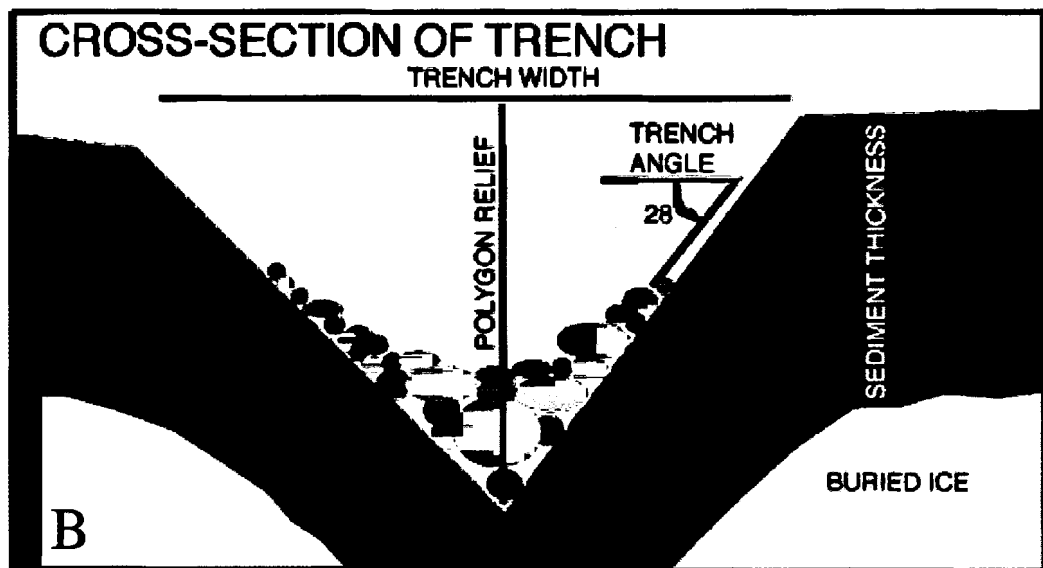
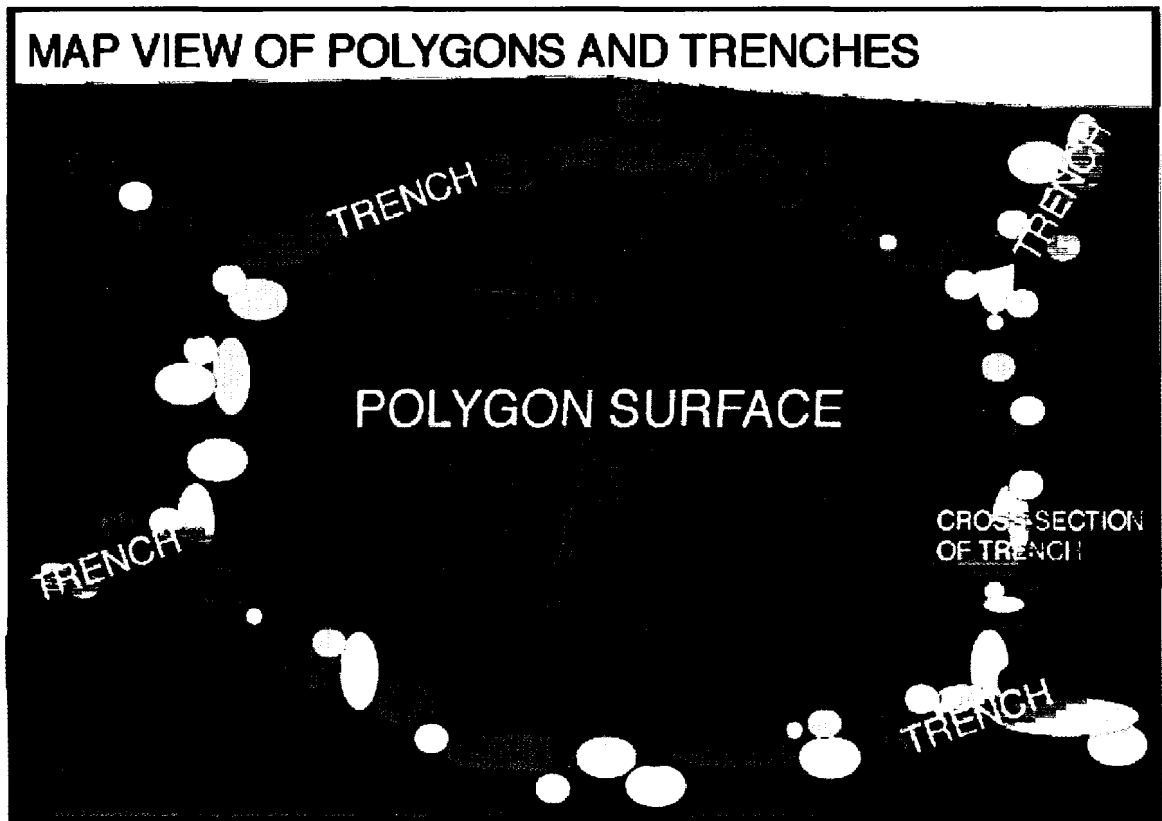


Figure 9 - Map view (A) and cross-section (B) of polygonal landform and bordering trench depicting where measurements of physical and sedimentological characteristics of polygons and associated trenches were taken.

All characteristics of polygons and the trenches bordering them were measured at 42 individual localities on the debris-covered glacier surface in Mullins and upper Beacon Valley. At each local, one polygon was surveyed out of a group of polygonal landforms that appeared to have similar traits (Figure 9). All measurements taken at each site can be found in Appendix B. Sediment thickness was measured vertically, from the surface of a polygonal landform to the surface of the buried ice within that landform. Most vertical profiles of sediment thickness could be measured effectively at the junction of the polygon surface and the upper edge of the trench that bordered an individual polygon. Polygon area was measured using the lengths of the long and short axes of a polygon surface. Determination of the long and short axes of a landform was a simple task when there was an obvious asymmetry to the polygonal landform. In the case of polygonal landforms that were nearly symmetrical, length and width measurements were taken across the surface of the polygon and normal to one another.

The polygons and the trenches bordering them were zoned both across and along the length of the debris-covered glacier surface (Figure 10A-E). The somewhat systematic survey of physical characteristics of polygons and trenches has highlighted the existence of a unique distribution for all of the measured polygon characteristics throughout Mullins and Beacon Valley. These characteristics appear to be related to the areal position of an individual polygon within the ablation zone of a debris-covered glacier.

Sediment thickness of the debris-covered glacier mantle increased from less than one cm depth to buried ice at the head of Mullins Valley to greater than 50 cm depth to

buried ice in upper Beacon Valley (**Figure 10A**). Polygon surface area was observed to increase along the longitudinal axis of the debris-covered glacier, from landforms having a radius of less than two meters, close to the head of the debris-covered glacier in Mullins Valley, to greater than 50 m on the floor of upper Beacon Valley (**Figure 10B**). Polygon relief was nearly non-existent at the head of the debris-covered glacier in Mullins Valley; however, relief of individual landforms increased downvalley to greater than 4.5 m for some of the more massive polygonal landforms (**Figure 10C**). Trench angle was also nearly nonexistent at the head of the debris-covered glacier in Mullins Valley, but increased to greater than 32° in upper Beacon Valley (**Figure 10D**). Trench width increased from 40 cm to greater than four m across in upper Beacon Valley (**Figure 10E**).

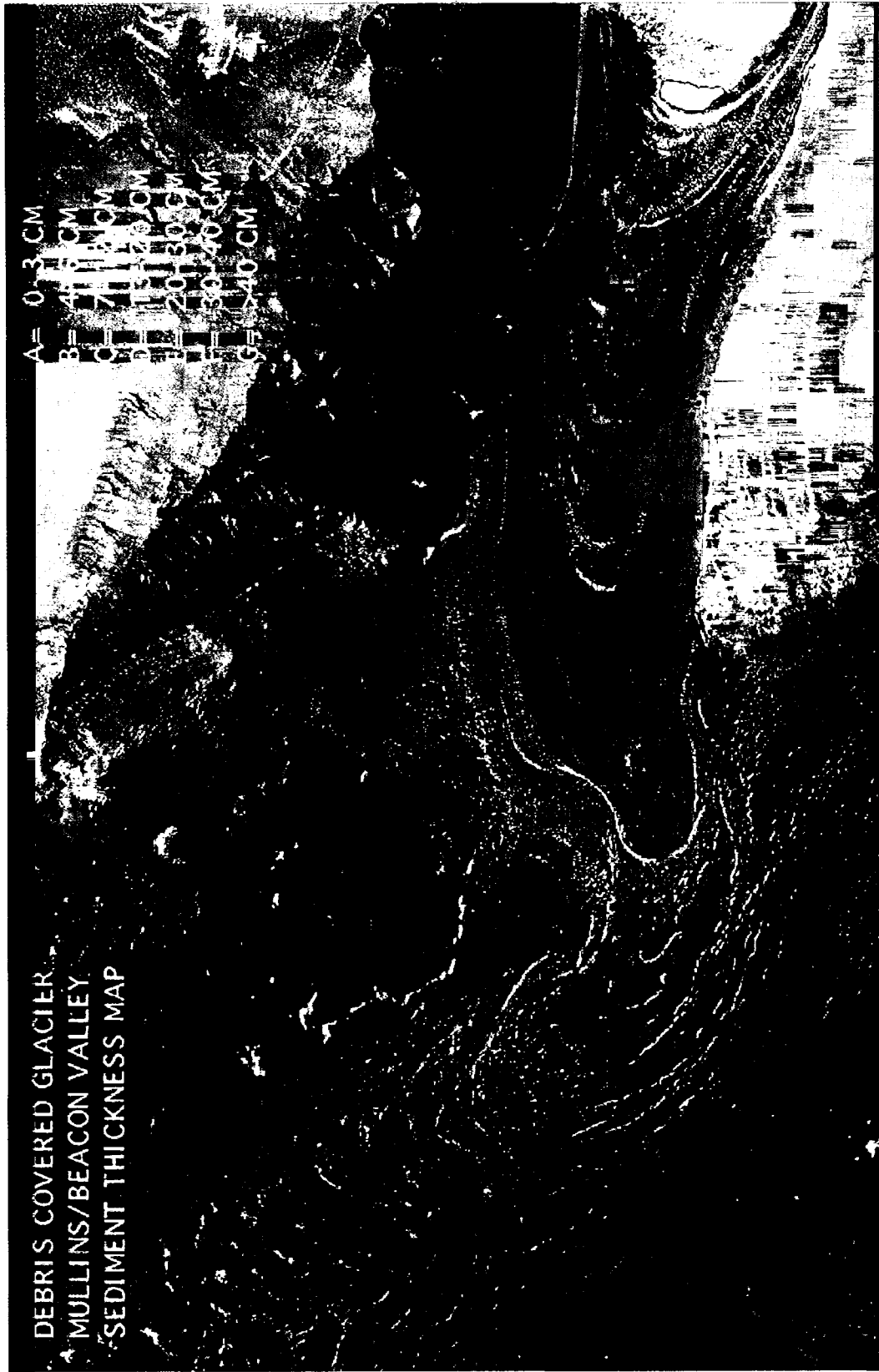


Figure 10- Aerial Photograph of Beacon and Mullins Valley
 A) Zones of sediment thickness on the debris-covered glacier surface Beacon/ Mullins Valley, Antarctica. Base map from vertical aerial photograph TMA 3079, #297/TMA-3081#147. Height 15500'.

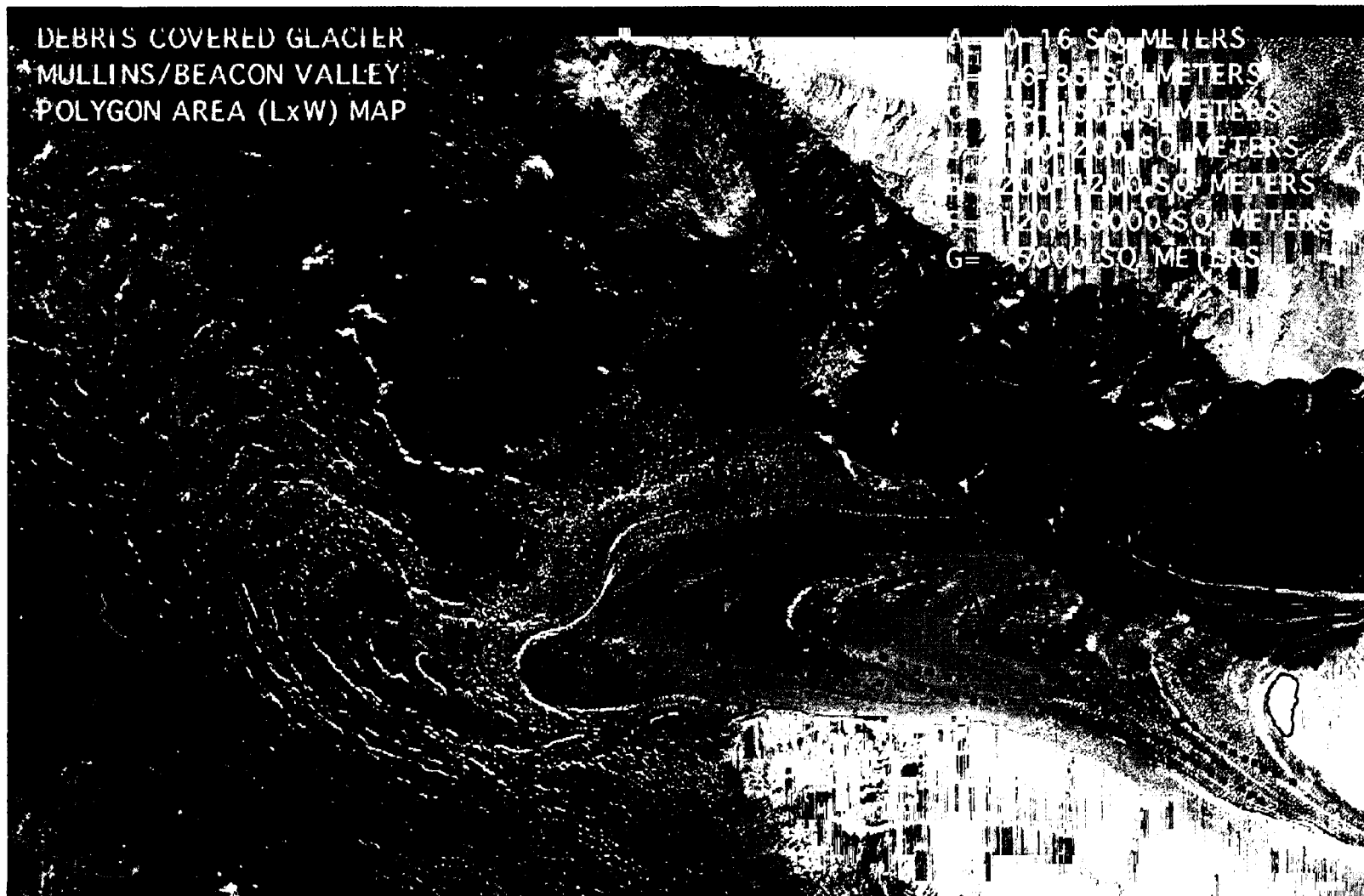


Figure 10- Aerial Photograph of Beacon and Mullins Valley

B)- Aerial photograph with zones of polygon area on the debris-covered glacier surface Beacon/ Mullins Valley, Antarctica. Base map from vertical aerial photograph TMA 3079, #297/TMA-3081#147. Height 15500'.

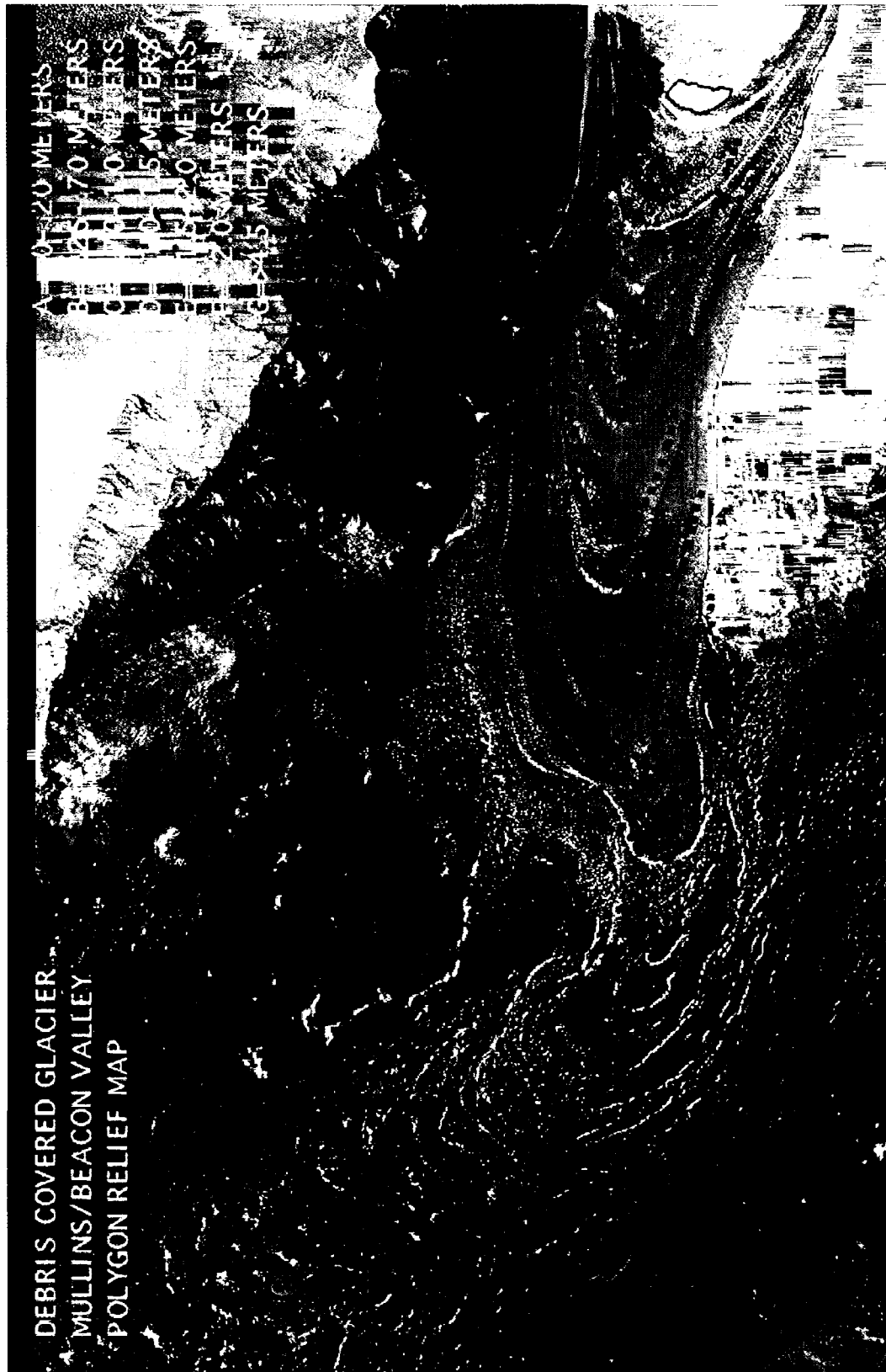


Figure 10- Aerial Photograph of Beacon and Mullins Valley
C)- Aerial photograph with zones of polygon relief on the debris-covered glacier surface Beacon/ Mullins Valley, Antarctica. Base map from vertical aerial photograph TMA 3079, #297/TMA-3081#147. Height 15500'.

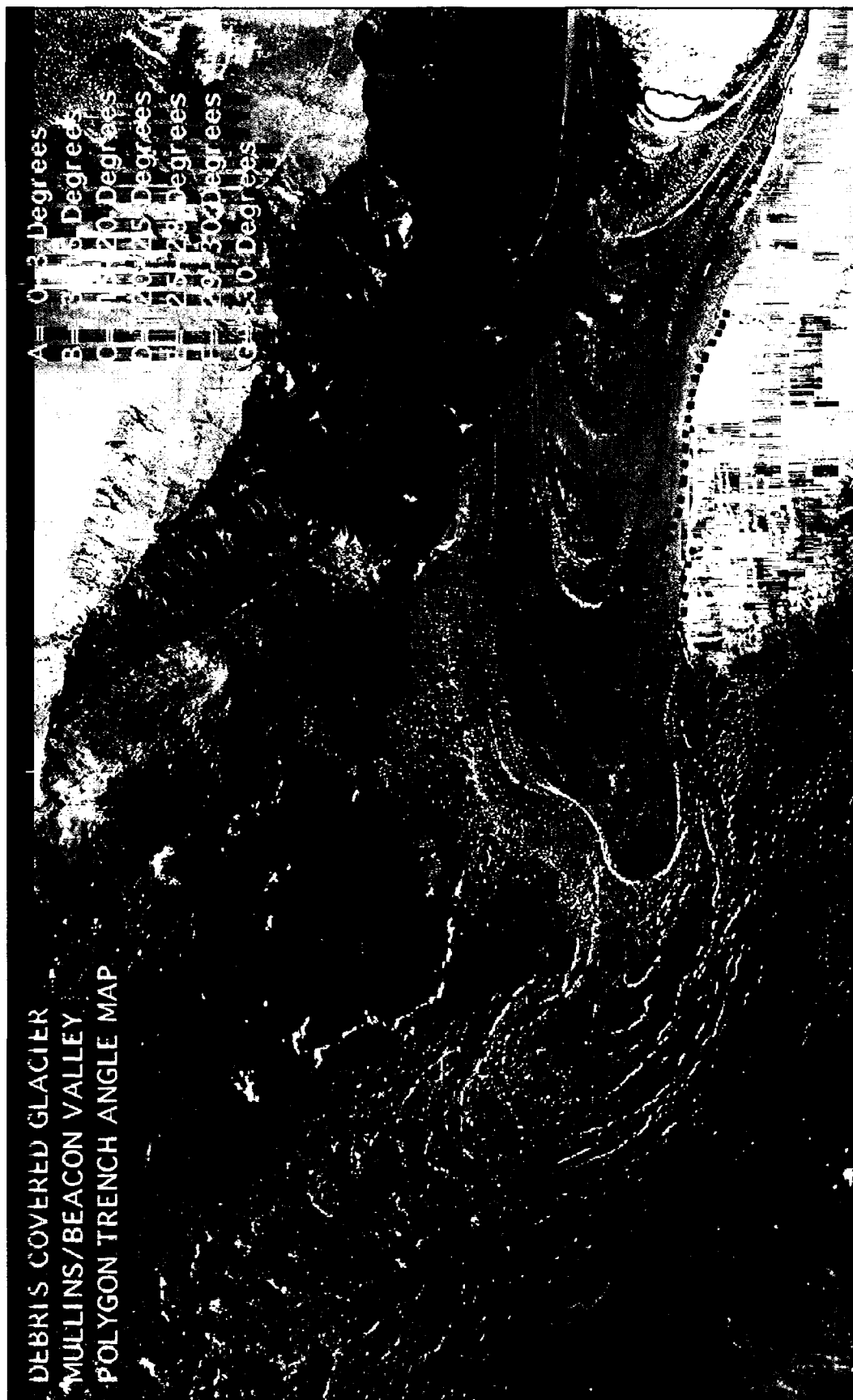


Figure 10- Aerial Photograph of Beacon and Mullins Valley

D) - Aerial photograph with zones of polygon trench angle on the debris-covered glacier surface Beacon/ Mullins Valley, Antarctica. Base map from vertical aerial photograph TMA 3079, #297/TMA-3081#147. Height 15500'.

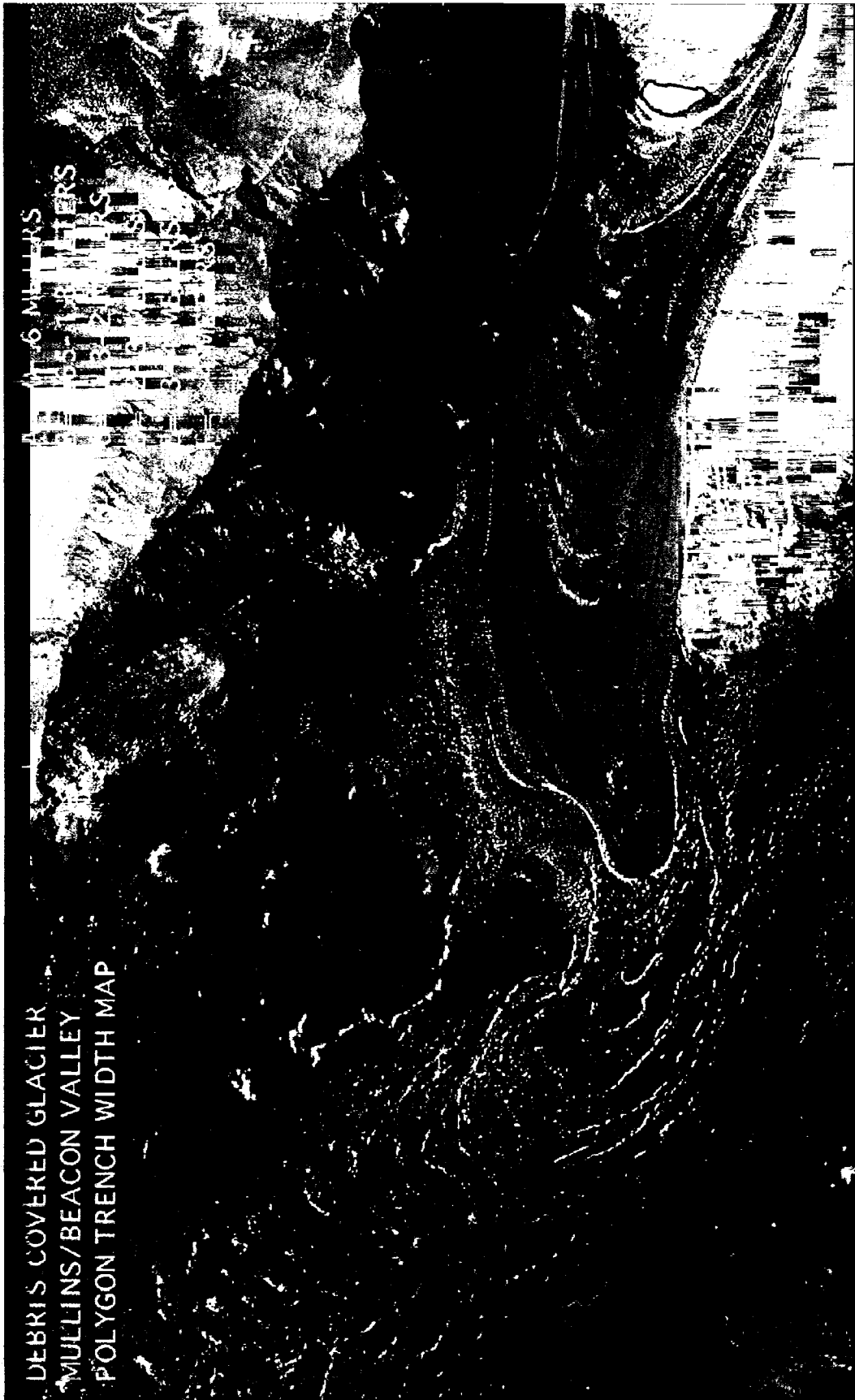


Figure 10- Aerial Photograph of Beacon and Mullins Valley

E)- Aerial photograph with zones of polygon trench width on the debris-covered glacier surface Beacon/ Mullins Valley, Antarctica. Base map from vertical aerial photograph TMA 3079, #297/TMA-3081#147. Height 15500'.

Stratigraphy in Excavations

Excavation DLE 98-004

This excavation was undertaken into the side of a polygon at 77.88523 °S latitude, 160.54528 °E longitude. This particular polygon had a length and width of 10 m, and a relief of 1.75 m. The surrounding crack width did not exceed one m at this site.

Sediments and Stratigraphy

The southeast wall of the excavation (**Figure 11A**) contained interbedded quartz and dolerite sand layers (DLE 98-004A). The interbedded sands were inclined, and had an apparent dip of approximately 18° to the northeast. Individual beds widened toward the bottom of the pit. Contacts between individual, successive beds were diffuse and some were hard to recognize (**Figure 11B**). A tangential relationship between beds of quartz and dolerite sands and the floor of the excavation was not established because bedding was not well preserved toward the bottom of the exposure. Ice-cemented sand and fine-gravel capped the buried ice in this pit. The ice-cemented sand was concentrated in a pinnacle on the highest point on the floor of the excavation. A 10 cm exposure from the top of the excavation to the buried ice surface was sampled on the northeast exposure of the excavation for sedimentological analysis. Two units were sampled, from 0-6 cm and 6-10 cm. These units were distinguished in the field on the basis of increased oxidization at depth. Sediments at 0-6 cm depth had a composition of



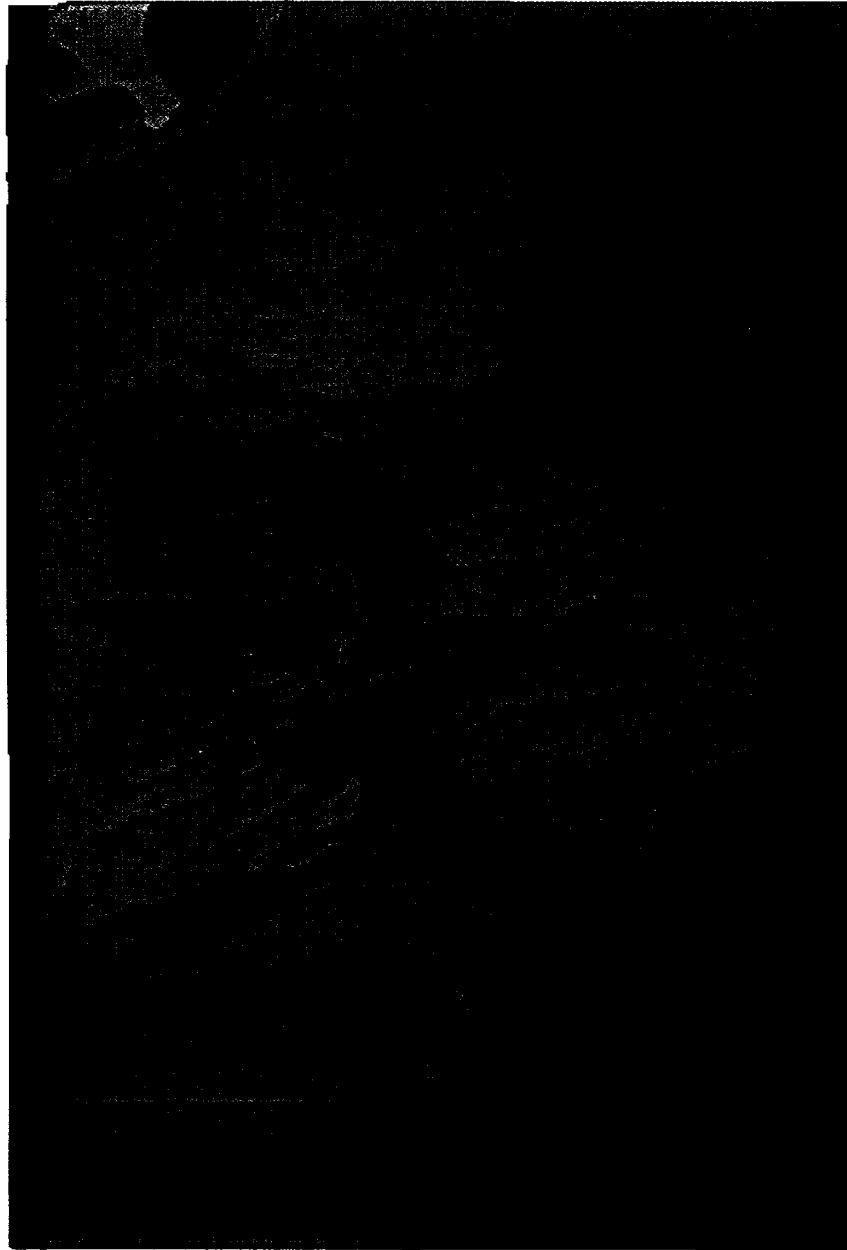
Figure 11 Excavation DLE 98-004

A) This photograph shows the southeast wall of excavation DLE 98-004. Visible above the camera lens cap (five cm diameter) are inclined beds of oxidized quartz and dolerite sand.

NE

DLE 98-004A

SW



<p>Latitude S 77.88523 Longitude E 160.54528</p> <ul style="list-style-type: none"> Weathered Sands Dolerite Sands Mixed Quartz and Dolerite Sand	<p>Samples Analyzed</p> <p>A DLS 98-004A</p>
--	--

Figure 11 Excavation DLE 98-004

B) An illustration of the southeast wall of excavation DLE 98-004 containing the inclined beds of oxidized quartz and dolerite sand. The letter "A" marks where sediment was sampled.

77% sand, 16% gravel and 7% mud (sample DLS 98-004 0-6). Sediments at slightly greater depth, 6-10 cm in this pit, had a composition of 87% sand, 7% gravel, and 6% mud (sample DLS 98-004 6-10).

Buried Ice

The buried ice at this locality contains only a few dispersed sand grains.

Debris Bands

Bands of dispersed sand were oriented in a crude, planar fashion in the buried ice. Two dolerite gravel clasts protruded from the ice. The long axis of both clasts were oriented up valley. A flat, planar surface on a large dolerite clast that was emerging from the buried provided a surface to measure the orientation of the protruding clast. The dip measurement along the long axis of this dolerite clast was 27° up valley. This orientation appeared to be similar for smaller debris bands in composed of dispersed sand grains in the buried ice.

Stratigraphic Interpretation

The stratigraphic unit seen in the surficial material overlying the buried ice in excavation DLE 98-004 is classified as a relict sand wedge. The repetitive geometry of the bedding indicates that sand had collapsed into an open ice-cemented sand wedge multiple times. The bedded quartz and dolerite sand preserved in the center of the polygon thickens toward the present ice surface. The thick part of each bed is interpreted as the former top of a contraction crack deposit. The entire sequence of sand wedge

sediment in this pit has been turned on its side, probably due to slumping caused from sublimation of the buried ice.

Excavation DLE 98-005

A linear excavation approximately two m long by 1.5 m wide by one m deep was made into the side of a polygon at 77.88364 °S latitude, 160.53825 °E longitude. This particular polygon was eight m long by 3.5 m wide, with a relief of 1.1 m. This polygon was similar in size to the other polygons in the immediate area. The width of the trench bordering this polygon was two m. The surface of this polygon and others surrounding it displayed relict networks of boulders and cobbles connected in polygonal patterns. Networks of relict polygons encompassed flat areas on the polygon surface that contained surficial sediment composed of sand and fine-gravel (**Figure 12**). The excavation into the surficial sediment also uncovered a small stringer of disseminated volcanic ash that was sampled.

Sediments and Stratigraphy

The buried ice at this locality was covered with a 50 cm layer of sandy dolerite grus containing very few clasts larger than granules. The sand component of the grus had a blackish hue. This unit was sorted to 84% sand, 12% gravel, and 4% mud (sample DLS 98-005 A). Some of the sand grains in the grus were composed of pyroxene. An upper layer of dolerite and sandstone boulders capped the sandy dolerite grus.

Buried ice

The buried ice appeared to be relatively free of sand-sized debris, with the exception of one angular pebble of dolerite protruding from the ice surface. A depression

ring having a radius of five cm surrounded the angular dolerite clast that had emerged from the buried ice. The depression ring gradually

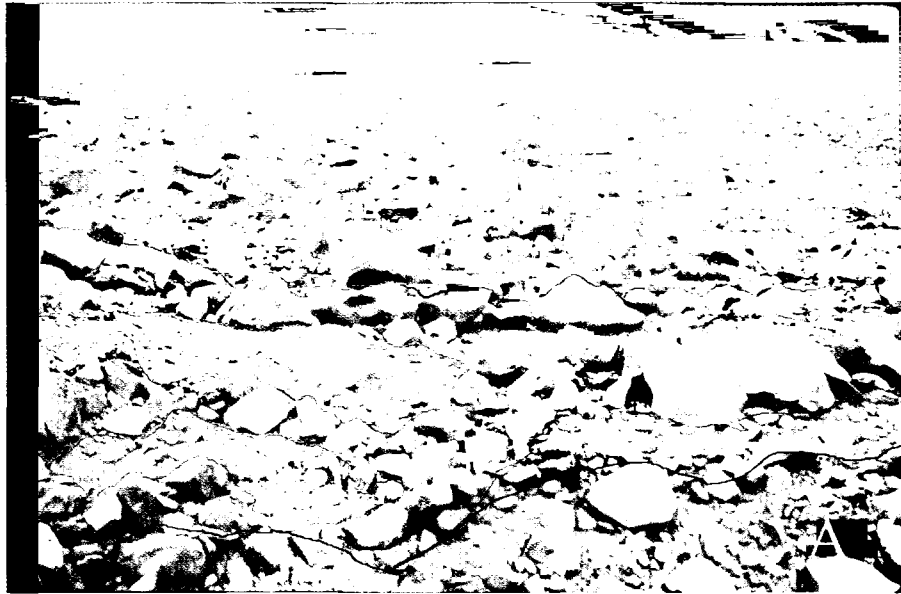


Figure 12- Relict polygon nets

Pictured here (outlined in magenta) are examples of relict polygon nets. Notice that the relict nets are distinguishable from the central polygon plateau on the basis of grain-size. The blue line in the upper picture marks the edge of an active polygon trench. The upper picture was taken in central Beacon Valley (map site LL, Appendix C) the lower picture in Mullins Valley (map site CC, Appendix C). The ice axe in both pictures is 85 cm long.

increased at depth around the dolerite clast, and was approximately two cm deep at its lowest point. Small, boil-like topographic undulations (1-1.5 cm high and 2-2.5 cm in diameter) are dispersed on the buried ice surface. The surface colors of the ice in this excavation varied from white, that was almost exclusively free of debris to a blue-gray, that contained fewer bubbles, and had sand grains and sand stringer inclusions. The topographically highest point on the floor of the pit was a wide pinnacle of buried ice capped by a layer of ice-cemented sand 6 cm thick.

Debris Bands

The dominant feature in this excavation is an ice-cemented sand wedge that penetrated to an unknown depth in the buried ice (**Figure 13A and 13B**). This large sand wedge had multiple folds and kinks. Additional, smaller debris bands flanked the large sand wedge. The smaller bands followed the fold geometry of the large ice-cemented sand wedge in the floor of the excavation. A cross section of the ice cemented sand wedge and surrounding ice exposed slight variations in ice texture and sediment concentration (**Figure 14A and 14B**) with increasing distance from the ice-cemented sand wedge. The white and bubbly ice on the outermost portions of the excavation floor was less brittle and contained fewer sand grains than the blue-gray ice that was found next to the large, ice-cemented sand wedge. In addition, the blue-gray ice contained multiple, small sand stringer pods that were vertically oriented and slightly curved to depth.



Figure 13- Excavation DLE 98-005

A) This photograph depicts the floor of excavation DLE 98-005. Contained in the buried ice in this pit is a large, ice-cemented sand wedge that appears to have been slightly folded. The cloth tape measure on the floor of the pit is 1 m long.

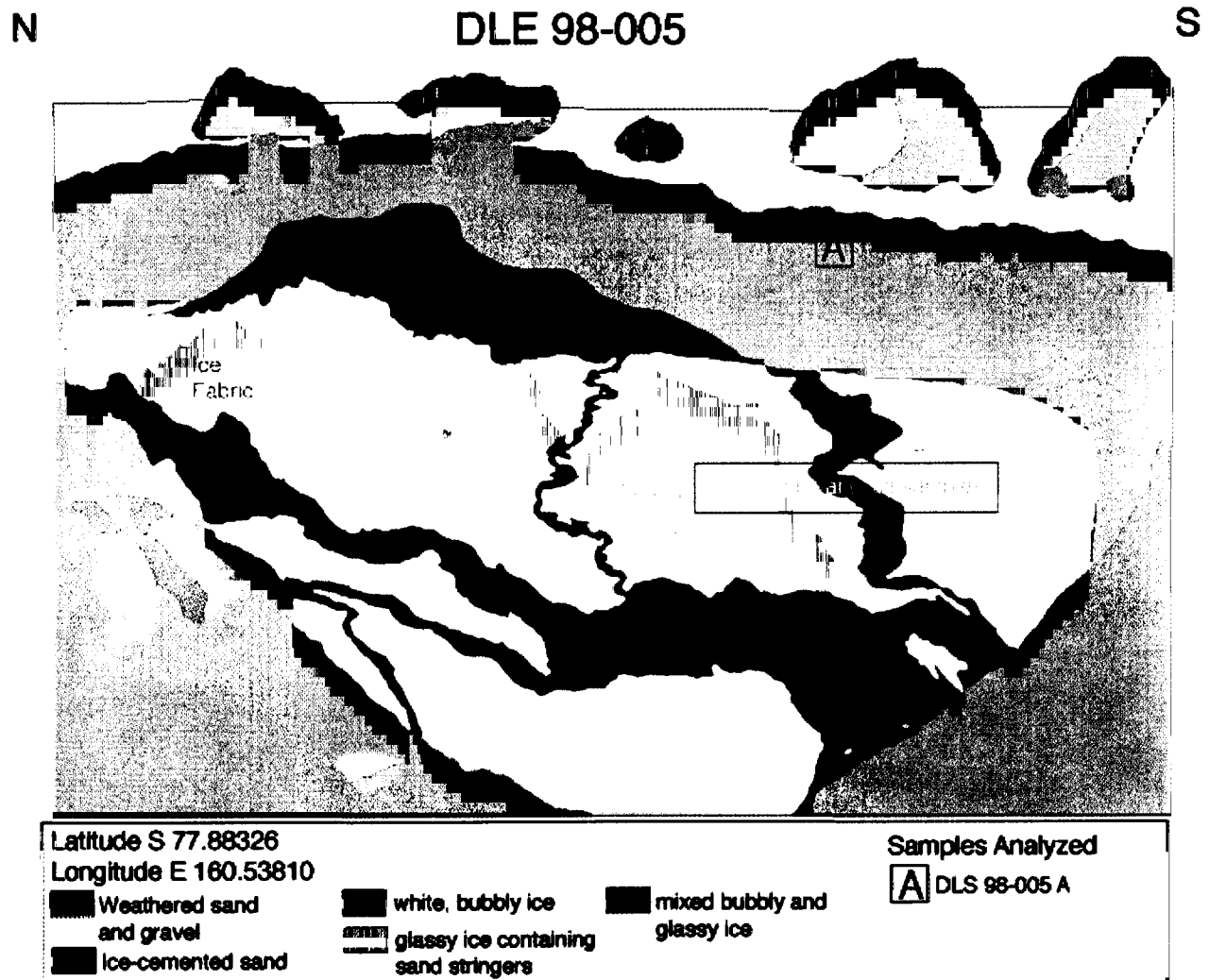


Figure 13- Excavation DLE 98-005

B) Illustration of excavation DLE 98-005. The letter "A" marks where sediment sample DLS 98-005 A was taken. Figure 9A illustrates a cross section where ice cement and ice samples were taken.

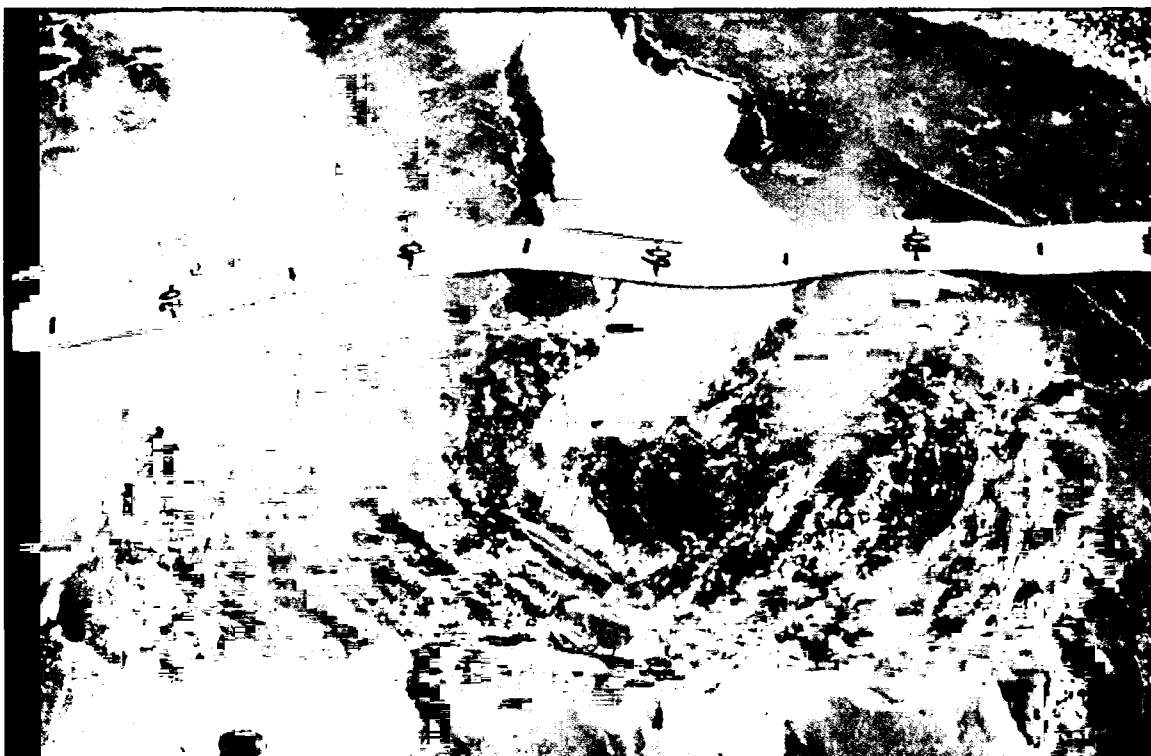


Figure 14- Cross-section through an ice-cemented sand wedge

A) This photograph shows a cross-section (DLE 98-005X) of the ice-cemented sand wedge and debris bands contained in the buried ice in excavation DLE 98-005. The scale on the cloth measuring tape is in centimeters.

Stratigraphic Interpretation

The ice-cemented sand wedge (sample DLI 98 005X D) in the floor of the excavation is interpreted as a relict sand wedge. This wedge no longer has an active, V-shaped polygon trench over it and does not mark the edge of a polygonal landform. The massive weathered sand overlying the ice is classified as slumped sand wedge sediment. The texture and sorting of the sediment overlying the excavation (DLS 98 005 A) is indistinguishable from the sediment contained in the relict sand wedge. This surficial material was likely part of the relict sand wedge that penetrates the buried ice in this excavation, and was probably let down onto the ice surface as sublimation has progressed.

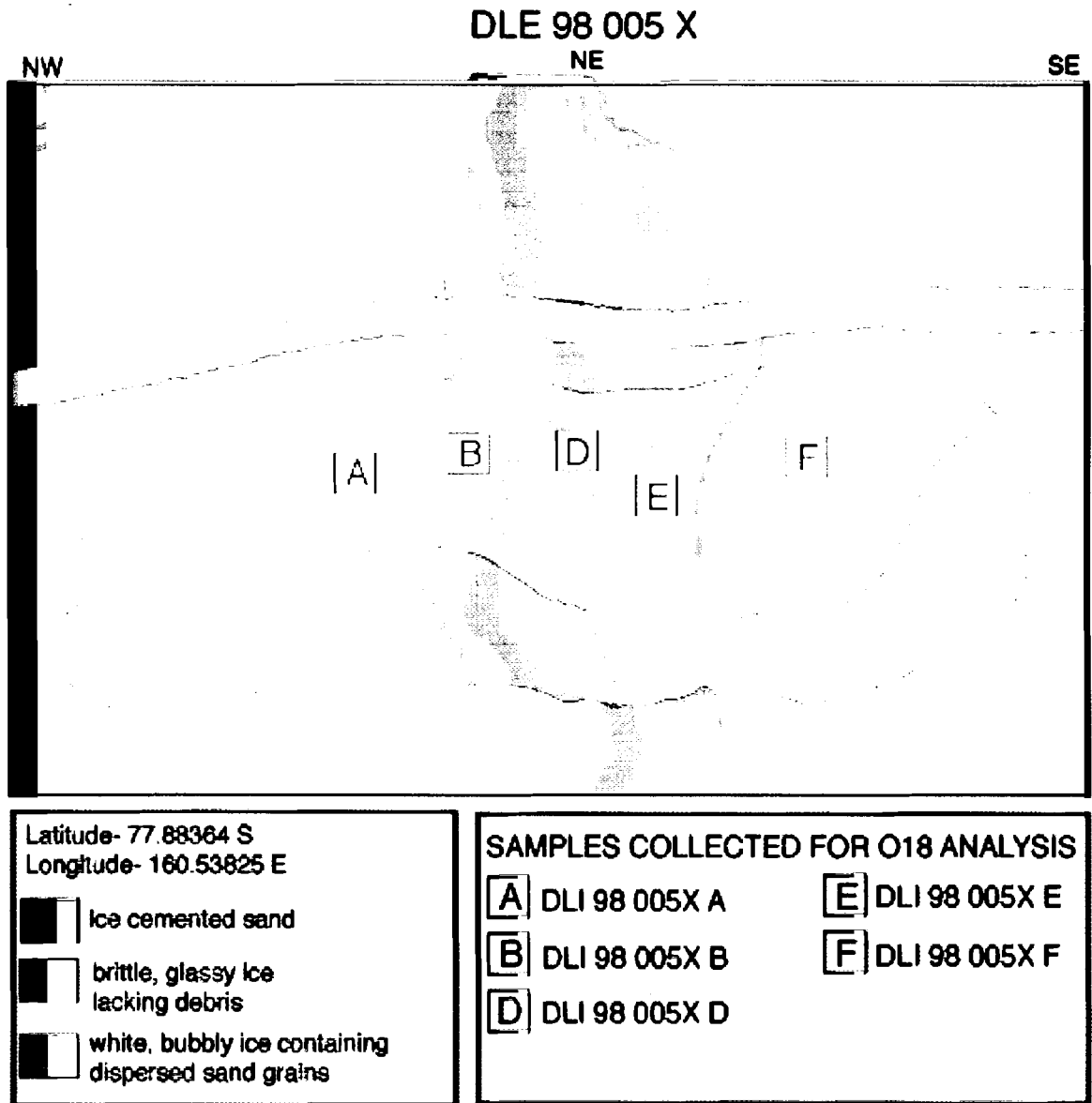


Figure 14- Cross-section through an ice-cemented sand wedge

B) Illustration of cross-section (DLE 98-005X) into the ice-cemented sand wedge on the floor of excavation DLE 98-005. The ice units in this diagram were differentiated in the field on observable debris concentration and on the degree of fissility upon removal with an ice axe. Sediment from unit DLI 98-005X D was sorted to 88% sand, 8% gravel, and 4% mud. This sediment was also texturally identical to the weathered sediment overlying the buried ice.

Excavation DLE 98-007

An excavation was undertaken into a polygon at 77.88195°S, 160.53591°E. The excavation was made into a polygon northeast of a bordering trench. Polygon relief was 1.5 m. Linear dimensions of polygon were six m by 25 m, and the long axis of the polygon was oriented perpendicular to the long axis of the valley.

Sediments and Stratigraphy

The surface layer of dolerite clasts was underlain by loose sediment with abundant dolerite sand. This layer was pervasively oxidized down to the first 2.5 cm depth. Oxidation of sediments decreased progressively to 20 cm depth. The northeast face of the excavation revealed several distinct sedimentological units, distinguished in the field on the basis of grain size. A wedge-shaped deposit of coarsening upward sediment was sampled for grain-size analysis (**Figure 15A and 15B**). The lower most unit (DLS 98-007D), directly overlying buried ice, was primarily composed of sand, although it contained some granules. This unit was sorted to 84% sand, 9% gravel and 7% mud. The unit overlying DLS 98-007D was crudely bedded. This particular unit (DLS 98-007C) was sorted to 65% sand, 30% gravel and 5% mud. Overlying DLS 98-007C was a coarse gravel pod, composed of pebbles, cobbles and boulders of dolerite with dispersed sandstone clasts. Directly overlying this unit was a massive sand layer, composed of oxidized and weathered quartz and dolerite sand, capped by the surface layer of weathered dolerite and sandstone boulders. The massive sand layer was sorted to 92% sand, 5% gravel and 3% mud.

Buried Ice with Included Clasts

The buried ice exposed in the floor of this excavation was predominantly clear, white and bubbly. It was capped with a thin veneer of ice-cemented sand and granules. There were two larger, cobble-sized angular clasts of unweathered dolerite protruding from the buried ice surface. The long axes of both of these clasts were dipping down into the ice and were oriented parallel to the long axis of the valley.

Stratigraphic Interpretation

The stratigraphic features preserved in the center of this polygon (excavation DLE 98-007) indicate the collapse of sediment into a mature polygon trench. The entire sequence is classified as a relict polygon trench deposit. The relict polygonal net excavated in the center of this polygon was observed to have sorting and arrangement of sediments similar to those contained in active polygon trenches. Superposed, coarsening upward sedimentologic units, oriented in a V-shaped geometry, indicate widening and deposition of sediment into a growing polygon trench. The complete coarsening-upward sequence is capped by a massive weathered sand unit (sample DLS 98 007B), which indicates sand deposition into a fully mature contraction crack. The massive oxidized sand cap is likely a slumped sand wedge deposit, superposed over the relict trench deposit as sublimation of the buried ice occurred.

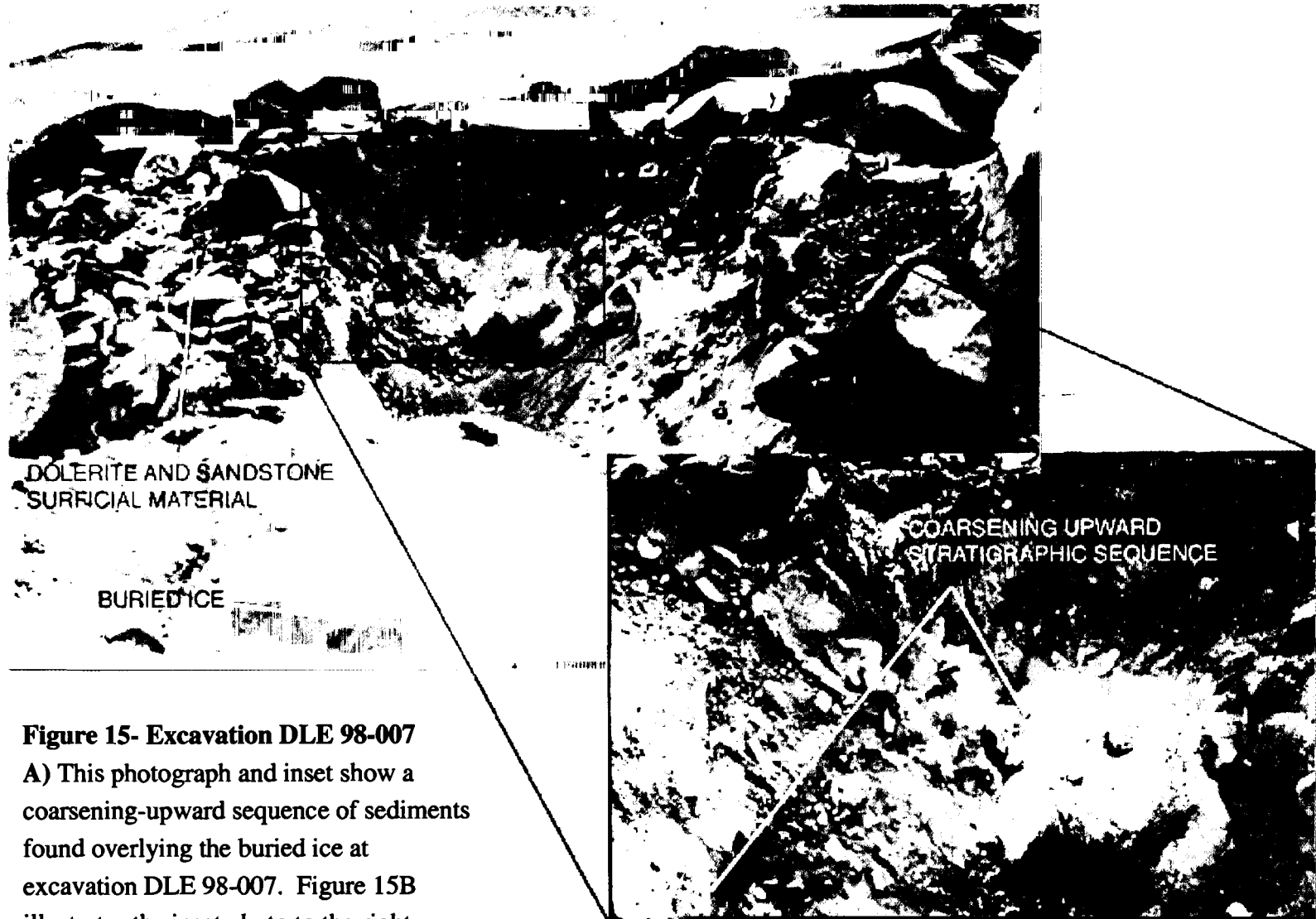


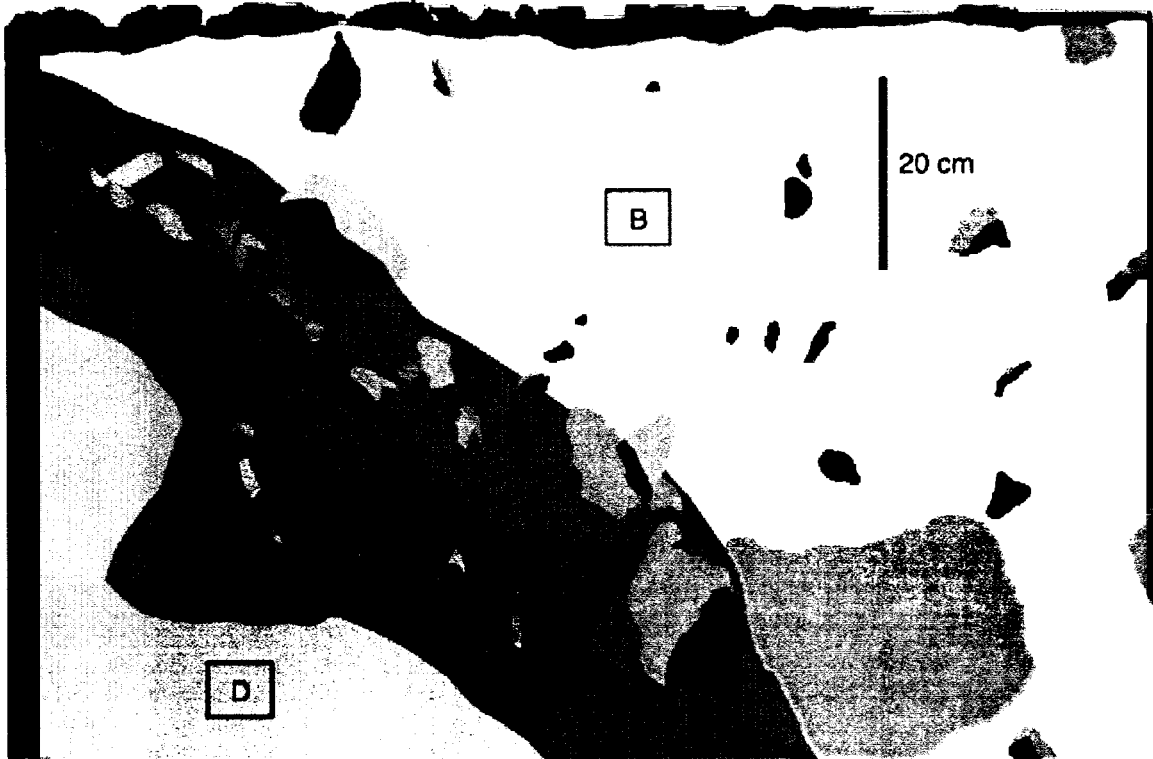
Figure 15- Excavation DLE 98-007
 A) This photograph and inset show a coarsening-upward sequence of sediments found overlying the buried ice at excavation DLE 98-007. Figure 15B illustrates the inset photo to the right.

DLE 98 007 A






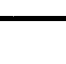
NW

NE

SW



Latitude- 77.88195 S
Longitude- 160.53591 E

-  weathered sand with dispersed fine gravel
-  oxidized sands and concentrated fine gravel
-  buried dolerite boulders
-  granules, pebbles and cobbles
-  surface dolerite boulders
-  weathered and oxidized quartz and dolerite sand

SAMPLES ANALYZED




-  DLS 98 007 B
-  DLS 98 007 C
-  DLS 98 007 D

Figure 15- Excavation DLE 98-007
B) Illustration of coarsening upward sequence of sediment found in excavation

Excavation DLE 98-010

An excavation was made into the south side of a large polygon near central Beacon Valley, 75 m northeast of 77.86795° S, 160.55689° E. A wedge of volcanic ash was uncovered and sampled (sample DLS 98-010A) near the surface of this excavation. This volcanic ash wedge penetrated into the upper four cm of the lowermost stratigraphic unit excavated in this particular excavation. The ash wedge pinched out and abruptly terminated as the northwest face of the exposure was excavated.

Sediments and Stratigraphy

The surface of this excavation was covered with dolerite pebbles, cobbles and boulders and a few sandstone clasts. Directly beneath the surface clasts were oxidized quartz and dolerite sands, commonly adhering to one another in the upper two cm, forming a highly oxidized surface crust. From two cm to 65 cm depth was a layer of massive oxidized quartz and dolerite sand that contained a few dispersed maroon siltstone granules. The oxidized and weathered sand also occurred directly next to the trench bordering the polygon and displayed some crude bedding, dipping toward the bottom of the polygon trench. The oxidized and weathered sands (sample DLS 98-010C) were sorted to 86% sand, 4% mud and 1% gravel. A sharp lower stratigraphic contact separated the massive oxidized sand unit from a gray diamicton, which continued to depth for 25 cm and terminated conformably on contact with the buried ice surface (**Figure 16A and 16B**). The gray diamicton was sorted to 22% sand, 3% mud and 76% gravel, having a high dolerite content. The dolerite clasts were angular, unoxidized and often exhibited impact blemishes on some surfaces.

Buried Ice

At this locality the buried ice was very debris rich, with numerous angular granules of dolerite. A large dolerite boulder protruded from the ice surface. This boulder was unoxidized and angular, with fresh bruises on the surface.

Stratigraphic Interpretation

In this excavation, the unweathered gray diamicton was in direct contact with the buried ice surface, draping it conformably. The sediments contained in the buried ice, as well as emerging directly from the buried ice, were observed to have the same physical characteristics of the unweathered gray diamicton, including composition, texture, sorting and degree of weathering. On this basis, I interpret the gray unweathered diamicton as a sublimation till. As sublimation occurs, this till progressively accumulates at the ice surface, and hence is added to the bottom of the overlying stratigraphic column.

Weathered quartz and dolerite sand was found directly beneath the present ground surface of weathered dolerite and sandstone gravel clasts. The weathered sand overlies the sublimation till. The weathered sand also contained a wedge of very fine-grained volcanic ash. The ash wedge, along with the surrounding weathered sediments, were likely part of a relict sand wedge deposit that slumped over the till as the buried ice surface was lowered by sublimation.



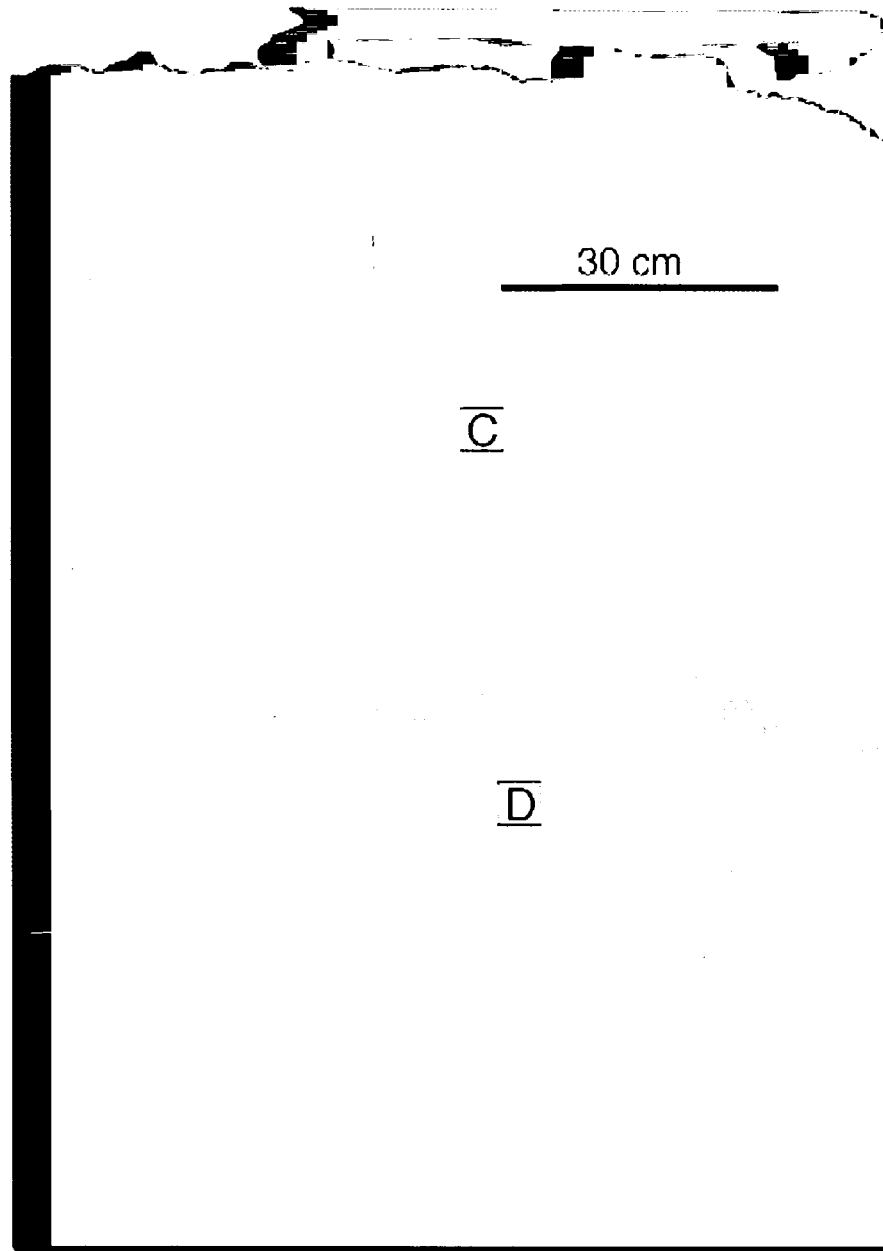
Figure 16- Excavation DLE98-010

A) This photograph shows excavation DLE 98-010. Seen in this photograph is buried ice (underlying the trowel) with emerging angular dolerite gravel. The sediment directly overlying the buried ice is unweathered, angular, and has a high gravel and mud component. This sediment is classified as a sublimation till (sample DLS 98-010D). The sediment directly under the surface cap of weathered dolerite is composed of weathered and oxidized quartz and dolerite sand, and is classified as slumped sand wedge sediment (sample DLS 98-010C)(See Figure 16B for interpretation).

W

DLE 98-010

E






Latitude S	Samples Analyzed
Longitude E	C DLS 98-010 C
 Weathered Sands	D DLS 98-010 D
 Unweathered, angular dolerite sand and gravel	
 Debris rich, buried ice	

Figure 16- Excavation DLE98-010

B) Illustration of excavation DLE 98-010. The letters in the diagram show where sediment samples were taken.

Excavation DLE 98-013

This excavation was undertaken approximately 450 m downslope from the supraglacial lake at the head of Mullins Valley. Polygon landforms were inconspicuous in this area. Individual landforms were not recognized because of sorting of coarse and fine sediments; however the polygon network of trenches were recognized by topographic depressions of about five to 10 cm that collected wind blown snow. The excavation proceeded in a fashion to remove the thin sediment cover overlying buried ice in this locality, so that the ice surface could be examined.

Sediments and Stratigraphy

The sediment mantle covering the buried ice did not exceed five cm in thickness in this excavation. The overlying sediment consisted of loose grus made up mostly of dolerite granules and pebbles. Larger dolerite boulders were dispersed across the surface at this locality. Underlying the dolerite grus cover was a thin layer of ice cemented sands with dispersed granules. The layer of ice cement overlying the buried ice appeared to be sorted by grain-size toward the bottom of the stratigraphic column, with thin layers of glassy ice containing mud-sized particles.

Buried Ice and Debris Bands

The buried ice at this local was white and bubbly. A few lenses of sand were contained in the ice. The sediments contained in the debris bands were composed entirely of rounded sand grains.

Contraction Cracks

The dominant feature of this pit was a four-cm-wide contraction crack in the buried ice (**Figure 17A**). The crack was exposed in strike section in an attempt to determine its' geometry and to see how deep it penetrated into the ice. The excavation was abandoned at a depth of 75 cm, before the bottom of the crack had been reached. However the excavation revealed a geometry that indicated the crack was terminating gradually at depth, and most likely somewhere around two meters depth into the ice.

The sediments contained in the crack exhibited a coarsening upward trend (**Figure 17B**). The sediments sampled in the deepest, narrowest portion appeared to be composed of very fine sand to silty material. The fine portion of this deposit also contained some disseminated volcanic ash. Some of the fine-grained material was adhering to the sidewalls of the contraction crack. The uppermost portion of the crack contained poorly sorted dolerite grus mixed with sediments similar to those found near the bottom.

Stratigraphic Interpretation

The contraction crack observed in the ice is classified as an active thermal contraction crack on the basis that the sediment filling the crack is not consolidated or ice-cemented. The sediment contained in the contraction crack is composed of slightly weathered sublimation till. However, the sediment from the till has been vertically sorted by grain size. I interpret the deposit in the contraction crack as a sieve deposit, derived from the overlying sublimation till and sorted as the thermal contraction crack opened.

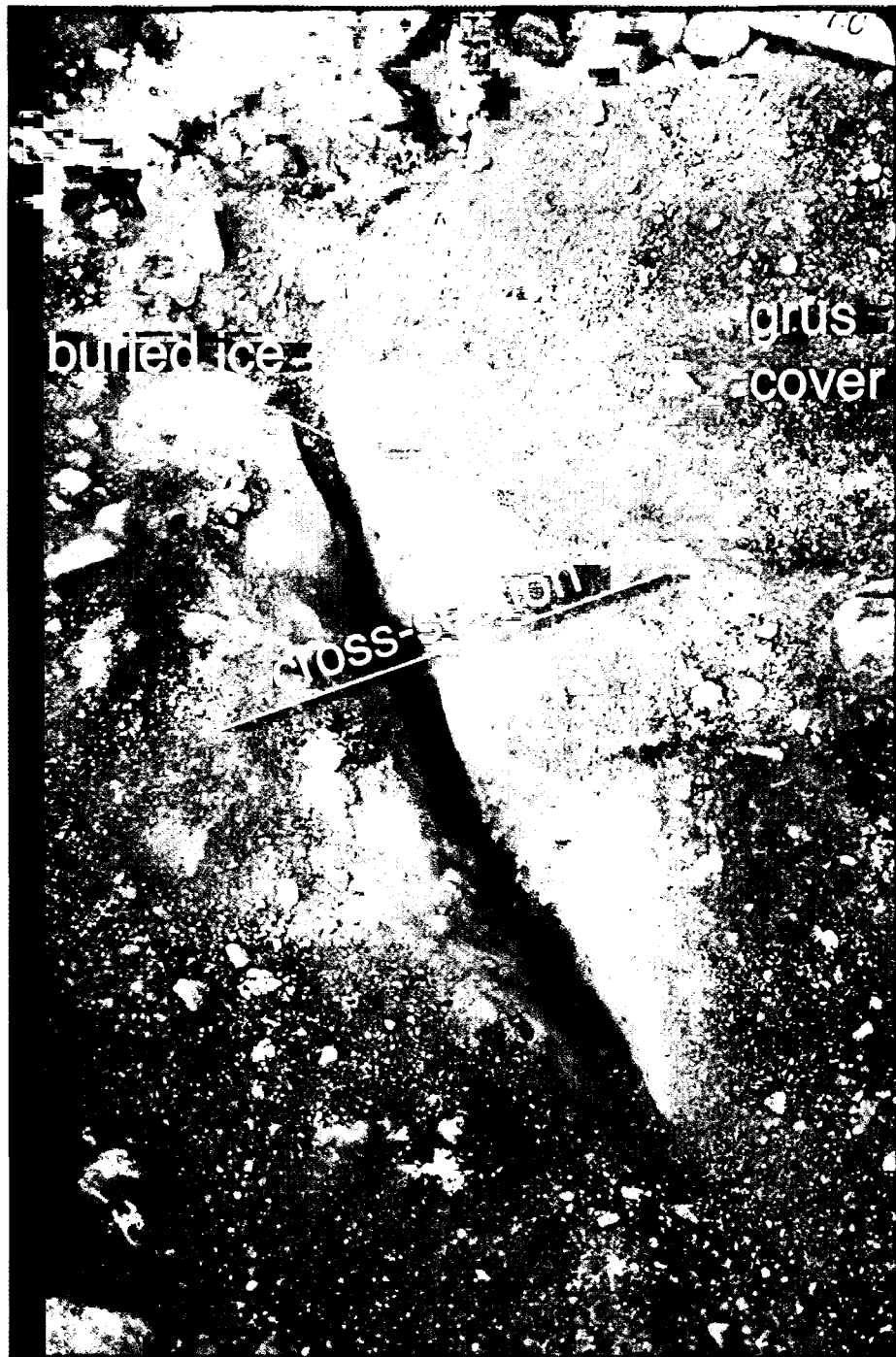


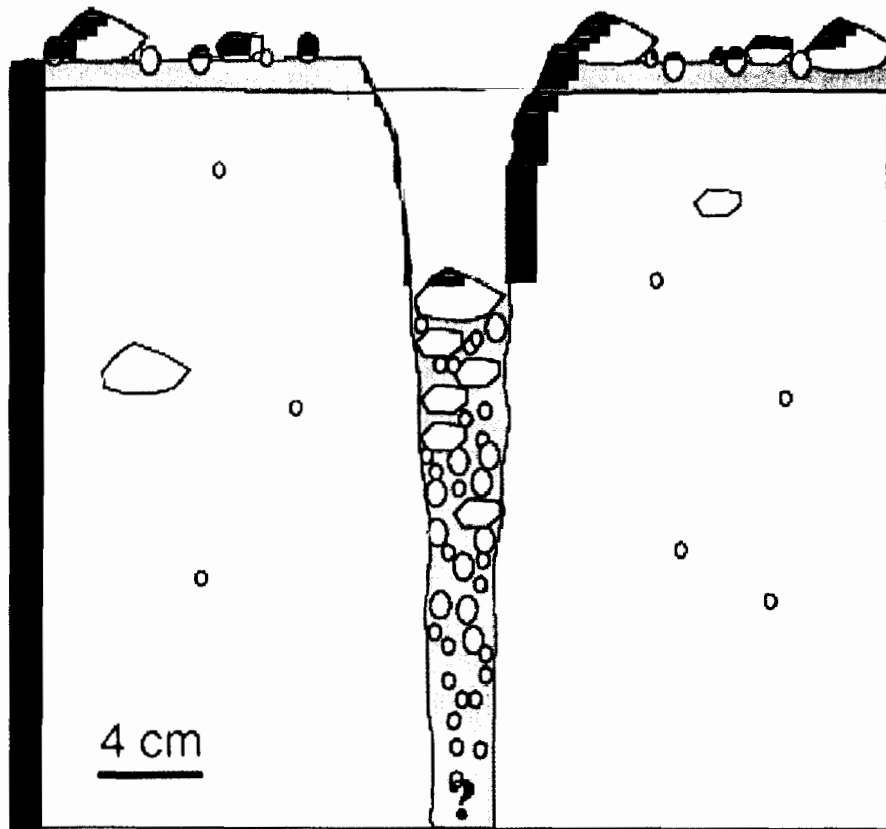
Figure 17- Excavation DLE 98-013

A) This photograph depicts a contraction crack in the buried ice found in excavation DLE 98-013. The upper 10 centimeters of the contraction crack was filled with the same dolerite grus seen overlying the buried ice surface. The grain-size of material contained in the contraction crack progressively decreased with depth.

NE

DLE 98 013

SW






-  slightly oxidized and weathered gray diamicton
-  angular and unweathered dolerite gravel
-  white, bubbly ice containing fresh, angular dolerite gravel

Figure 17- Excavation DLE 98-013

B) An illustration showing the cross-section of excavation DLE 98-013. Depicted is a thermal contraction crack that has been filled with sediment derived from the sublimation till on the buried ice surface. Notice that the upper portion of the contraction crack is not filled with sediment. The sediment in the lower parts of the crack contained disseminated volcanic ash.

Excavation DLE 98-014

This excavation was prompted by the presence of an unusually high polygonal mound standing above the mean elevation of the land surface in central Beacon Valley.

Sediments and Stratigraphy

This excavation revealed several stratigraphic units (**Figure 18A and 18B.**) The dolerite and dispersed sandstone boulder surface was directly underlain by 45 cm of oxidized and weathered quartz and dolerite sand. This sand unit was sorted to 85% sand, 7% gravel and 8% mud. The sand unit conformably terminated at 45 cm depth on contact with a different unit. Directly underlying the weathered sand unit was an unweathered gray diamicton that contained large boulder-to-pebble-sized angular dolerite clasts. This unit was sorted to 27% sand, 70% gravel and 3% mud. The unweathered gray diamicton terminated at a depth of 110 cm upon direct contact with a layer of cobble-to-boulder-sized oxidized and weathered dolerite clasts.

Buried Weathered Dolerite Clasts

A layer of interlocked weathered and oxidized dolerite clasts was exposed at a depth of 110 to 115 cm. This layer was parallel to the present-day landscape surface. The buried dolerite clasts displayed weathering characteristics similar to those of dolerite clasts found at the present-day desert surface in Beacon Valley. These characteristics included faceted sides, a high degree of oxidation, pitting, staining, and weathering rinds that were fragile and partially broken off. Of particular interest, several clasts exhibited prominent manganese oxide stains.

Directly below the buried weathered dolerite clasts was a thin layer of highly oxidized dolerite sand grains at 120 cm depth. The sand grains were cemented together to form a crude crust. Beneath this dolerite sand crust was weathered and oxidized quartz and dolerite sand unit. This unit was sorted to 53% sand, 41% gravel and 6% mud. Within this sand unit, a few pebble-sized sandstone ghosts were found. The ghosts readily crumbled into quartz sand grains. The buried weathered and oxidized sand unit was excavated to a depth of 150 cm. Buried ice was not found.

Stratigraphic Interpretation

The weathered quartz and dolerite sand unit overlying unweathered gray diamicton was superimposed on a layer of interlocked weathered dolerite gravel clasts. The clasts exhibited extensive oxidation, staining, and pitting. One clast had purple manganese oxide stains across its surface. The surface textures of the gravel in this layer are indicative of the dolerite clasts having been exposed at the surface of a polygon or in a polygon trench for some extensive period of time. At the surface, the clasts would have developed their physical characteristics from subaerial erosion. On the basis of weathering, the buried dolerite cobbles and boulders in excavation DLE 98-014 are interpreted as being constituents of a former desert pavement. The weathered state of the buried clasts suggests that they must have existed at the surface of a polygon, in a trench bordering a polygon or in both localities for an extensive period of time.

The unweathered gray diamicton (sample DLS 98-014B) superposed on the buried desert pavement is inferred to be a sublimation till. The basis of this interpretation is supported by fresh sediment that is unweathered and appears to be sorted to the same

degree as the sediment sublimating out of the buried ice at other excavations (excavation DLE 98-010). Overlying this sublimation till is a massive weathered sand unit (sample DLS 98-014C) that is interpreted as slumped sand wedge sediment. The entire stratigraphic package containing the sequence of sublimation till (sample DLS 98-014B) superposed by slumped sand wedge sediment (DLS 98-014C) was likely emplaced over the buried desert pavement by slumping as sublimation of the buried ice occurred.



Figure 18- Excavation DLE 98-014

A) A photograph of excavation DLE 98-014. The exposure of the interior of this polygon contained a complex stratigraphic package of sediment that was composed of a weathered and oxidized quartz and dolerite sand unit superposed on an unweathered, gray diamicton. The entire sequence was found to overlie an interlocked layer of oxidized, pitted and stained dolerite boulders.

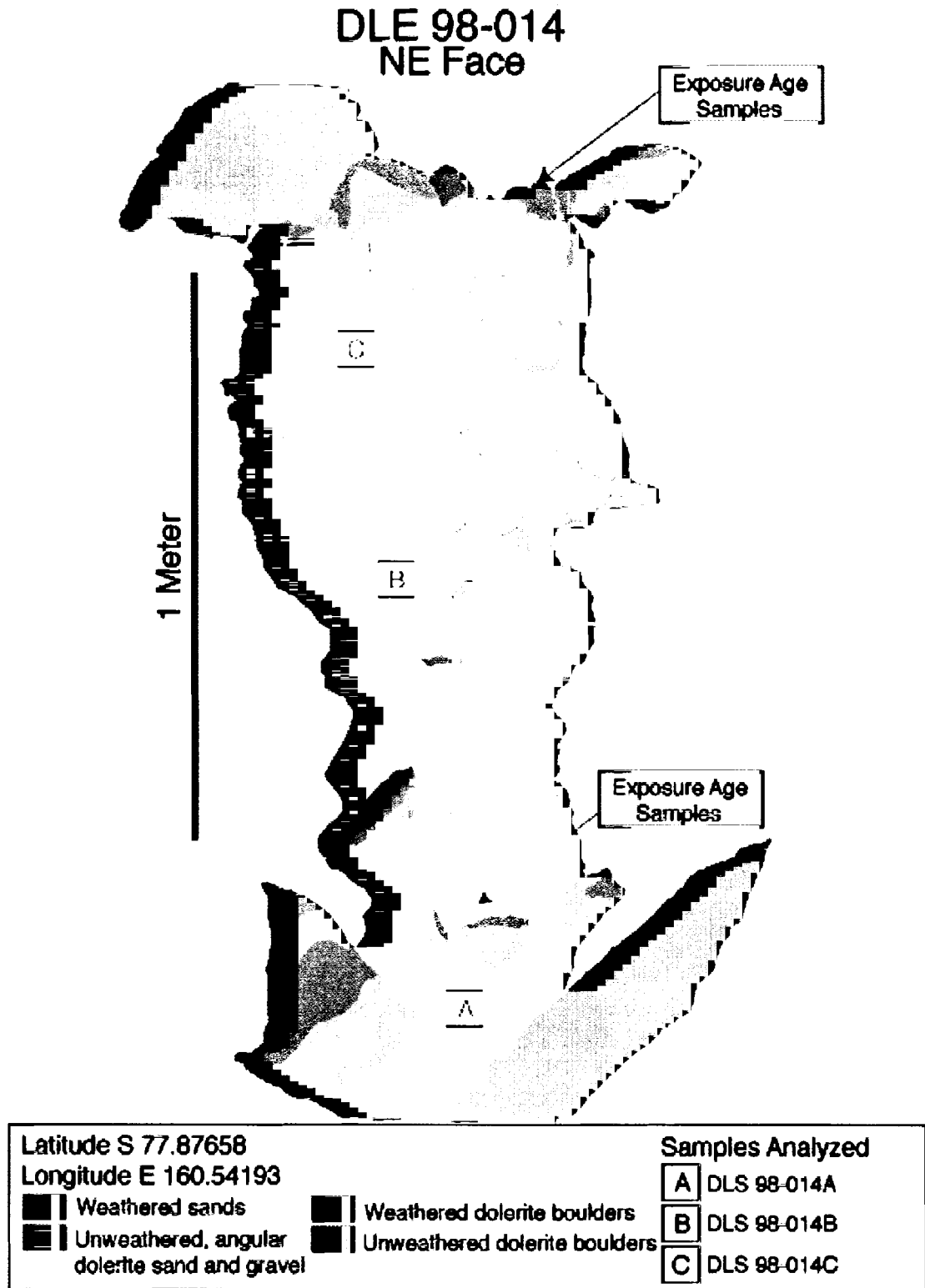


Figure 18- Excavation DLE 98-014

B) Illustration of excavation DLE 98-014. The letters mark where sediment samples were taken.

Excavation DLE 98-017

A pit was dug into the edge of a polygon at 77.87658°S latitude, 160.54193°E longitude. Polygon relief at this site was approximately 1.5 m and the slope angle from the polygon plateau to the bottom of the adjacent trench was near the angle of repose. Two sedimentary units were readily visible on the trench slope surface bordering this particular polygon.

Sediments and Stratigraphy

The landscape surface at this locality was covered with highly weathered dolerite cobbles and boulders that displayed horned and hollowed surfaces, pitting, oxidation and weathering rinds. Directly underneath this surface was an 80 cm thick layer of weathered and oxidized quartz and dolerite sand (sample DLS 98-017D) (**Figure 19A**). This unit was sorted to 92% sand, 1% gravel, and 7% mud. Contained in this layer was a thin stringer of concentrated black volcanic ash. A small pod of concentrated unweathered gray diamicton was draped over the buried ice. This unit was sorted to 31% sand, 67% gravel, and 2% mud (sample DLS 98-017C).

Volcanic Ash Stringers

A stringer of black volcanic ash was uncovered in this excavation. The stringer was 1.5 m in length, and dipped at 15° in a planar fashion toward the bottom of the pit. The upper portion contained some oxidized quartz and dolerite sand grains, but became coarser and less disseminated toward the bottom of the excavation. Here, the ash deposit displayed a tangential relationship to the buried ice surface at the bottom of the

excavation. Two cm above the buried ice surface, the unconsolidated ash became partially ice-cemented to a six cm wide by two cm thick volcanic ash lens.

Ice-cemented Volcanic Ashes

The ice-cemented volcanic ash lens at the bottom of the excavation was fused with a massive ice-cemented volcanic ash layer that overlay the buried ice. When the ash was exposed in a strike section in the buried ice, it was seen to be part of an ice-cemented ash wedge that was flanked on both sides by ice-cemented quartz and dolerite sand (**Figure 19B**). The grain-size of the volcanic ash in the ice-cemented wedge decreased upward toward the widest portion of the wedge.

Buried Ice

The exposed buried ice had two distinct textures. The ice surrounding the ice-cemented sand wedge was brittle and displayed a high degree of fissility. This ice was relatively clear and had a glassy texture to it. The ice that was not in contact with the ice-cemented sand wedge was white, contained numerous air bubbles and angular pieces of fine dolerite gravel and quartz sand grains.



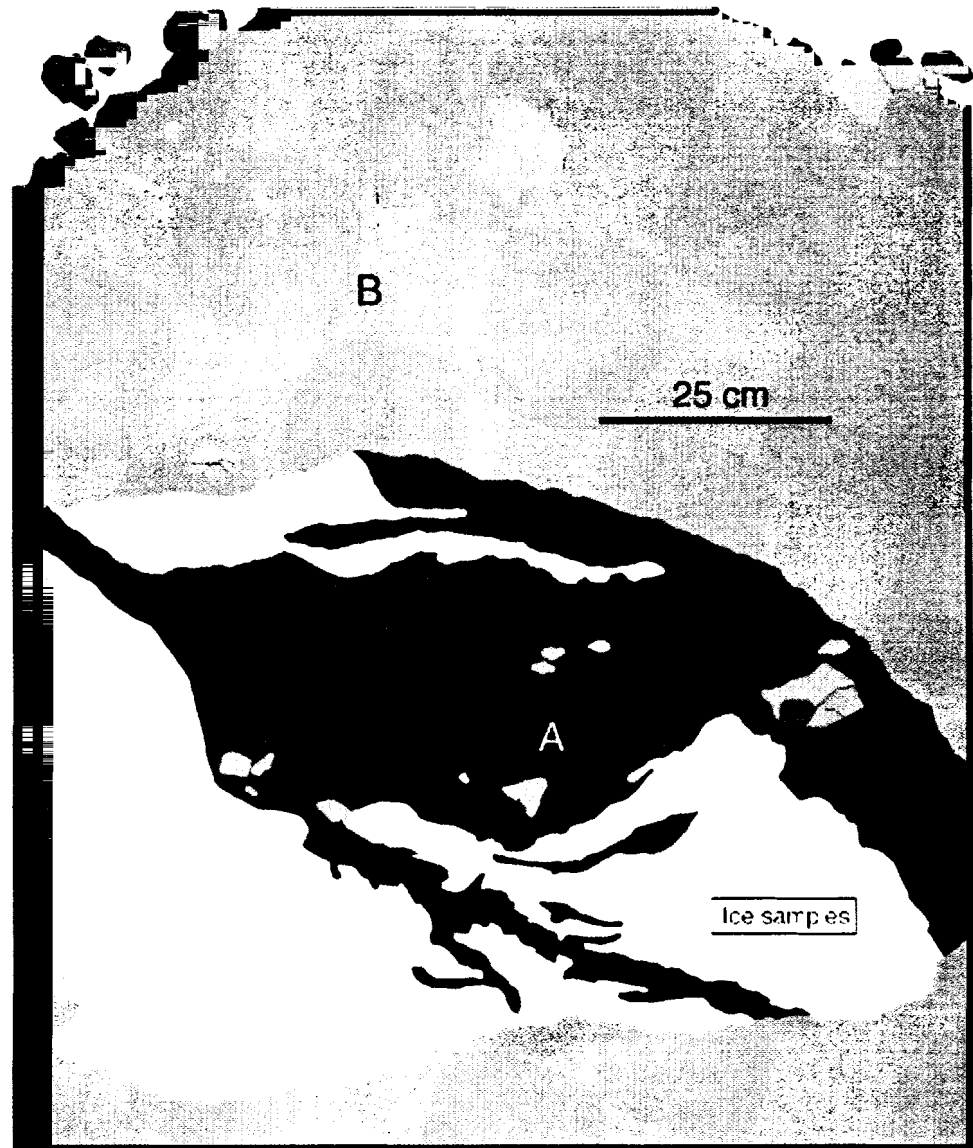
Figure 19 Excavation DLE 98-017

A) This picture shows excavation DLE 98-017. The sediment on the floor of the pit is composed of weathered and oxidized quartz and dolerite sand. Contained in the floor of the pit is an ice-cemented volcanic ash wedge within an ice-cemented sand wedge. The sand wedge is flanked by buried ice. Lens cap is five cm in diameter.

NE

DLE 98-017

SW



Latitude S 77.87658		Samples Analyzed	
Longitude E 160.54193		A	DLS 98-017 A
Weathered Sands	Ice-cemented sand	B	DLS 98-017 B
Ice-cemented sand and fine gravel	Volcanic Ash		
	White, bubbly ice		

Figure 19 Excavation DLE 98-017

B) Illustration of excavation DLE 98-017. The letters in the diagram mark where sediment and volcanic ash were sampled.

Stratigraphic Interpretation

The sharp contact between the volcanic ash wedge within the ice-cemented sand wedge indicates that the process of thermal contraction is repetitive at a single locality (excavation DLE 98-017). The sorting of the ash suggests that the contraction crack opens wide enough for only coarse sand sized material to penetrate to depth. Because this crack is filled with a fining-upward sequence of volcanic ash, the crack must have been void of sediment during volcanic ash fall. This illustrates that the contraction cracks are sediment starved, and volcanic ashes that filled this contraction crack represent near instantaneous filling of this crack after it opened.

A seamless transition occurs between the ice cemented sand/ash wedge contained in the floor of the excavation and the overlying weathered sand containing the volcanic ash stringer. The fining-upward trend of the ice-cemented ash wedge continued into the ash stringer overlying the buried ice. The stringer of volcanic ash (sample DLS 98-017A) is thought to be a distorted portion of the top of a volcanic ash wedge, on the basis of its identical grain-size, composition, and is in direct contact with the underlying ice-cemented volcanic ash wedge. The upper portion of the volcanic ash wedge was probably stretched into a linear strand from slumping that resulted from the sublimation of the buried ice. The weathered sand (sample DLS 98-017D) surrounding the volcanic ash stringer are inferred to be slumped sand wedge sediment. This sand was likely the upper part of the ice-cemented sand wedge that flanked the volcanic ash wedge. As the buried ice sublimated, the sediments ceased to be ice-cemented and were stretched and slumped. The unweathered gray diamicton (DLS 98-017C) overlying the ice and underlying the slumped sand wedge sediment is interpreted as a sublimation till.

Sedimentology

Sorting

A visual distinction could be applied to the stratigraphic units contained in all of the excavations. The sediments composing all the stratigraphic units were initially separated in the field as composed of either weathered quartz and dolerite sands or an unweathered gray diamicton (**Table 1**). The sublimation till and the sediment in and emerging from the buried ice were composed of the unweathered gray diamicton. The sediment contained in the sand wedges, the ice-cemented sand wedges, contraction cracks, and slumped sand wedge deposits were composed of weathered quartz and dolerite sand. A ternary plot of the weight percentages of gravel, sand, and mud in all samples show no overlap between the sediments that were incorporated into a sand wedge and the sublimation till that originated from the buried ice (**Figure 20**).

TABLE 1- DESCRIPTIONS AND INTERPRETATIONS OF STRATIGRAPHIC UNITS SEEN IN THE FIELD

STRATIGRAPHIC UNIT	FIELD UNIT	DESCRIPTION	INTERPRETATION
Sediment in the buried ice	Unweathered gray diamicton	Angular sand and gravel composed of dolerite that is fresh, unoxidized and often exhibits impact chips. Found in buried ice.	Unweathered englacial sediment
Sublimation till	Unweathered gray diamicton	Unweathered poorly sorted sand and gravel composed of dolerite and some sandstone. Green and Maroon siltstone clasts are common. Conformably drapes the buried ice.	A till deposited at the ice surface from sublimation of buried ice
Sand wedge sediments	Weathered and oxidized sand	Well-sorted sand composed of oxidized and weathered quartz and dolerite. Found bordering active polygon landforms.	A deposit formed at the edge of a polygon as a thermal contraction crack opens in the buried ice
Slumped sand wedge sediment	Weathered and oxidized sand	Massive well-sorted sand composed of oxidized and weathered quartz and dolerite. Distorted vertical bedding and volcanic ash stringers are common. Found superposed over the buried ice and/or over buried ice and sublimation till.	A sand wedge bordering a polygon that slumped over the buried ice and any till overlying the ice as sublimation occurred.
Ice-cemented sand wedges	Weathered and oxidized sand	Ice-cemented wedges of well-sorted sand composed of weathered quartz and dolerite. Located in the buried ice beneath the center of polygon landforms.	A relict sand wedge deposit that formed at the edge of a polygon as a thermal contraction crack opened in the buried ice.
Open contraction cracks	Weathered and oxidized sand and some fine-gravel	Well-sorted sand and fine-gravel composed of oxidized and weathered quartz and dolerite. Located in the buried ice at the edge of new or older, active polygon landforms.	Active contraction crack sediment
Ice-cemented debris-bands	Weathered and oxidized sand	Well-sorted sand composed of oxidized and weathered quartz and dolerite. Concentrated in linear bands only 1-2 cm wide. Located in the buried ice beneath the center of polygon landforms.	Healed thermal contraction crack sediment

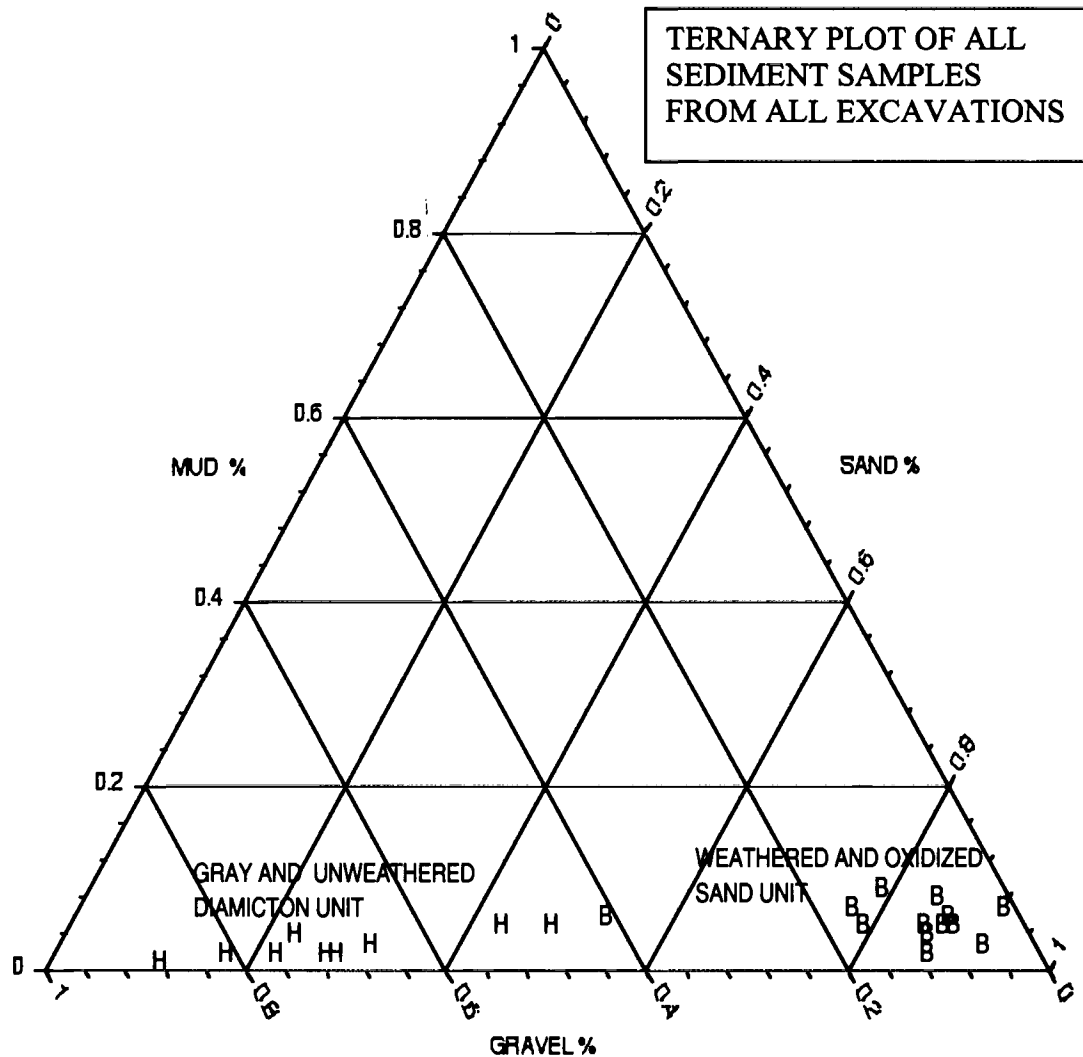
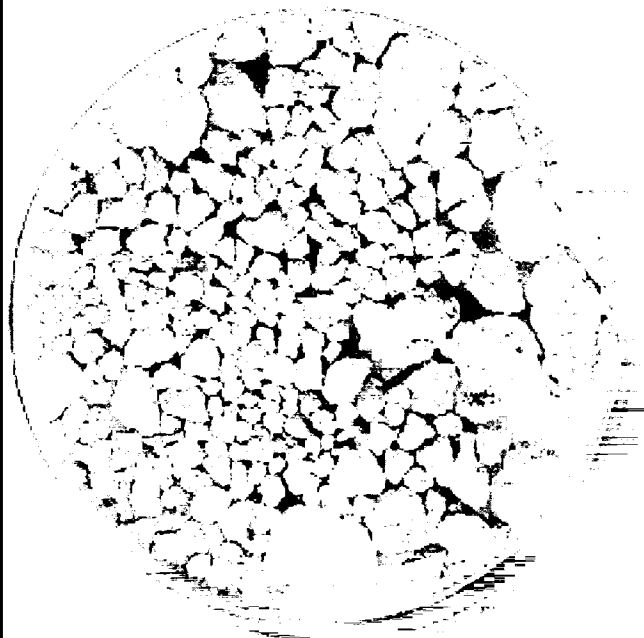


Figure 20- Ternary plot of all sediment samples

This ternary plot depicts the distribution of all sediment samples from all excavations by weight percent of sand, gravel and mud. All units were distinguished in the field as being composed of the gray, unweathered diamicton unit (H) or the weathered and oxidized sand unit (B). All sublimation till and all the sediment in the buried ice were composed of the unweathered gray diamicton. The sediment contained in the sand wedges, ice-cemented sand wedges, slumped sand wedge deposits, debris bands and contraction cracks was composed of the weathered and oxidized sand. Note that there is no overlap between the two units. Supporting data listing weight percentages of sand, gravel and mud can be found in Appendix A, and field classification and composition all the sedimentary units sampled can be found in Appendix D.

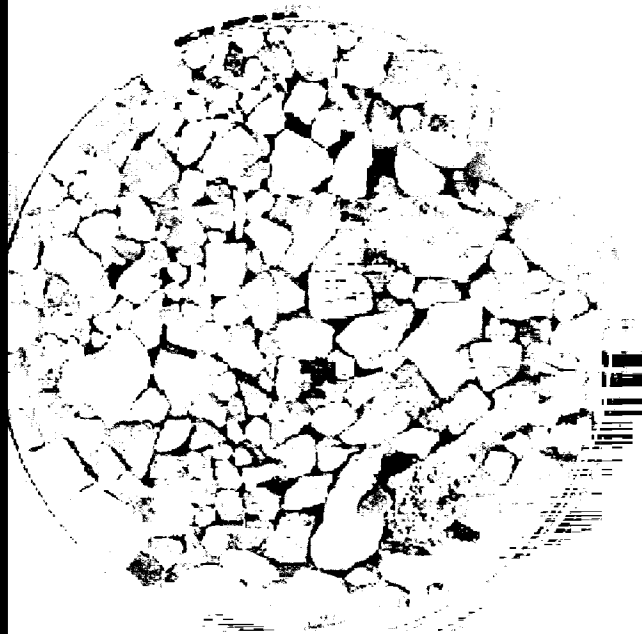
Grain Maturity

The weathering of the sublimation till and the sand wedge sediments can be qualitatively assessed through an examination of the surface textures and grain maturity of gravel clasts contained in both units. The gravel clasts in the sand wedge sediments are pitted and have developed weathering rinds, similar to larger clasts of dolerite on the surface of the debris-covered glacier. In addition, the grain shape of the sand wedge sediments is more well-rounded than that of the sublimation till, suggesting that they have been subjected to a greater degree of subaerial weathering processes (**Figure 21**).



DLE 98-010 C

1 INCH



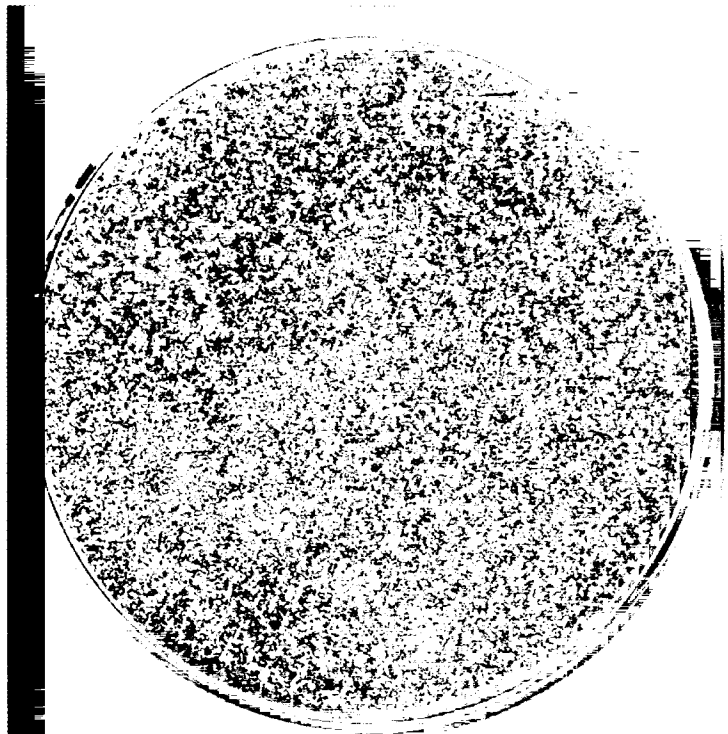
DLE 98-010 D

Figure 21 – Contrast in grain maturity

Pictured here are fine-gravel samples from excavation DLE 98 010 (Figure 16A). The sediment is from a slumped sand wedge (sample DLE 98-010C) and the sublimation till (DLE 98-010D). Visual differences in angularity, oxidation and surface texture of small gravel clasts contained in the sand wedge sediment (DLE 98-010C) are seen here. In addition, note the large amount of maroon siltstone present in the unweathered gray diamicton (DLE 98-010D). The siltstone is not observed to survive subaerial weathering at the surface of the debris-covered glacier.

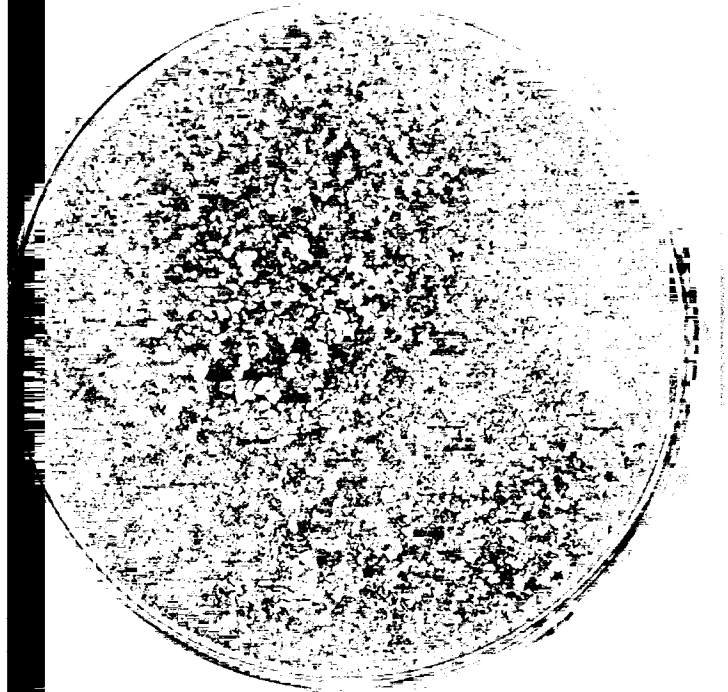
Oxidation and Lithology

The sand wedge sediments can be distinguished from the sublimation till by examining lithologic composition. The sand wedge sediment is primarily composed of quartz with a minor dolerite component. The sublimation till is primarily composed of dolerite, however there is a noticeable component of gravel clasts in this unit composed of green and maroon siltstone (**Figure 22**). The sand wedge sediment has no observable siltstone component, and large gravel clasts of green and maroon siltstone were not observed on the debris-covered glacier surface. The composition and sedimentological immaturity of the material constituting the sublimation till illustrate that it has not been subjected to subaerial weathering processes.



DLS 98-010 C

1 INCH



DLS 98-010 D

Figure 22 – Contrast in oxidation and lithology

Pictured here are visual differences in oxidation and lithologic composition between samples from excavation DLE 98-010 (Figure 16A.) The sediments contrasted are from the sand fraction of the slumped sand wedge sediment (sample DLS 98-010C) and the sublimation till (sample DLS 98-010D)

Note the pieces of green siltstone in the coarse sand fraction of the sublimation till.

VI. DISCUSSION

Morphology

Progressive geometric changes of all polygon characteristics occur along the long-axis of the debris-covered glacier. A series of diagrams (**Figure 23**) illustrate progressive changes in polygon characteristics from the head to the snout of the debris-covered glacier on the long axis of symmetry. These diagrams are useful because they show how polygons change with distance from the equilibrium line.

The thermal contraction cracks in the buried ice are root cause of the polygons seen at the surface of the debris-covered glacier. Without thermal contraction of the buried ice, there would be no surface manifestation of cracks, and therefore no polygonal network or polygon characteristics. The contraction cracks exist and remain open because the rate of ice flow, and hence the rate of closure of the contraction cracks, is slower than the rate of sublimation. As contraction cracks in the buried ice begin to open, fine-grained sediment contained in overlying, poorly sorted sublimation till penetrates to depth, causing a surface depression to form directly over the crack. Because the contraction crack is a plane in the buried ice oriented perpendicular to the debris-covered glacier surface, it will appear as a shallow, linear furrow on the landscape. Sublimation of the contraction crack walls, chiefly the upper part where the sediment cover is thin, initiates the formation of a polygon trench. As thermal contraction of the buried ice continues through time, the linear dimensions of the polygon and the surrounding trench increase. Because the buried ice is lost by sublimation, the water vapor that once was ice has to be transported through the sediment mantle. It is probable that the layer of sediment over the buried ice can be sufficiently thick as to slow down the vapor transport.

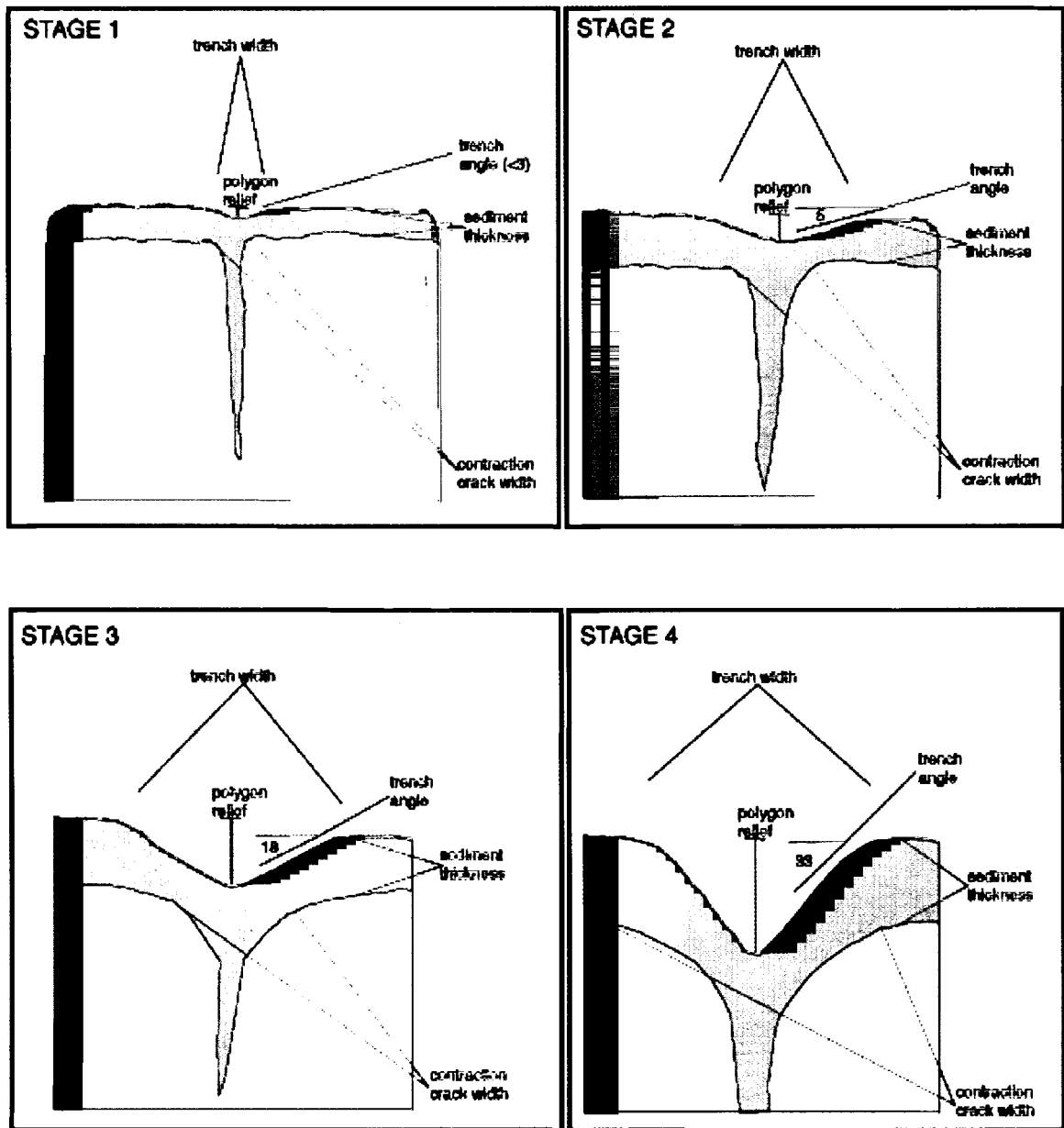


Figure 23- Observed changes in polygon morphology

A series of illustrations depicting observed changes in thermal contraction crack size in buried ice. Also shown are observed down-glacier (Stage 1= head of glacier, Stage 4= proximal to toe of glacier) changes in polygon and surrounding trench characteristics. The polygon trenches form when a contraction crack opens in the buried ice. Sublimation of the upper portion of the thermal contraction crack, where the sediment cover is thinnest, causes the development of the polygon trench.

Development of Trenches

The thermal contraction cracks in the buried ice define the borders of a polygon landform. Sublimation of the upper part of the contraction crack lowers the surface elevation of the landscape directly over the crack. The vertical change in topography over the crack caused by sublimation creates the polygon relief (**Figure 24**). Trench angle and trench width are directly affected by growth and widening of the underlying thermal contraction crack in the buried ice. An increase in trench relief is accompanied by increases in both trench angle and trench width (**Figures 25 and 26**). The trench angle eventually stabilizes at the angle of repose ($\sim 32^\circ$), while the polygon relief and the trench width continue to increase. All of the polygon trench traits increase with distance from the equilibrium line. A comparison of trench relief, trench angle, and trench width to distance from the equilibrium line indicates that the most mature polygons are the farthest away from the head of the debris-covered glacier, have the greatest relief, and the widest trench widths (with steep sides $\sim 32^\circ$). The trenches define the borders of the polygonal landform, and hence the trench characteristics control the size of the overall polygon area.

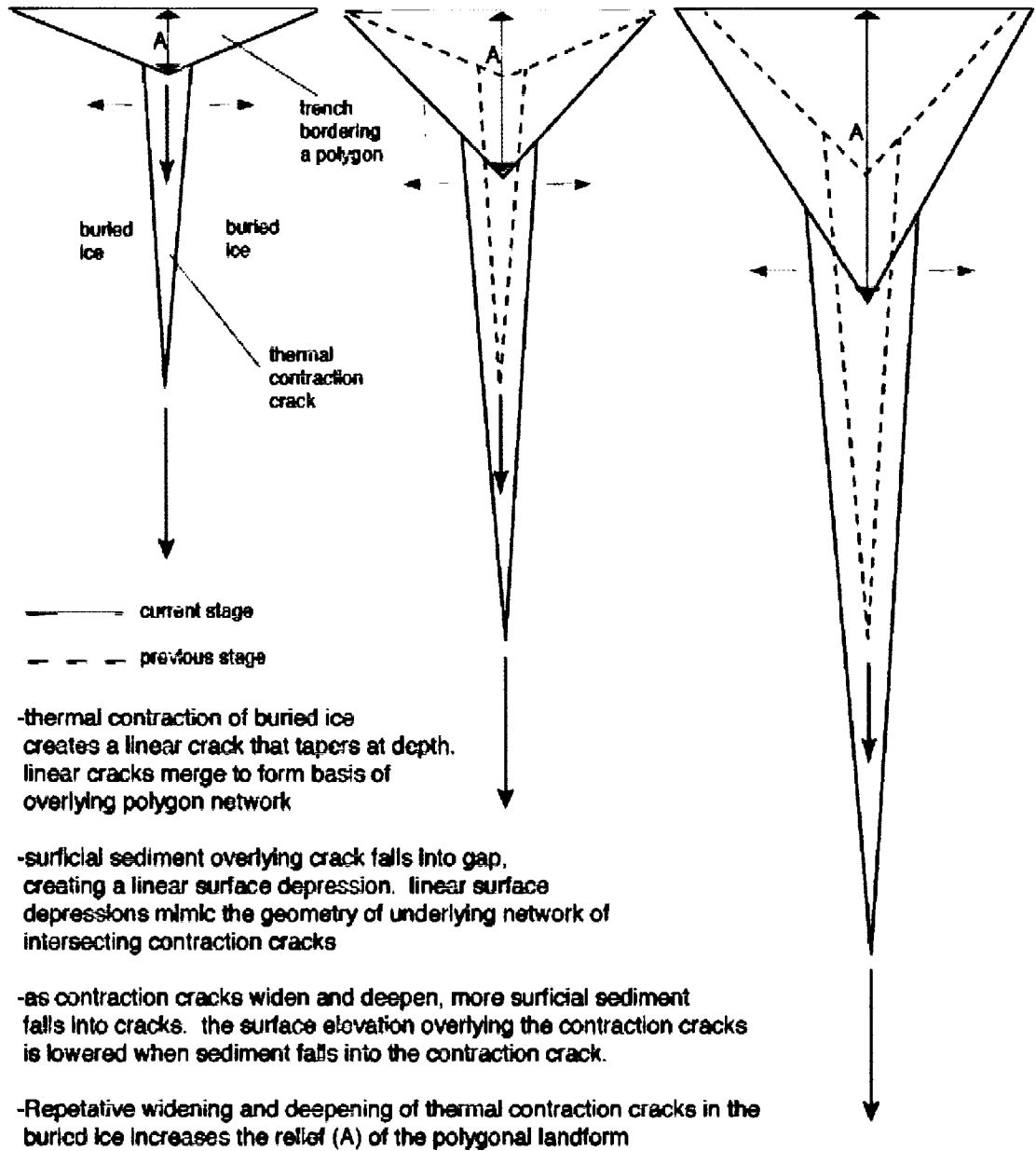
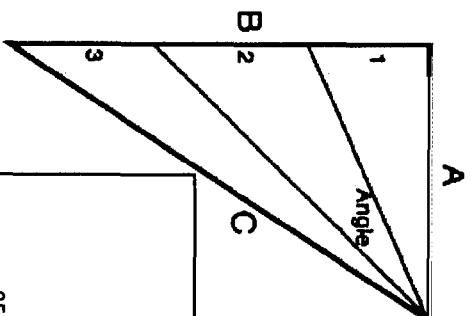


Figure 24- Diagram of change in polygon relief

Depiction of change in polygon relief, as well as other trench characteristics as a result of continual thermal contraction crack growth.



- Retain a fixed length for side A (1/2 trench width)
- By increasing the length of side B (Polygon Relief), side C (hypotenuse and side of polygon) lengthens
- an increase in side B (polygon relief) has and result of widening its opposite interior angle (trench angle)

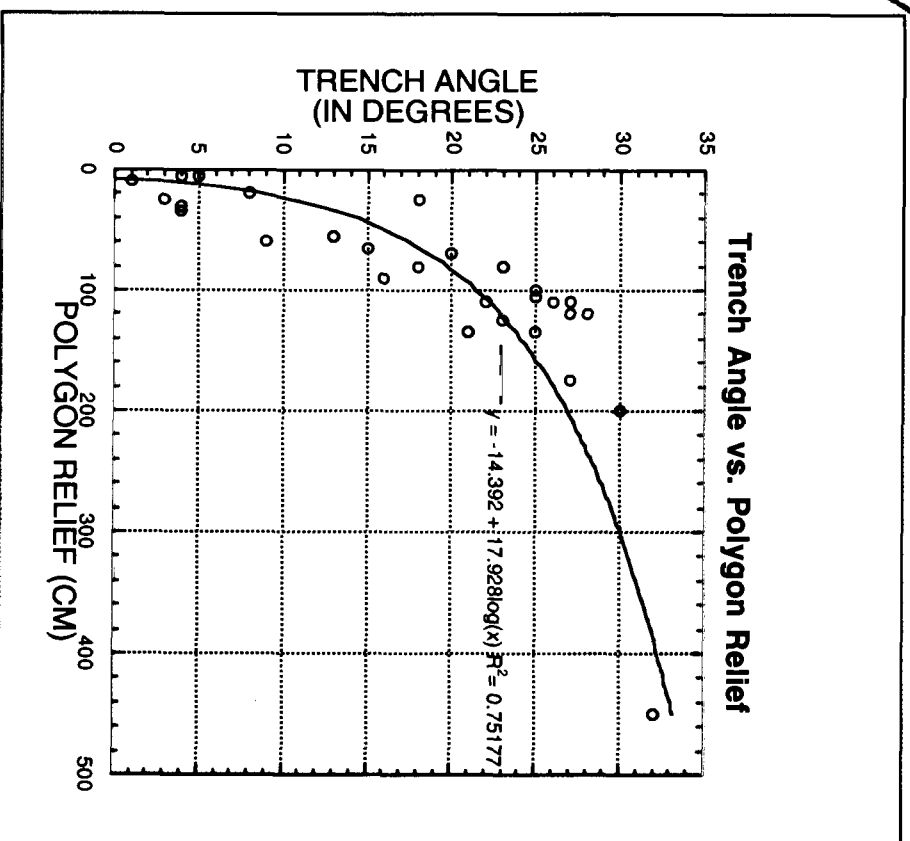


Figure 25- The relationship between polygon relief and trench angle. Data are from survey sites listed in Appendix B. Notice that the trench stabilizes at the angle of repose while the relief of the landform continues to develop. Sublimation of the buried ice occurs at the upper part of contraction cracks because the sediment cover is thinner than that on the polygon plateau. When the angle of repose is reached, the depth of sediment cover becomes the same along the trench sidewall. It is probable that the even sediment thickness causes sublimation to occur at an equal rate over the buried ice along the trench sidewall. In this case, the relief of the polygon can continue to develop and the trench angle will remain consistent.

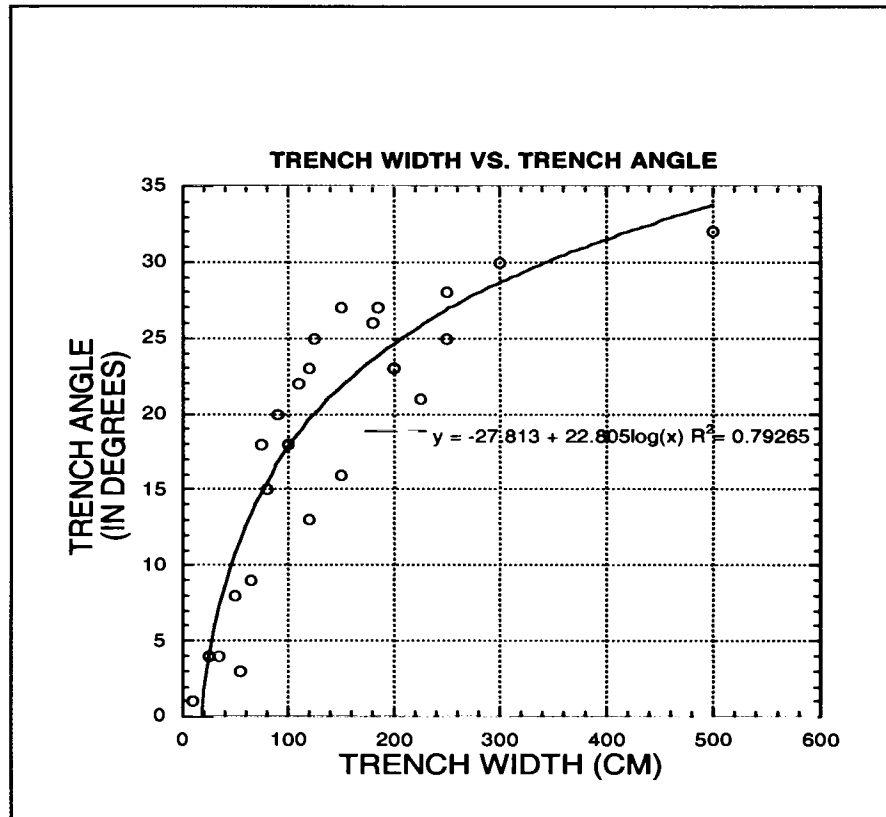
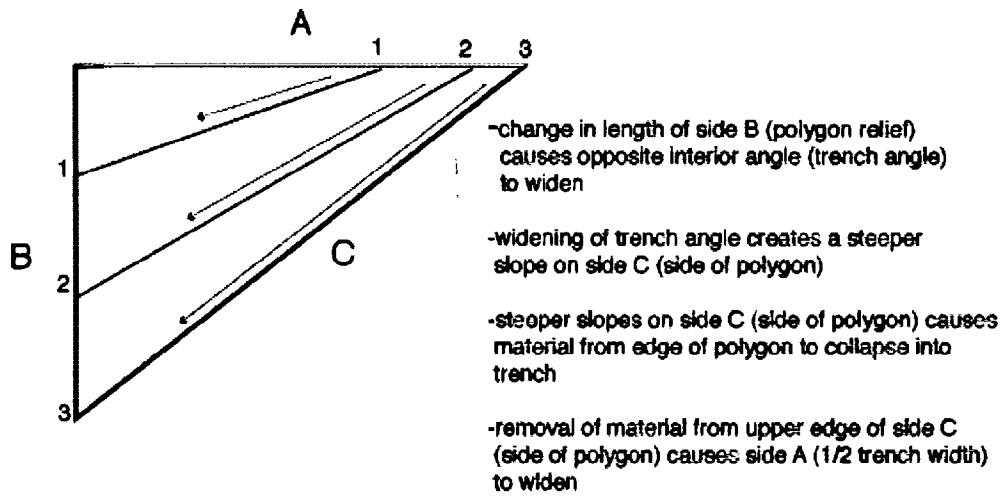


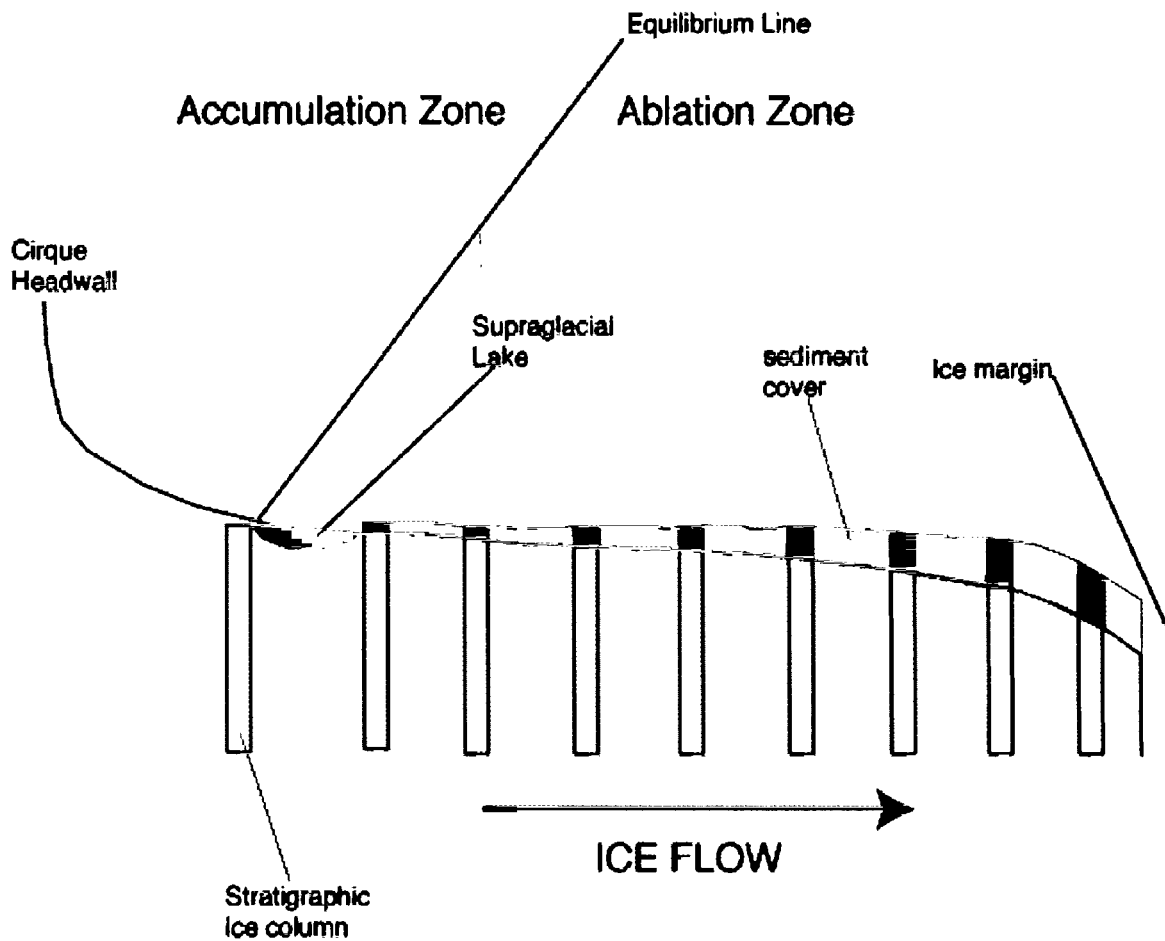
Figure 26- The relationship between trench width and trench angle.

Data are from survey sites listed in Appendix B.

Sediment Distribution

As glacier ice is transported from the accumulation zone, past the equilibrium line into the ablation zone, ice loss begins (**Figure 27**). Ablation (by way of sublimation) of the upper surface of the ice column occurs in the ablation zone. A layer of formerly englacial sediment is deposited at the glacier surface as an ablation till as result of sublimation of the buried ice. The buried ice is continually subjected to sublimation as it is transported through the ablation zone. Thus, ice that has been in the ablation zone for a long period of time (near the snout of the glacier) has experienced a greater degree of sublimation than ice that has been in the ablation zone for a short period of time (near the head of the glacier). Thus, the sediment that overlies the buried ice should become progressively thicker toward the snout of a debris-covered glacier.

PROFILE OF A DEBRIS-COVERED GLACIER



- assume a constant rate of ice flow
- as stratigraphic column of ice progresses through the ablation zone, sediment is added to the surface of the ice as a function of distance travelled and time spent in the ablation zone
- note the ratio of sediment added to ice loss is unequal, so there is a net reduction in surface elevation of glacier with increasing distance into the ablation zone

Figure 27- Profile of a debris-covered glacier. Viewpoint is along the long axis of symmetry. Depicted is a column of ice and the resulting meltout of sediment from that column as it travels further into the ablation zone.

A relationship between increasing distance into the ablation zone and sediment thickness is observed in the debris-covered glacier contained in Mullins/Beacon Valley. The relationship between increasing distance from the equilibrium line and sediment thickness illustrates that as a column of ice has traveled down valley, more sediment has been added to the stratigraphic column (Figure 28).

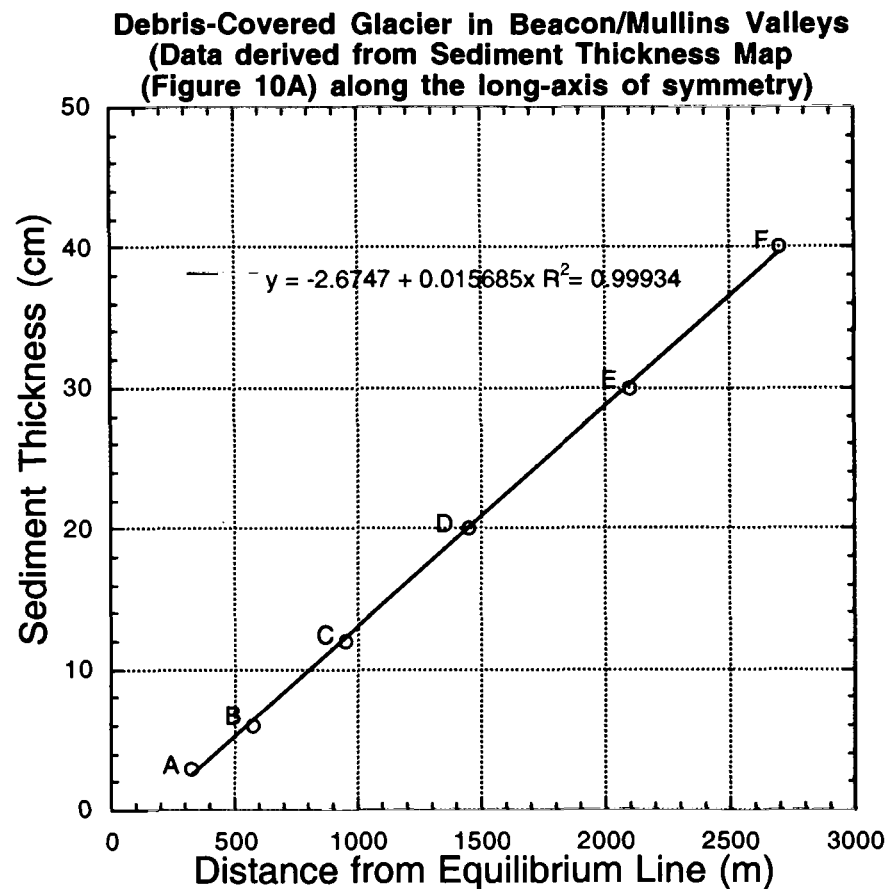


Figure 28- Relationship between sediment thickness and distance from equilibrium line.

Data points are derived from endpoints of zones of sediment thicknesses from Figure 10A, at the intersection with the long axis of symmetry.

The increased sediment thickness overlying the buried ice that coincides with an increase in distance into the ablation zone illustrates the dependence of sedimentation on the rate of ice flow in a debris-covered glacier. The rate of flow is a function of distance traveled over a period of time. The amount of sediment added to the surface of the buried ice has remained constant with increasing distance and time spent in the ablation zone of the debris-covered glacier. This linear relationship highlights a fundamental stability of ablation and rate of glacier flow that has not wavered through time. A preliminary ^3He cosmogenic exposure age date at site DLE Core 1 (located approximately 1700m downhill from the equilibrium line) from a dolerite boulder on the surface of the debris-covered glacier in Mullins Valley yielded an exposure age of 320 Ka (Marchant, Personal Communication).

The preliminary exposure age date can be used to provide a maximum flow rate for the debris-covered glacier, because it only provides a minimum age for time of entry into the ablation zone. An older exposure age would yield a slower rate of glacier flow. Using the preliminary exposure age date of 320 ka at the DLE Core 1 site 1700 m downslope from the equilibrium line, the above mathematical relationship indicates a maximum flow rate of 5.3 mm/year for the debris-covered glacier in Mullins Valley.

Linkage Between Polygon Characteristics

The cause-effect relationships that connect changes in one polygon characteristic to another can be related to specific controlling mechanisms (**Figure 29**). Seasonal temperature change in Beacon Valley causes thermal contraction cracks to open in the buried ice. With cracking, the polygon network is initiated and is first visually noticeable with a change in relief of polygons. The change in relief is a direct result of sediment

over contraction cracks being displaced as fine sediment filters downward into the crack. Contraction cracks also afford important additional surface area for sublimation to occur on. The continual growth of cracks eventually produces trenches. The trench formation is probably enhanced by the differences in relative humidity and saturation of the air with water vapor at depth in the cracks that contain unconsolidated sediment.

Loss of ice by sublimation causes sediment to be deposited as an ablation till on the buried ice in the ablation zone. As a column of ice is transported downglacier, the amount of sediment deposited on top of the buried ice is a function of distance traveled and length of time spent in the ablation zone (**Figure 27**).

During ablation, thermal contraction cracks continue to form in the buried ice. The poorly sorted ablation sediment that is added to the surface of the debris-covered glacier surface through sublimation is preferentially sieved by grain-size because the width of the thermal contraction crack width dictates sediment size. As the sieving process begins, polygon relief is initiated. The increase in polygon relief has a direct influence on two other physical properties; trench angle and trench width. The trench angle, trench width and relief of the polygon compose the defining edges of a polygonal landform.

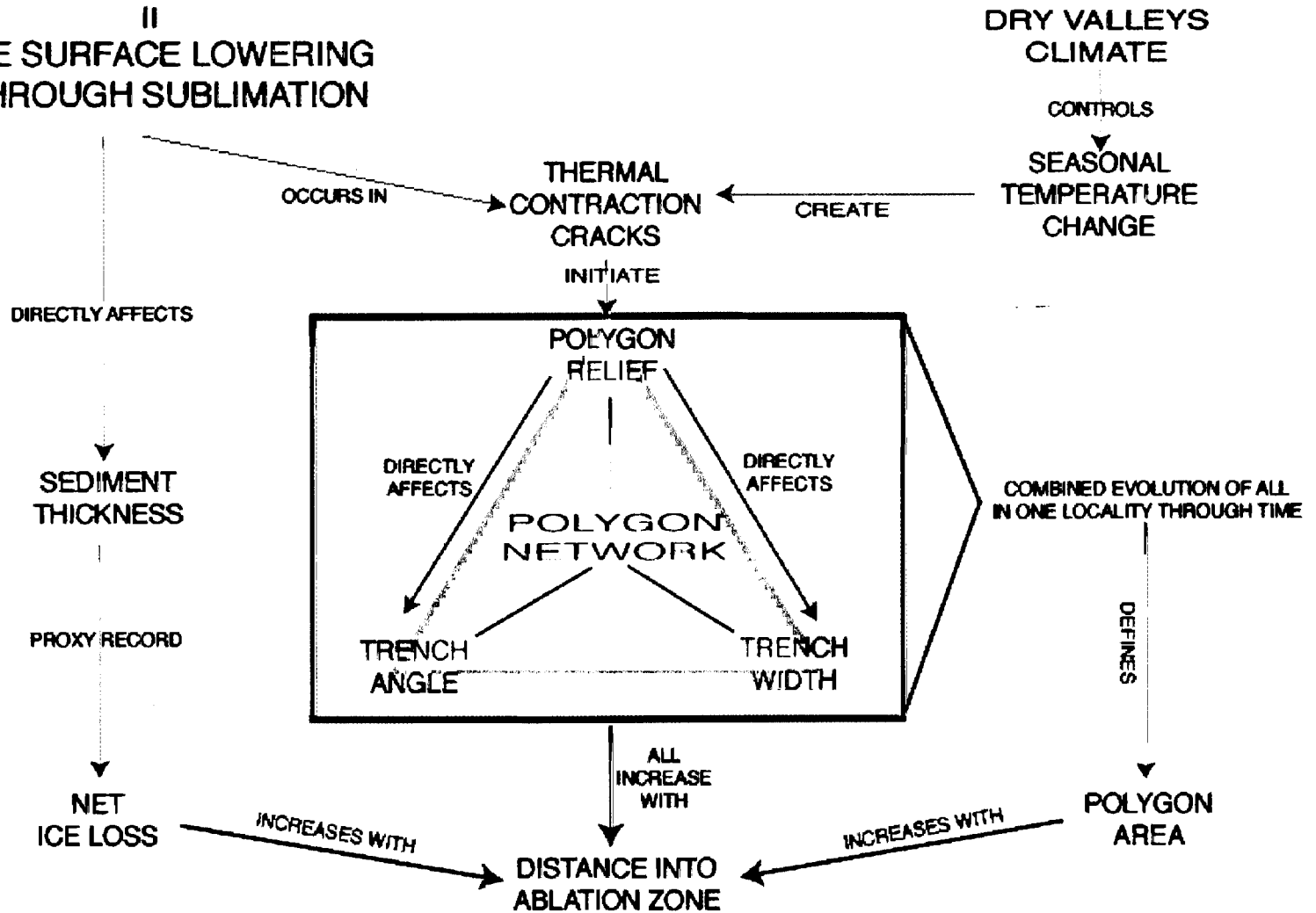
The polygon trenches define the areal extent of an individual landform. The initiation of polygon relief through thermal contraction of buried ice is the catalyst for polygon formation. Sublimation causes thermal contraction cracks to widen and sediment to be deposited at the surface of the debris-covered glacier. The rate of ice flow in the ablation zone is slow, which prevents the thermal contraction cracks from annealing. Because the contraction cracks remain open, polygon trenches can form.

One possible interpretation from the polygon distribution would be that the rate of glacier flow has diminished in a downglacier direction. In this scenario, the largest landforms would have developed near the snout of the debris-covered glacier because the ice is moving very slow or is stagnant. However, all of the polygon characteristics mimic the geometry of the sediment distribution across the debris-covered glacier surface. An alternative explanation would be that the rate of glacier flow has not varied through the existence of the debris-covered glacier. The sediment thickness is a function of ice flow rate through the ablation zone. The linear relationship derived from field measurements illustrates an increasing sediment thickness with increasing distance into the ablation zone (**Figure 28**). This relationship suggests that the flow rate has been constant through the entire length of the ablation zone. Hence, the development of the overall size of the landform is a direct reflection of time spent and distance traveled into the ablation zone (**Figure 29**). Existing polygons and trenches are engulfed and cannibalized by larger, developing landforms through time, as the buried ice and overlying sediment are transported into the ablation zone (**Figure 30**).

ABLATION

II
ICE SURFACE LOWERING
THROUGH SUBLIMATION

Figure 29- Schematic diagram of a polygon environment on a debris-covered glacier.



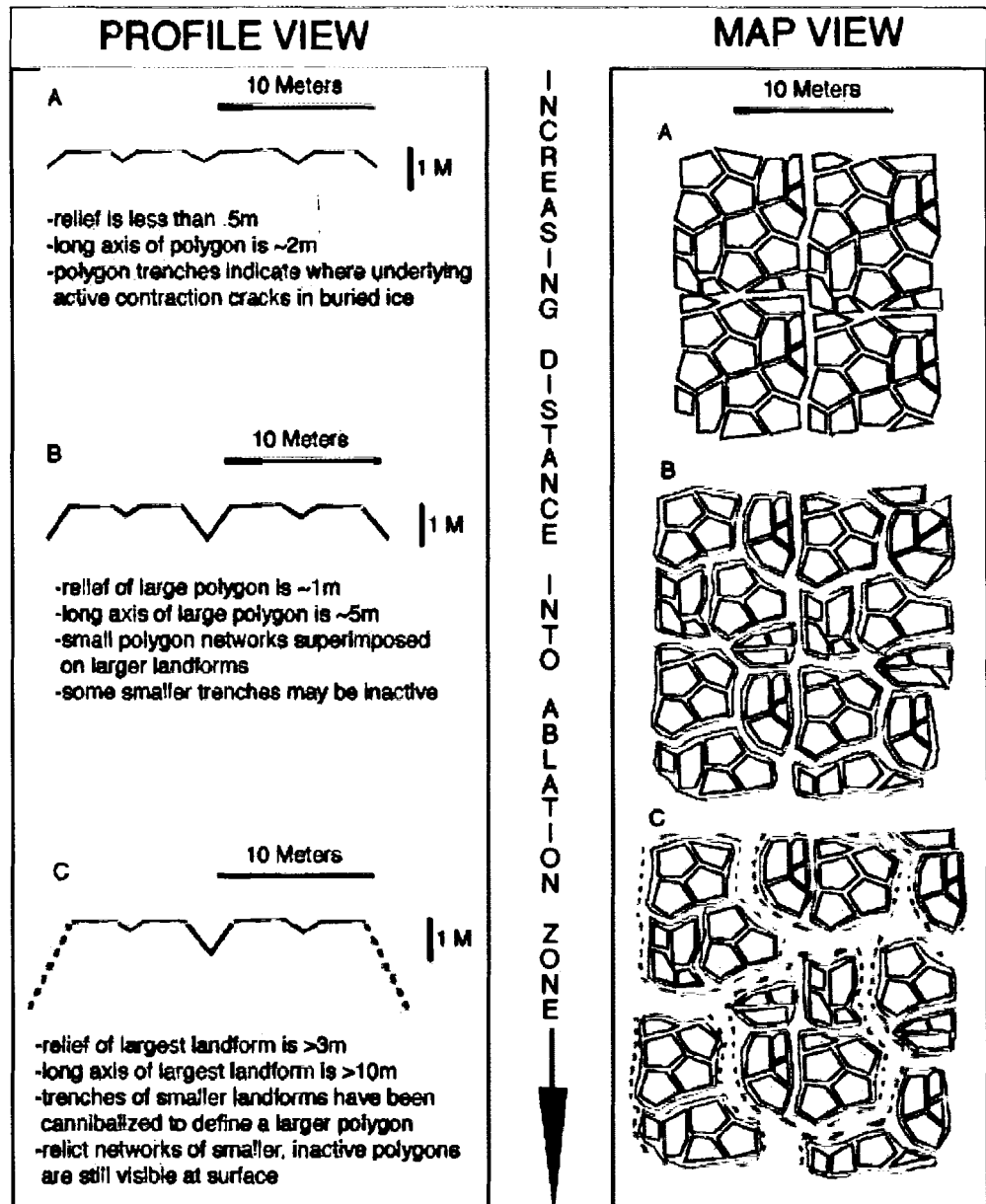


Figure 30-Polygon cannibalization process

The process diagram above illustrates the relative sizes of polygons and their bordering trenches with increasing distance down valley. Smaller polygons and trenches are engulfed and cannibalized by larger, developing landforms through time, as the buried ice and overlying sediment are transported into the ablation zone.

All of the polygon characteristics illustrate that the buried ice is a prerequisite for the formation of polygonal landforms contained in Mullins and Beacon Valley. The polygons themselves, and stratigraphy created during their formation, are both younger than the buried ice. In addition, the polygonal characteristics and landforms have been related directly to thermal contraction and ablation processes on a debris-covered glacier. The distribution of polygonal characteristics and landforms show that the buried ice was subsequently transported from the accumulation zone downvalley. The buried ice is inferred to be a singular, cohesive glaciogenic unit in the ablation zone of a debris-covered glacier. The buried ice can be traced back to the accumulation zone in Mullins Valley and is therefore glacial in origin.

Stratigraphy

Development of Stratification

The stratigraphy that was seen in the field can be attributed to the contraction crack/sublimation polygon process (**Figure 31**). Sublimation till (**Figure 31, Unit 3**) forms at the buried glacial ice (**Figure 31, Unit 1**) surface in Mullins and Beacon Valley. Larger clasts may have been added to this developing debris cover from Beacon Supergroup sedimentary rocks and Ferrar Dolerite in the upper portion of Mullins Valley. Bruises and impact chip marks on clasts in the buried ice (**Figure 31, Unit 2**) and the sublimation till are evidence of such rockfall.

As a thermal contraction crack opens, only the fine-grain sediment in the sublimation till penetrates to depth in the small opening. The crack within the buried ice usually opens and closes to the same width. The expansion-contraction process of an opening and closing contraction crack creates vertically bedded sand wedges (**Figure 33**). The preferential sieving of the sublimation till by the width of the contraction crack explains why nearly all fillings are sand-sized material (**Figure 31, Unit 4**). Volcanic ashes can also fall in the crack and become interbedded with weathered sand in a sand wedge. Because such wedges postdate the opening of the contraction crack and the buried ice, they afford a minimum age for the buried ice.

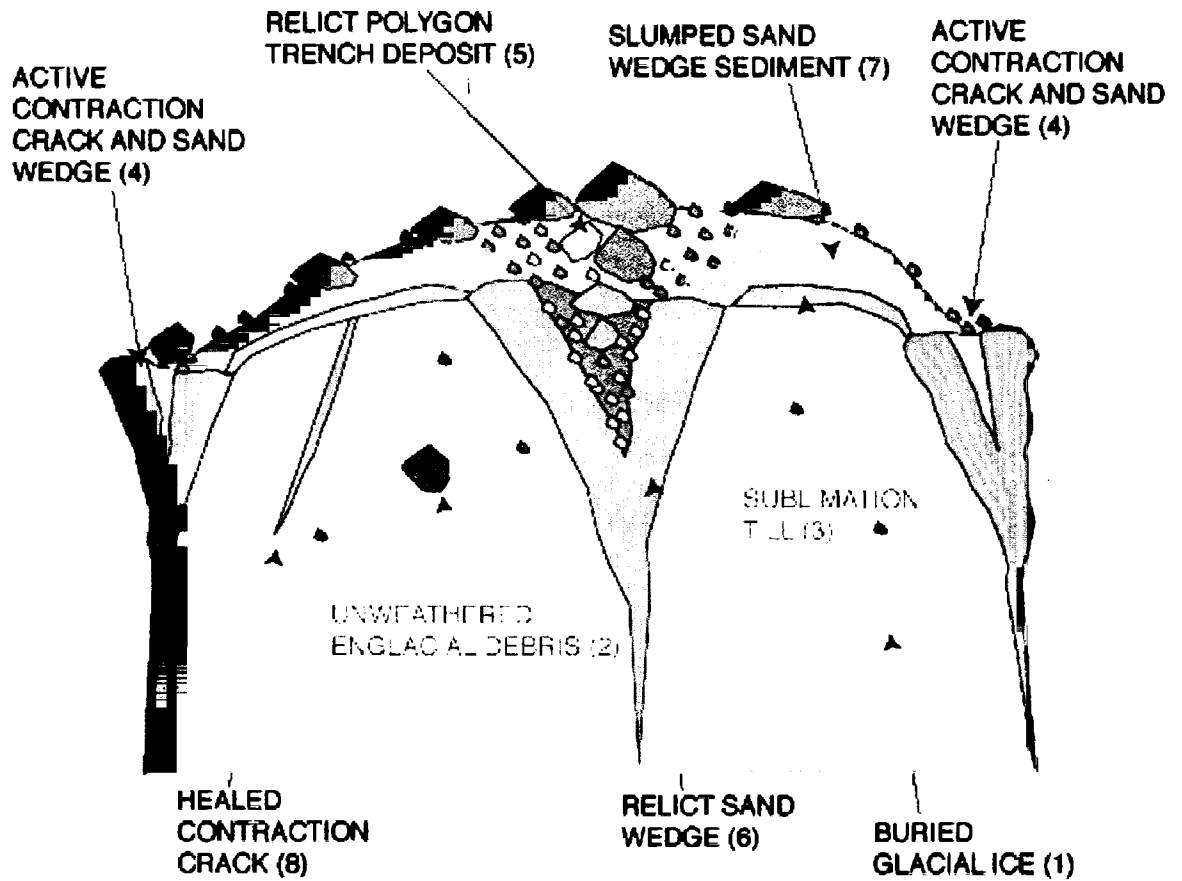
The top of a sand wedge usually occurs at the same level as the surface of the adjacent buried ice. Therefore, the flanks of the sand wedge are no longer supported the when the buried ice surface sublimates downward. As a result, the sediment contained in the wedge collapses (**Figure 31, Unit 7**) on top of the buried ice and sublimation till. The

material contained slumped sand wedges can be progressively distorted by further sublimation of the buried ice (**Figure 32**).

Figure 31- Contraction crack/sublimation polygon

This diagram depicts a cross-section of a polygon with flanking, active contraction cracks. Contained in this polygon are healed and relict contraction cracks. In this scenario, the sub-surface ice (Unit 1) is of glacial origin. The englacial sediment (Unit 2) is originally encased in snow in the accumulation zone, and is eventually encapsulated in ice. Other minor amounts of material accumulate on the glacier surface from rock fall in the accumulation and ablation zones. Ablation occurs primarily through sublimation. The ablation till produced by sublimation accumulates on the ice surface. Sublimation till (Unit 3) is continually added to the bottom of the surface layer as ablation of the buried ice proceeds. Thermal contraction cracks in underlying glacial ice allow weathered, fine-grained sediment to penetrate to depth. The collection of vertically bedded sediment deposited in the contraction crack forms sand wedges (Unit 4). Some cracks may heal (Unit 8) by ice closure shortly after opening. Other cracks may continue to increase in width for some time, and the development of a polygon trench overlying the sand wedge may ensue. In this situation, a relict polygon trench deposit (Unit 5) can contain both sublimation material and a relict sand wedge (Unit 6). Volcanic ash may be preserved in a relict sand wedge in the center of a polygon. As sublimation progresses, slumped sand wedge sediment (Unit 7) may be emplaced over the sublimation till that had already accumulated on the buried ice. In this way, layers of volcanic ashes that were originally vertical in the sand wedges may become stretched into thin stringers across the surface of the buried ice as sublimation occurs (**Figure 32**).

Figure 31- Contraction Crack/Sublimation Polygon Model



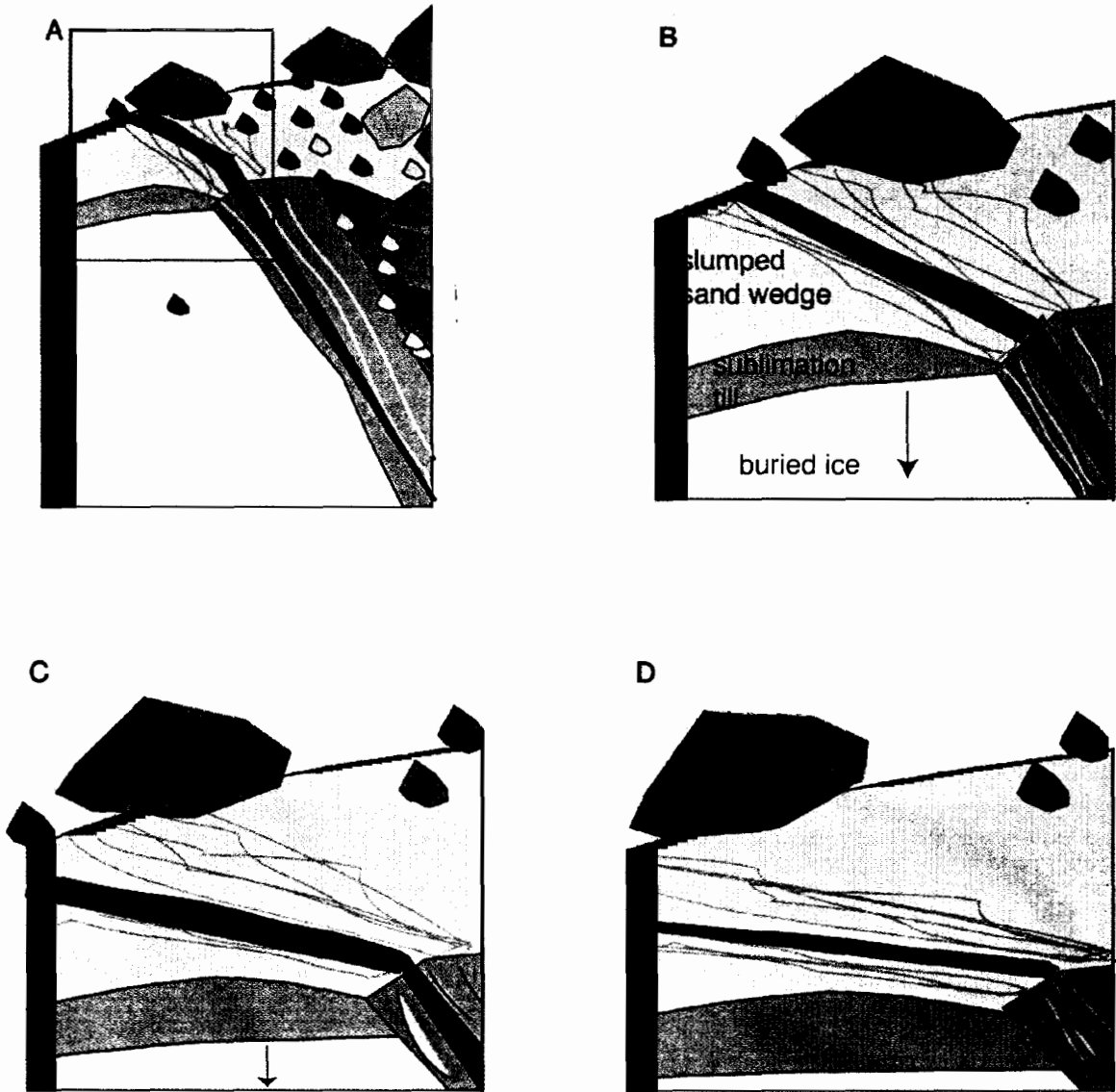


Figure 32- Stretching of volcanic ash wedge into a stringer

This illustration shows a relict sand wedge deposit in the middle of a polygon. The black box in part A focuses on the upper part of the sand wedge, the sublimation till and the buried ice. In this scenario, the relict sand wedge contains a nearly upright wedge of black volcanic ash contained in vertical beds of sand. As the buried ice sublimates (part B), the stratigraphy of sublimation till and overlying sand wedge sediment slumps slowly (to the left in this case) over the buried ice. As the sediment slumps, the upper portion of the ash wedge is stretched out into a long stringer of ash (parts C and D). In time, the stringer will become very thin, long, and parallel to the buried ice surface.

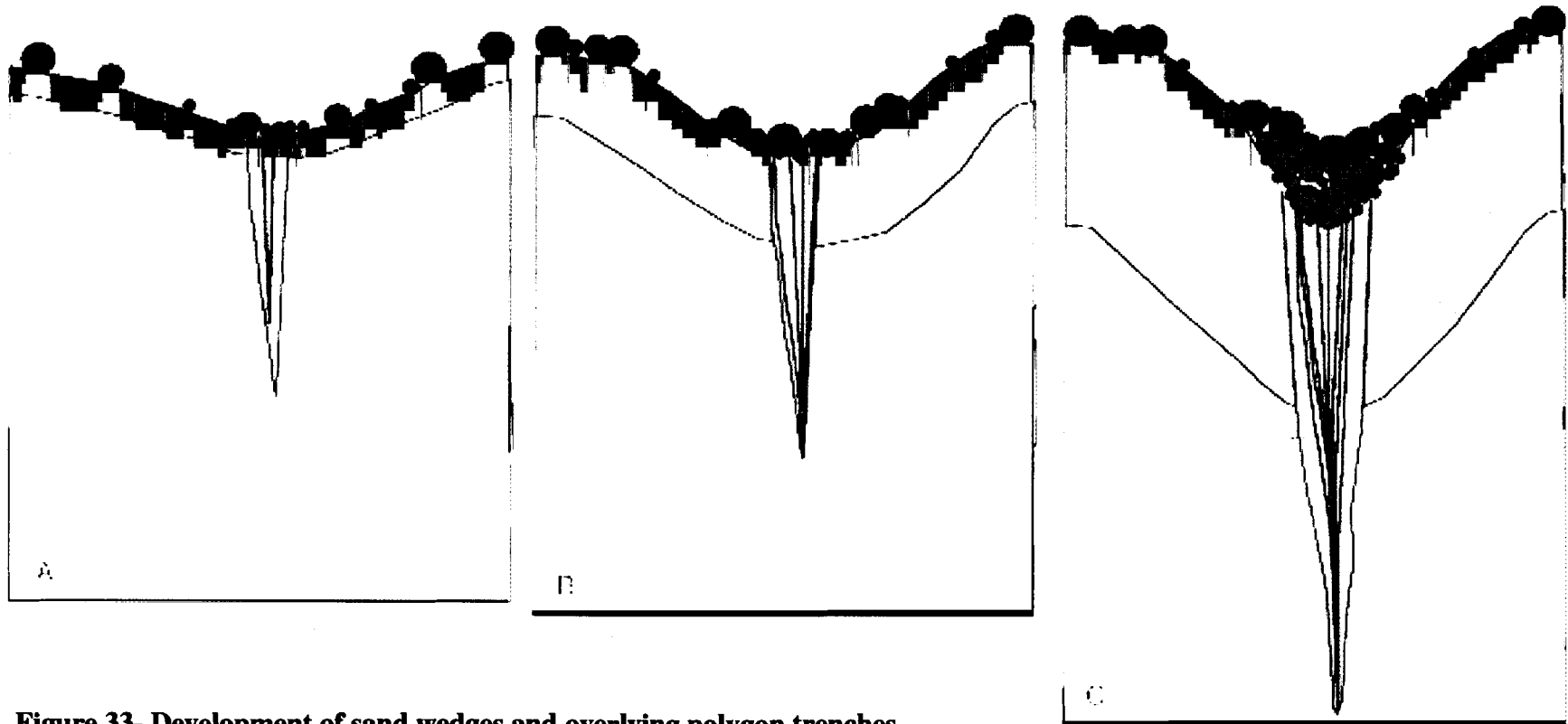


Figure 33- Development of sand wedges and overlying polygon trenches

This diagram depicts development of a sand wedge and an overlying polygon trench. As a thermal contraction crack opens in the buried ice (A), sand sized particles fall into the crack. Relief of the overlying polygon trench increases, and sand and fine-gravel avalanches into the bottom of the trough. As the process of thermal contraction continues, the sand wedge grows in size, but only allows sand size particles to fall to depth. Larger clasts avalanche into the overlying polygon trench (B). As this process continues, a vertically sorted, V-shaped deposit of gravel forms in the overlying polygon trench(C).

The cross-cutting relationship of ice-cemented vertical debris bands in the buried ice indicates that some of the thermal contraction cracks do not reopen (**Figure 31**, Unit 8), and that the process can take place time and again, and in different directions (**Figure 34**). Active sand wedges and trenches form as a result of repetitive thermal contraction at a specific locality for an extensive period of time.

If a thermal contraction crack develops into an active sand wedge, the polygon trench overlying the crack will continue to increase in width and depth. Large gravel-size sediment can then fall into the trench forming over the active sand wedge. Thus, a preferential sieving of sediments also exists in the trench directly above a sand wedge. The maximum grain size contained in the trench overlying an active thermal contraction crack is likely to be related to the size of the underlying ice-cemented sand wedge. Some well-developed sand wedges and overlying trenches cease to be active. It is possible that a large sediment thickness contained a well-developed polygon could cause the cessation of thermal contraction crack and sand-wedge growth. It is likely that a relict trench deposit (**Figure 31**, Unit 5) and relict sand wedge (**Figure 31**, Unit 6) will become distorted within the body of a polygonal landform during sublimation of the underlying buried ice (**Figure 32**).

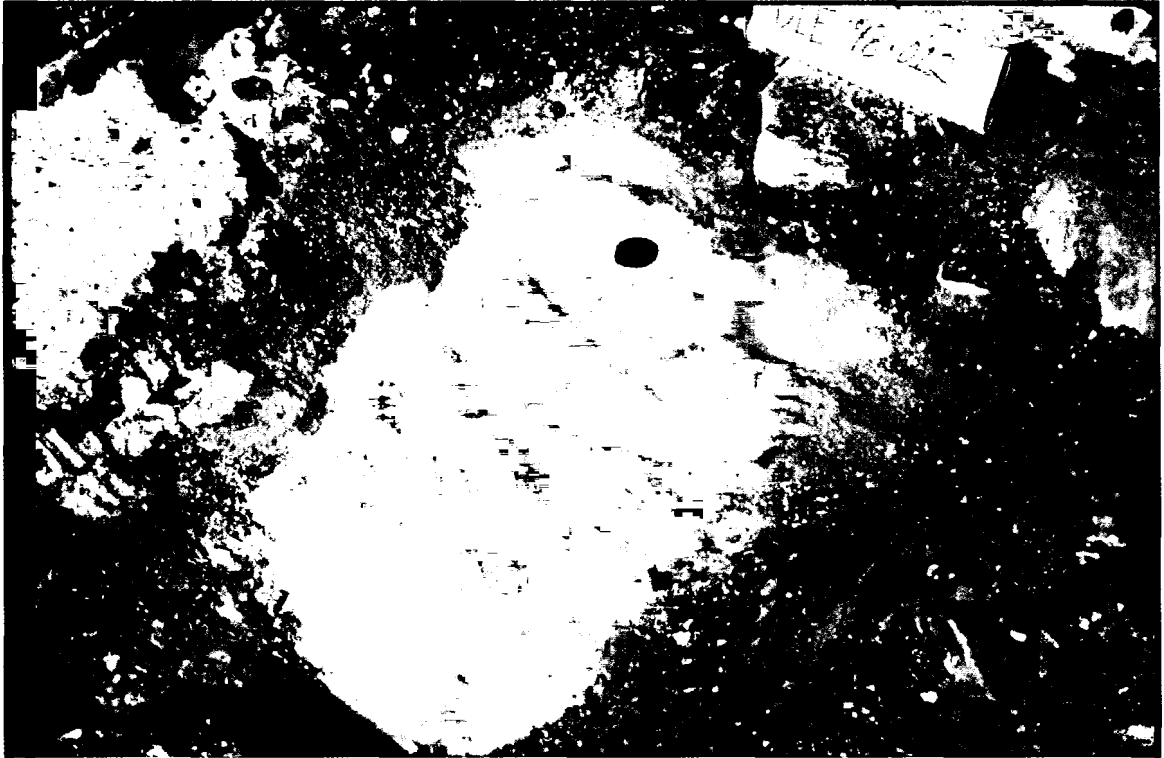


Figure 34- Photograph of healed contraction cracks

Pictured here beneath a thin sediment mantle of dolerite grus and boulders is buried ice (excavation DLE 98-012). The brown debris bands in the ice are vertically oriented ice-cemented sand layers. The ice-cemented sands are healed contraction cracks (**Figure 31**, Unit 8). Notice that the bands cross cut one another, indicating that thermal expansion and contraction of the buried ice can take place in multiple directions at the same locality.

The buried desert pavement in excavation DLE 98-014 is the only stratigraphic feature that cannot be explained by slow slumping of all the stratigraphic units described above. The pavement of buried dolerite boulders was located in an area that contained steep-sided polygons and trenches in excess of 2 meters depth. It is likely that massive, rapid slumping of material on the side of a trench bordering a polygon is responsible for burial of the former desert surface (Figure 35). The stratigraphic succession in excavation DLE 98-014 indicates that some material is able to move as cohesive stratigraphic packages in areas containing steep-sided polygons.

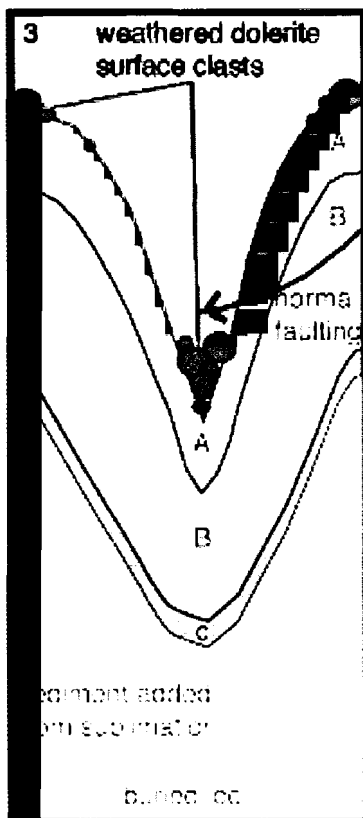
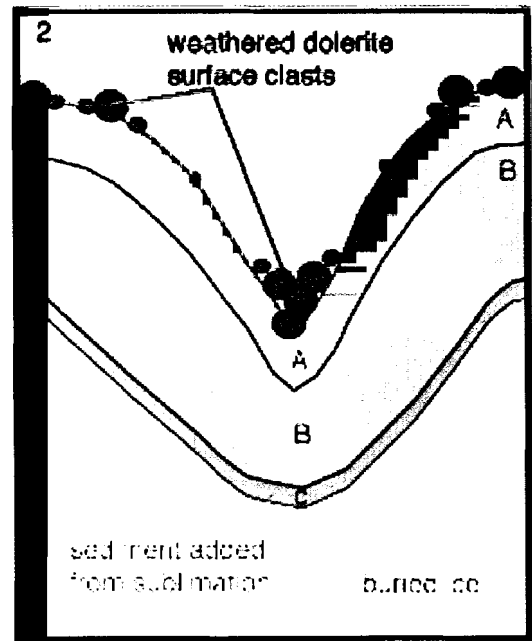
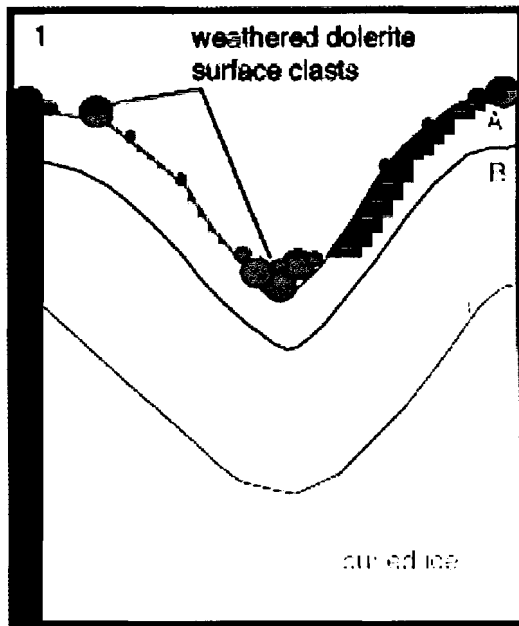
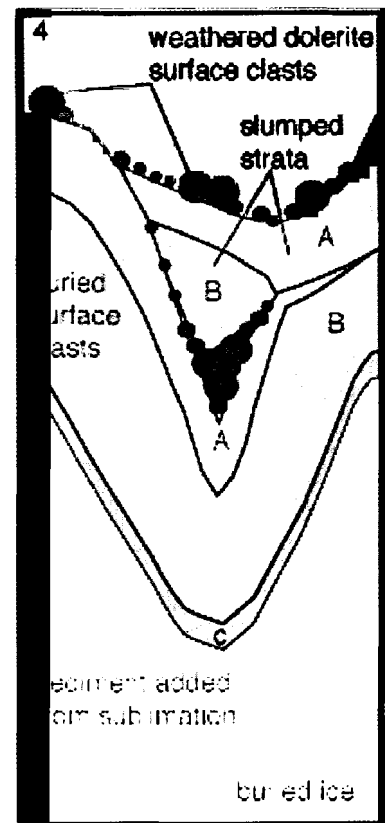


Figure 35- Burial of former desert pavements
 Growth of a trench bordering a polygon. As trench widens and deepens (2 and 3) during progressive sublimation, sidewalls at the angle of repose become unstable (3) and slumping of sediment occurs. Cohesive stratigraphic packages move as entire units in this situation, and are responsible for burial of former desert surfaces.



VI. CONCLUSIONS

- The polygons and trenches in upper Beacon and Mullins Valleys can be grouped into zones by size. The borders of these zones are arcuate. The morphology of the borders appears to be perpendicular to the flow paths of buried ice in the ablation zone of the debris-covered glacier. Polygonal landforms develop along these transport pathways. The distribution of polygons and trenches can be used to outline the ablation zone and the transport pathways of the buried ice in the ablation zone. The path that the buried ice in upper Beacon and Mullins Valleys has taken indicates that it originated in the cirque at the head of Mullins Valley, is a singular unit, and has a glacial origin.
- Sublimation causes englacial sediment to be deposited at the surface of the buried glacial ice as a till in upper Beacon and Mullins Valley. Thermal contraction of the buried ice sieves fine-grained material out of the sublimation till, forming active sand wedges. As the buried ice sublimates, sediment contained in the upper part of sand wedges can collapse onto the ice surface. Both the cracks and the sand wedges postdate the buried ice.
- Stratigraphically diverse units were composed either of sand wedge sediment that is well-sorted and highly weathered, or of sublimation till that is poorly sorted and unweathered. Sediment emerges from the buried ice and is sorted and weathered as the sand wedges form. Surficial sediment may be repetitively recycled from slumped

sand wedges into new sand wedges, but is never recycled back into the buried ice.

On this basis, cryoturbation as a means of forming the polygons is refuted.

- Volcanic ash is found within a sand wedge because the thermal contraction cracks in the buried ice were sediment starved. Polygon trenches overlying the sand wedges are ideal for trapping wind-blown volcanic ash because they shield loose sediment from high winds. Any volcanic ash trapped in a polygon trench would fall into the underlying sand wedge upon thermal contraction of the buried ice. Because sand wedges are younger than the buried ice, volcanic ashes contained in active, relict, or distorted sand wedge sediment provide a minimum age for the underlying glacial ice.
- Ashes from sand wedge sediment overlying buried ice in Beacon Valley have been dated at 8.1 Ma (Sugden *et al.*, 1995). The existence of the ancient buried glacial ice in Beacon Valley argues for persistent polar conditions since at least middle Miocene time.

REFERENCES

- Ackert Jr., R.P. 1998. A rock glacier/debris-covered glacier system at Galena Creek, Absaroka Mountains, Wyoming. *Geografiska Annaler* Vol. 80 A No. 3-4. Pp. 267-276.
- Barrett, P.J., Adams, C.J., McIntosh, W.C., Swisher III, C.C., and Wilson, G.S. 1992. Geochronological evidence supporting Antarctic deglaciation three million years ago. *Nature* Vol. 359 October 29. Pp. 816-818.
- Barrett, P.J. 1996. Antarctic Palaeoenvironment through Cenozoic Times- A Review. *Terra Antarctica* Vol. 3 No. 2. Pp. 103-119.
- Barrett, P.J. 1997. Antarctic Paleoenvironment through Cenozoic Times- A Review. In proceedings of VII Antarctic Earth Science Symposium. Siena, Italy.
- Berg, T.E. and Black, R.F. 1966. Preliminary measurements of growth of nonsorted polygons, Victoria Land, Antarctica. In J.C.F. Tedrow(Ed.), *Antarctic Research Series* (Vol. 18) Washington D.C., American Geophysical Union.
- Black, R. F. 1982. Patterned-ground studies in Victoria Land. *Antarctic Journal of the United States*. Vol. 17. Pp. 53-54.
- Black, R.F. 1973. Growth of patterned ground in Victoria Land, Antarctica. *Permafrost: The North American Contribution to the Second International Conference* (13-28 July 1973, Yakutsk, USSR). Washington, D.C.: National Academy of Sciences.
- Brady, H. and McKelvey, B. 1979. The interpretation of a Tertiary tillite at Mount Feather, Southern Victoria Land, Antarctica. *Journal of Glaciology* Vol. 22 No. 86. Pp. 189-193.
- Burckle, L. H. and Pokras, E. M. 1991. Implication of a Pliocene stand of *Nothofagus* (southern beech) within 500 kilometers of the South Pole. *Antarctic Science* Vol. 3, No. 4. Pp. 389-403.
- Burckle, L. H. and Potter Jr., N. 1996. Pliocene-Pleistocene diatoms in Paleozoic and Mesozoic sedimentary and igneous rocks from Antarctica: A Sirius problem solved. *Geology* Vol. 24 No. 3. Pp. 235-238.
- Chinn, T.J. 1980. "Glacier balances in the Dry Valleys area, Victoria Land, Antarctica." In Proceedings of the Riederalp workshop IAHS-AISH Publication no. 125. Pp. 237-247.
- Clark, D.H., Steig, E.J., Potter Jr., N., and Gillespie, A.R. 1998. Genetic variability of rock glaciers. *Geografiska Annaler* Vol 80 A No. 3-4 Pp. 175-182.

- Denton, G.H., Prentice, M.L., Kellogg, D.E., and Kellogg, T.B. 1984. Late Tertiary history of the Antarctic ice sheet: Evidence from the Dry Valleys. *Geology* Vol. 12 May. Pp. 263-267.
- Denton, G.H., Prentice, M.L., and Burckle, L.H. 1991. Cainozoic history of the Antarctic Ice Sheet. *In: The Geology of Antarctica* (R.J. Tingey, ed.) Pp. 365-433. Oxford University Press, New York.
- Denton, G.H., Sugden, D. E., Marchant, D. R., Hall, B. L., and Wilch, T. I. 1993. East Antarctica ice sheet sensitivity to Pliocene climatic change from a Dry Valleys perspective. *Geografiska Annaler* Vol. 75A No. 4. Pp. 155-204.
- Drewry, D.J. 1982. Ice flow, bedrock, and geothermal studies from radio-echo sounding inland of McMurdo Sound, Antarctica. *In: Antarctic Geoscience* (C. Craddock, ed.) Pp. 977-983. University of Wisconsin Press, Madison.
- Elliot, D.H., Fleck, R.J., and Sutter, J.F. 1985. Potassium-Argon age determinations of Ferrar Group rocks, central Transantarctic Mountains. *In: Geology of the Central Transantarctic Mountains. Antarctic Research Series 36(10)*. Pp. 197-224.
- Flower, B. P. and Kennett, J. P. 1994. The middle Miocene climatic transition: East Antarctic ice sheet development, deep ocean circulation and global carbon cycling. *Palaeogeography, Palaeoclimatology, Palaeoecology* Vol 108. Pp. 537-555.
- Gutzler, D. S. 2000. Evaluating Global Warming: A Post-1990 s Perspective. *GSA Today* Vol. 10 No. 10. Pp. 1-7.
- Hall, B.L., Denton, G.H., Lux, D.R., and Bockheim, J.G. 1993. "Late Tertiary Antarctic paleoclimate and ice-sheet dynamics inferred from surficial deposits in Wright Valley. *Geografiska Annaler* Vol. 75A No. 4. Pp. 239-268.
- Hallet, B. 1990a. Self-organization in freezing soils: from microscopic ice lenses to patterned ground. *Canadian Journal of Physics* Vol. 68. Pp. 842-852.
- Hallet, B. 1990b. Spatial self-organization in geomorphology: from periodic bedforms and patterned ground to scale-invariant topography. *Earth-Science Reviews* Vol. 29. Pp. 57-75.
- Hallet, B. and Prestrud, S. 1986. Dynamics of Periglacial Sorted Circles in Western Spitsbergen. *Quaternary Research* Vol 26. Pp. 81-99.

- Hill, R. S. and Truswell, E. M. 1993. *Nothofagus* fossils in the Sirius Group, Transantarctic Mountains: Leaves and pollen and their climatic implications. *Antarctic Research Series* Vol. 60. Pp. 67-73.
- Hughes, T.J. 1998. *Ice Sheets*. Oxford University Press, New York.
- Kellogg, D.E. and Kellogg, T.B. 1996. Diatoms in South Pole ice: Implications for eolian contamination of Sirius Group deposits. *Geology* Vol. 24 No. 2, Pp. 115-118.
- Kellogg, D.E. and Kellogg, T.B. 1997. Diatoms in a South Pole ice core: Serious implications for the age of the Sirius Group. *Antarctic Journal* — Review 1997. Pp. 213-218.
- Kennett, J.P. 1977. Evolution of Antarctic glaciation, the Circum-Antarctic Ocean, and their impact on global paleoceanography. *Journal of Geophysical Research* Vol. 82. Pp. 3843-3860.
- Lewis, A. R. 2000. The Paleoclimate Significance of Massive Buried Glacial Ice in Beacon Valley, Antarctica. Unpublished Master s Thesis, Institute for Quaternary Studies. University of Maine.
- Marchant, D.R., 1998. Personal Communication.
- Marchant, D.R., Denton, G.H., Bockheim, J.G., Wilson, S.C., and Kerr, A.R. 1994 Quaternary changes in level of the upper Taylor Glacier, Antarctica: implication for paleoclimate and East Antarctic Ice Sheet dynamics. *Boreas* Vol. 23. Pp. 29-43.
- Marchant, D.R. and Denton, G.H. 1996. Miocene and Pliocene paleoclimate of the Dry Valleys region, Southern Victoria land: a geomorphological approach. *Marine Micropaleontology* Vol. 27. Pp. 253-271.
- Marchant, D.R., Denton, G.H., and Swisher III, C.C. 1993a. Miocene-Pliocene-Pleistocene glacial history of Arena Valley, Quartermain Mountains, Antarctica. *Geografiska Annaler* Vol. 75A No. 4. Pp. 269-302.
- Marchant, D.R., Denton, G.H., Sugden, D.E., and Swisher III, C.C. 1993b. Miocene glacial stratigraphy and landscape evolution of the Western Asgard Range, Antarctica. *Geografiska Annaler* Vol. 75A No. 4. Pp. 303-330.
- Margolis, S. and Kennett, J.P. 1970. "Antarctic glaciation during the Tertiary recorded in sub-Antarctic deep-sea cores." *Science* Vol. 170. Pp. 1085-1087.

- McElroy, C.T. and Rose, G. 1987. Geology of the Beacon Heights area, Southern Victoria Land, Antarctica. 1:50,000. New Zealand Geological Survey miscellaneous series map 15 (1 sheet) and notes. Wellington, New Zealand. Department of Scientific and Industrial Research.
- McKelvey, B.C., Webb, P.N., and Kohn, B.P. 1977. Stratigraphy of the Taylor and lower Victoria groups (Beacon Supergroup) between the Mackay Glacier and Boomerang Range, Antarctica. *New Zealand Journal of Geology and Geophysics*. Vol. 20 No. 5. Pp. 813-863.
- Miller, K.G., Fairbanks, R.G., and Mountain, G.S. 1987. Tertiary oxygen isotope synthesis, sea level history, and continental margin erosion. *Paleoceanography* Vol. 2 No. 1. Pp. 1-19.
- Potter Jr., N. and Wilson, S. C. 1984. Glacial geology and soils in Beacon Valley. *Antarctic Journal of the United States* Vol. 18 No. 5. Pp. 100-103.
- Rosato, A., Strandburg, K.J., Prinz, F., and Swendsen, R.H. 1987. Why the Brazil nuts are on top: size segregation of particulate matter by shaking. *Physical Review Letters* Vol. 58 No. 10. Pp. 1038-1040.
- Schfer, J. M., Ivy-Ochs, S., Wieler, R., Ingo, L., Baur, H., Denton, G.H., and Schlichter, C. 1999. Cosmogenic noble gas studies in the oldest landscape on earth: surface exposure ages of the Dry Valleys, Antarctica. *Earth and Planetary Science Letters* Vol. 167. Pp. 215-226.
- Schwerdtfeger, W. 1984. Weather and climate of the Antarctic. *In: Developments in Atmospheric Science* 15. Elsevier Publishing Company, Amsterdam.
- Sugden, D. E. 1996. The East Antarctic Ice Sheet: unstable ice or unstable ideas? Vice-Presidential Address delivered at the Annual Conference of the Royal Geographical Society (with the Institute of British Geographers) University of Strathclyde.
- Sugden, D.E., Denton, G.H., and Marchant, D.R. 1991. Subglacial meltwater channel systems and ice sheet overriding, Asgard Range, Antarctica. *Geografiska Annaler* Vol. 73 A No. 2. Pp. 109-121.
- Sugden, D. E., Denton, G. H., and Marchant, D. R. 1995. Landscape evolution of the Dry Valleys, Transantarctic Mountains: Tectonic implications. *Journal of Geophysical Research* Vol. 100 No. B7. Pp. 9949-9967.
- Sugden, D. E., Marchant, D. R., Potter Jr., N., Souchez, R. A., Denton, G. H., Swisher III, C. C., and Tison, J. 1995. Preservation of Miocene glacier ice in East Antarctica. *Nature* Vol. 376 August 3. Pp. 412-414.

- Sugden, D.E., Summerfield, M.A., Denton, G.H., Wilch, T.I., McIntosh, W.C., Marchant, D.R., and Rutherford, R.H. 1999. Landscape development in the Royal Society Range, southern Victoria Land, Antarctica: stability since the mid-Miocene. *Geomorphology* Vol. 28. Pp. 181-200.
- Summerfield, M.A., Stuart, F.M., Cockburn, H.A.P., Sugden, D.E., Denton, G.H., Dunai, T., and Marchant, D.R. 1999. Long-term rates of denudation in the Dry Valleys, Transantarctic Mountains, southern Victoria Land, Antarctica based on in-situ-produced cosmogenic ^{21}Ne . *Geomorphology* Vol. 27. Pp. 113-129.
- Webb, P.N. and Harwood, D.M. 1991. Late Cenozoic glacial history of the Ross Embayment, Antarctica. *Quaternary Science Reviews* Vol. 10. Pp. 215-223.
- Webb, P.N. and Harwood, D.M. 1987. Terrestrial flora of the Sirius Group: Its significance for late Cenozoic glacial history. *Antarctic Journal of the United States* Vol. 22 No. 4. Pp. 7-11.
- Webb, P.N., Harwood, D.M., McKelvey, B.C., Mercer, J.H., and Stott, L.D. 1984. Cenozoic marine sedimentation and ice-volume variation on the East Antarctic craton. *Geology* Vol.12 No. 5. Pp. 271-291.
- Zachos, J. C., Quinn, T. M., and Salamy, K. A. 1996. High-resolution (10^4 years) deep-sea foraminiferal stable isotope records of the Eocene-Oligocene climate transition. *Paleoceanography* Vol. 11, No. 3. Pp. 251-266.

APPENDIX A- SEDIMENTOLOGY DATA

Sedimentology data is classified in this appendix as into two groups on the basis of oxidation and weathering observed in the field

**TABLE A.1- WEATHERED QUARTZ AND DOLERITE SAND UNIT
(ACTUAL SAMPLE WEIGHTS IN GRAMS)**

Sample #	Total Weight (g)	Sand Weight	Gravel Weight	Mud Weight
DLS 98-003 17-19CM	657	574	55	28
DLS 98-004 0-6CM	849	655	140	54
DLS 98-004 6-10CM	537	465	38	34
DLS 98-005 X D	2272	1999	182	91
DLS 98-005 A	1445	1212	118	5984
DLS 98-006B	2004	1587	249	168
DLS 98-007B	2152	1984	115	53
DLS 98-008	609	527	68	14
DLS 98-009A	2159	1703	355	101
DLS 98-010C	1983	1710	200	73
DLS 98-014A	2795	1480	1135	180
DLS 98-014C	2095	1773	142	180
DLS 98-015C	2350	2008	225	117
DLS 98-016B	2601	1176	1344	81
DLS 98-017D	1456	1333	10	113

APPENDIX A- SEDIMENTOLOGY DATA

**TABLE A.2- WEATHERED QUARTZ AND DOLERITE SAND UNIT
(PERCENT GRAIN-SIZE BY WEIGHT)**

Sample #	% Sand	% Gravel	% Mud
DLS 98-003 17-19CM	87	8	5
DLS 98-004 0-6CM	77	16	7
DLS 98-004 6-10CM	87	7	6
DLI 98-005 X D	88	8	4
DLS 98-005 A	84	12	4
DLS 98-006B	79	12	9
DLS 98-007B	92	5	3
DLS 98-008	87	11	2
DLS 98--009A	79	16	5
DLS 98-010C	86	10	4
DLS 98-014A	53	41	6
DLS 98-014C	85	7	8
DLS 98-015C	85	10	5
DLS 98-016B	88	7	5
DLS 98-017D	92	1	7

APPENDIX A- SEDIMENTOLOGY DATA

**TABLE A.3- UNWEATHERED GRAY DIAMICTON UNIT
(ACTUAL SAMPLE WEIGHTS IN GRAMS)**

Sample #	Total Weight (g)	Sand Weight	Mud Weight	Gravel Weight
DLS 98-006 C	1701	811	87	803
DLS 98-006 D	2086	347	54	1685
DLS 98-009 B	1826	207	11	1608
DLS 98-010 D	4272	938	108	3226
DLS 98-011 B	2387	1026	110	1250
DLS 98-014 B	4648	1253	118	3277
DLS 98-015 D	2965	829	60	2076
DLS 98-016 A	3250	750	131	2369
DLS 98-017 C	2019	632	50	1336

APPENDIX A- SEDIMENTOLOGY DATA

**TABLE A.4- UNWEATHERED GRAY DIAMICTON UNIT
(PERCENT GRAIN-SIZE BY WEIGHT)**

Sample #	% Sand	% Mud	% Gravel
DLS 98-006 C	48	5	47
DLS 98-006 D	16	3	81
DLS 98-009 B	11	1	88
DLS 98-010 D	22	3	75
DLS 98-011 B	43	5	52
DLS 98-014 B	27	3	70
DLS 98-015 D	28	2	70
DLS 98-016 A	23	4	73
DLS 98-017 C	31	2	67

APPENDIX B- POLYGON DATA

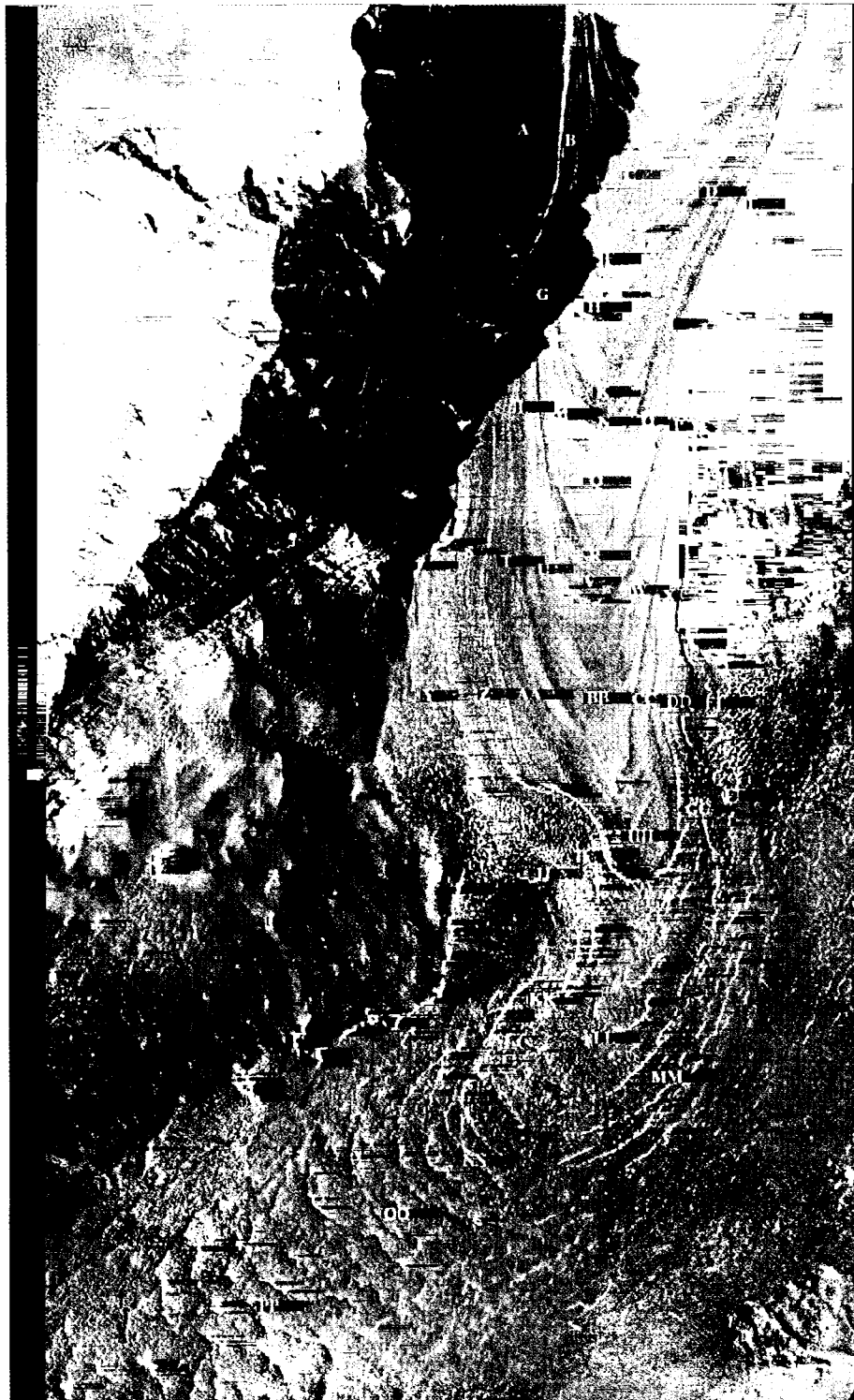
TABLE B.1

MAPPING SITE	SEDIMENT THICKNESS (CM)	POLYGON AREA (Sq. Meters)	POLYGON RELIEF (CM)	TRENCH ANGLE (DEGREES)	TRENCH WIDTH (CM)
A	12	63	40		60
B	6	21		3	55
C	3		10		40
D	6	35	25	3	
E	8	59	35		150
F	4		0		
G	7	60	30	4	25
H	6	6	10	1	10
I	7	60	25		40
J	9	59	35	4	
K		9	5		
L	10				
M	7	9	5	4	35
N	12	12	20	8	50
O	8	16	5		35
P					
Q	8	12	15		45
R		13	15		45
S	26	39	80	23	120
T	20	17	70	20	90
U	16	17	60	9	65
V	18	23	65	15	80
W	28	35	55	13	120
X					
Y	45	195	100-110	25	100-150
Z	25	88	100-150	23	200
AA	15	30	80	18	100
BB	15	21	0-10	5	
CC	25	27	25	18	75
DD	35	110	80-100	16	150
EE	48	180	120-150	25	>200
FF		185	120-150	21	>200
GG	45	72	120	27	150
HH	20	96	100	25	125
II	48	75	120	28	150
JJ					>200
KK	38	165	100-120	27	185
LL	25		100-120	22	100-120
MM	40	153	100-120	26	180
NN	37	168	150-200	27	150
OO	40	1125	200	30	300
PP		5000	450	32	>>400

APPENDIX C-
MAP C.1 EXCAVATION SITES



APPENDIX C-
MAP C.2 POLYGON MAPPING SITES



BIOGRAPHY OF THE AUTHOR

Andrew Martin Lorrey was born in Lowell, Massachusetts on March 8, 1975. He was raised in Nashua, New Hampshire by his parents Jean and Martin, his sister Haidee, and his grandmother Estelle. He graduated upper quarter from Nashua High School in 1993. He graduated from Boston University in 1998 with a degree in Earth Sciences, specializing in Pleistocene geology of paleolakes in New Hampshire. After becoming fascinated with the geology of Maine on select fieldtrips, he began taking classes at the University of Maine in 1997 and became a full-time graduate student in 1998. While at the University of Maine, he was an active member of the Association of Graduate Students, serving as the Graduate Research Exposition Coordinator for the years 2000-2002 inclusive. He was also the Grant Review officer for the 2001-2002 academic year. As of July of 2002, Andrew will be pursuing a Doctor of Philosophy degree in Geography and Environmental Science at the University of Auckland, New Zealand. Andrew is a candidate for the Master of Science degree in Geological Sciences from The University of Maine in May, 2002.